Measurements of W±Z production cross sections in pp collisions at s=8TeV with the ATLAS detector and limits on anomalous gauge boson self-couplings

Measurements of $W^{\pm}Z$ production cross sections in pp collisions at $\sqrt{s} = 8$ TeV with the ATLAS detector and limits on anomalous gauge boson self-couplings

G. Aad *et al.*[*]
(ATLAS Collaboration)
(Received 8 March 2016; published 13 May 2016)

This paper presents measurements of $W^{\pm}Z$ production in pp collisions at a center-of-mass energy of 8 TeV. The gauge bosons are reconstructed using their leptonic decay modes into electrons and muons. The data were collected in 2012 by the ATLAS experiment at the Large Hadron Collider and correspond to an integrated luminosity of 20.3 fb^{-1}. The measured inclusive cross section in the detector fiducial region is $\sigma_{W^{\pm}Z\to\ell'\nu\ell\ell} = 35.1 \pm 0.9(\text{stat}) \pm 0.8(\text{sys}) \pm 0.8(\text{lumi})$ fb, for one leptonic decay channel. In comparison, the next-to-leading-order Standard Model expectation is 30.0 ± 2.1 fb. Cross sections for $W^{+}Z$ and $W^{-}Z$ production and their ratio are presented as well as differential cross sections for several kinematic observables. Limits on anomalous triple gauge boson couplings are derived from the transverse mass spectrum of the $W^{\pm}Z$ system. From the analysis of events with a W and a Z boson associated with two or more forward jets an upper limit at 95% confidence level on the $W^{\pm}Z$ scattering cross section of 0.63 fb, for each leptonic decay channel, is established, while the Standard Model prediction at next-to-leading order is 0.13 ± 0.01 fb. Limits on anomalous quartic gauge boson couplings are also extracted.

DOI: 10.1103/PhysRevD.93.092004

I. INTRODUCTION

The study of $W^{\pm}Z$ diboson production is an important test of the Standard Model (SM) for its sensitivity to the gauge boson self-interactions, related to the non-Abelian structure of the electroweak interaction. It provides the means to investigate vector boson scattering (VBS) processes, which directly probe the electroweak symmetry breaking sector of the SM, and to extract constraints on anomalous triple and quartic gauge boson couplings (aTGC and aQGC). Improved constraints can probe scales of new physics in the multi-TeV range and provide a way to look for signals of new physics in a model-independent way. Precise measurements of $W^{\pm}Z$ production will also help to improve the existing QCD calculations of this process.

This paper presents measurements of the $W^{\pm}Z$ production cross section and limits on the aTGC and aQGC obtained by analyzing proton-proton (pp) collisions at a center-of-mass energy of $\sqrt{s} = 8$ TeV. The leptonic decay modes of the W and Z bosons are used and all quoted fiducial production cross sections include the branching ratio of the gauge bosons into channels with electrons or muons. The analyzed data sample was collected in 2012 by the ATLAS experiment at the Large Hadron Collider (LHC), and corresponds to an integrated luminosity of 20.3 fb^{-1}. Experimentally, $W^{\pm}Z$ production has the advantage of a higher cross section than ZZ production. At the same time, with three charged leptons and the requirement that two of them originate from a Z boson, the leptonic $W^{\pm}Z$ final states are easier to discriminate from the background than the leptonic WW final states.

Measurements of the $W^{\pm}Z$ production cross section have been reported in proton-antiproton collisions at a center-of-mass energy of $\sqrt{s} = 1.96$ TeV by the CDF and D0 collaborations [1,2] using integrated luminosities of 7.1 fb^{-1} and 8.6 fb^{-1}, respectively, and for $\sqrt{s} = 7$ TeV proton-proton collisions, using an integrated luminosity of 4.6 fb^{-1}, by the ATLAS Collaboration [3]. Limits on anomalous charged-current gauge couplings were also reported previously by the LEP, Tevatron, and LHC experiments [4–6]. In hadron collisions, the selection of $W^{\pm}Z$ final states allows direct access to the WWZ gauge coupling without the need of disentangling it from the $WW\gamma$ gauge coupling as in $W^{\pm}W^{\mp}$ events from hadronic or $e^{+}e^{-}$ collisions.

Compared to the previously published measurements, this paper uses data collected at a higher center-of-mass energy with a fourfold increase in integrated luminosity and presents additional measurements. The production cross section is measured in a fiducial phase space inclusively and as single differential cross sections as a function of each of several kinematic variables: the transverse momentum p_{T} of the W and Z bosons, the jet multiplicity, the transverse mass of the WZ system, m_{T}^{WZ}, and the p_{T} of the neutrino associated with the W boson decay. An interesting

[*]Full author list given at the end of the article.

feature of this last distribution is its sensitivity to the polarization of the W boson, similar to the p_{T} of the lepton of the W boson decay. Finally, the distribution of the absolute difference between the rapidities of the Z boson and the lepton from the W boson decay is measured, which was proposed as an alternative variable to look for aTGC and was also found to be sensitive to the approximately zero helicity amplitude that is predicted at leading order (LO) in the SM [7,8]. Limits on aTGC are extracted from the m_{T}^{WZ} distribution, which is found to be less sensitive to higher-order perturbative effects in QCD [9] and electroweak (EW) theory [10,11] than other observables, e.g., p_{T}^{Z}.

The ratio of W^+Z/W^-Z integrated production cross sections, sensitive to the choice of parton distribution functions (PDF), is measured along with the evolution of this ratio as a function of the kinematic variables introduced above. Charge-dependent distributions may be helpful in investigating CP violation effects in the interaction between gauge bosons. This paper also includes a study of $W^{\pm}Z$ vector boson scattering, characterized by the presence of at least two forward jets, which is sensitive to quartic gauge couplings. Events with a $W^{\pm}Zjj$ final state are used to set limits on the VBS cross section and on aQGC in the $WZWZ$ vertex.

The results are compared with the SM cross-section predictions, which at present are fully calculated only up to the next-to-leading order (NLO) in QCD [12,13].

The paper is organized as follows. The ATLAS detector is described in Sec. II. The definition of the fiducial phase space used in this paper is presented in Sec. III. Section IV discusses the available theoretical predictions. Section V provides details of the simulated samples used for the measurements. A description of the data set and the selection criteria are given in Sec. VI. Section VII presents the background estimation, and Sec. VIII provides comparisons of observed and expected events and of kinematic distributions at the reconstructed level. The procedure used to correct for detector effects and for acceptance is described in Sec. IX. The treatment of the systematic uncertainties is detailed in Sec. X. Sections XI, XII, and XIII describe the combination procedure of the four leptonic $W^{\pm}Z$ decay channels and discuss the results. Finally, concluding remarks are presented in Sec. XIV.

II. THE ATLAS DETECTOR

The ATLAS detector [14] is a multipurpose detector with a cylindrical geometry and nearly 4π coverage in solid angle. The collision point is surrounded by inner tracking devices, which are followed in increasing distance from the center by a superconducting solenoid providing a 2 T axial magnetic field, a calorimeter system, and a muon spectrometer.

The inner tracker provides precise position and momentum measurements of charged particles in the pseudorapidity[1] range $|\eta| < 2.5$. It consists of three subdetectors arranged in a coaxial geometry around the beam axis: the silicon pixel detector, the silicon microstrip detector, and the transition radiation tracker.

Electromagnetic calorimetry in the region $|\eta| < 3.2$ is based on a high-granularity, lead/liquid-argon (LAr) sampling technology. Hadronic calorimetry uses a steel/scintillating-tile detector covering the region $|\eta| < 1.7$ and a copper/LAr detector in the region $1.5 < |\eta| < 3.2$. The most forward region of the detector $3.1 < |\eta| < 4.9$ is equipped with a dedicated forward calorimeter, measuring electromagnetic and hadronic energies using copper/LAr and tungsten/LAr modules.

The muon spectrometer comprises separate trigger and high-precision tracking chambers to measure the deflection of muons in a magnetic field generated by three large superconducting toroids arranged with an eightfold azimuthal coil symmetry around the calorimeters. The high-precision chambers cover a range of $|\eta| < 2.7$. The muon trigger system covers the range $|\eta| < 2.4$ with resistive plate chambers in the barrel, and thin gap chambers in the end cap regions.

A three-level trigger system is used to select events in real time. A hardware-based Level-1 trigger uses a subset of detector information to reduce the event rate to a value of at most 75 kHz. The rate of accepted events is then reduced to about 400 Hz by two software-based trigger levels, Level-2 and the event filter.

III. PHASE-SPACE DEFINITION

The phase-space definition used in this paper relies on final-state prompt leptons[2] [15] associated with the W and Z boson decay, as explained in detail below.

At particle level, the kinematics of final-state prompt electrons and muons is computed including the contributions from final-state radiated photons within a distance in the (η, ϕ) plane of $\Delta R = \sqrt{(\Delta\eta)^2 + (\Delta\phi)^2} = 0.1$ around the direction of the charged lepton.

These dressed leptons and the final-state neutrinos that do not originate from hadron or τ decays are associated with the W and Z boson decay products with an algorithmic approach, called "resonant shape." This algorithm is based on the value of an estimator expressing the product of the nominal line shapes of the W and Z resonances

[1] ATLAS uses a right-handed coordinate system with its origin at the nominal interaction point (IP) in the center of the detector and the z axis along the beam direction. The x axis points from the IP to the center of the LHC ring, and the y axis points upward. Cylindrical coordinates (r, ϕ) are used in the transverse (x, y) plane, ϕ being the azimuthal angle around the beam direction. The pseudorapidity is defined in terms of the polar angle θ as $\eta = -\ln[\tan(\theta/2)]$.

[2] A prompt lepton is a lepton that is not produced in the decay of a hadron or a τ or their descendants.

TABLE I. Phase-space definitions used for the total, fiducial, VBS cross-section measurements and for the extraction of limits on the aTGC and aQGC. The symbols ℓ_Z and ℓ_W refer to the leptons associated with the Z and W bosons, respectively. The symbol m_Z^{PDG} refers to the mean experimental mass of the Z boson from the Particle Data Group [16]. The other symbols are defined in the text.

Variable	Total	Fiducial and aTGC	VBS	aQGC
Lepton $\lvert\eta\rvert$	⋯	< 2.5	< 2.5	< 2.5
p_{T} of ℓ_Z, p_{T} of ℓ_W [GeV]	⋯	> 15, > 20	> 15, > 20	> 15, > 20
m_Z range [GeV]	66–116	$\lvert m_Z - m_Z^{\mathrm{PDG}}\rvert < 10$	$\lvert m_Z - m_Z^{\mathrm{PDG}}\rvert < 10$	$\lvert m_Z - m_Z^{\mathrm{PDG}}\rvert < 10$
m_{T}^W [GeV]	⋯	> 30	> 30	> 30
$\Delta R(\ell_Z^-, \ell_Z^+)$, $\Delta R(\ell_Z, \ell_W)$	⋯	> 0.2, > 0.3	> 0.2, > 0.3	> 0.2, > 0.3
p_{T} two leading jets [GeV]	⋯	⋯	> 30	> 30
$\lvert\eta_j\rvert$ two leading jets	⋯	⋯	< 4.5	< 4.5
Jet multiplicity	⋯	⋯	≥ 2	≥ 2
m_{jj} [GeV]	⋯	⋯	> 500	> 500
$\Delta R(j, \ell)$	⋯	⋯	> 0.3	> 0.3
$\lvert\Delta\phi(W, Z)\rvert$	⋯	⋯	⋯	> 2
$\sum \lvert p_{\mathrm{T}}^{\ell}\rvert$ [GeV]	⋯	⋯	⋯	> 250

$$P = \left| \frac{1}{m^2_{(\ell^+,\ell^-)} - (m_Z^{\mathrm{PDG}})^2 + i\Gamma_Z^{\mathrm{PDG}} m_Z^{\mathrm{PDG}}} \right|^2 \times \left| \frac{1}{m^2_{(\ell',\nu_{\ell'})} - (m_W^{\mathrm{PDG}})^2 + i\Gamma_W^{\mathrm{PDG}} m_W^{\mathrm{PDG}}} \right|^2, \quad (1)$$

where m_Z^{PDG} (m_W^{PDG}) and Γ_Z^{PDG} (Γ_W^{PDG}) are the world average mass and total width of the Z (W) boson, respectively, as reported by the Particle Data Group [16]. The input to the estimator is the invariant mass m of all possible pairs (ℓ^+, ℓ^-) and $(\ell', \nu_{\ell'})$ satisfying the fiducial selection requirements defined in the next paragraph. The final choice of which leptons are assigned to the W or Z bosons corresponds to the configuration exhibiting the highest value of the estimator. Using this specific association algorithm, the gauge boson kinematics can be computed using the kinematics of the associated leptons independently of any internal Monte Carlo (MC) generator details.

The integrated and differential cross-section measurements are performed in a fiducial phase space defined at particle level by the following requirements: the p_{T} of the leptons from the Z boson decay is greater than 15 GeV, the p_{T} of the charged lepton from the W decay is greater than 20 GeV, the absolute value of the pseudorapidity of the charged leptons from the W and Z bosons are less than 2.5, the invariant mass of the two leptons from the Z boson decay differs at most by 10 GeV from the world average value of the Z boson mass m_Z^{PDG}. The W transverse mass, defined as $m_{\mathrm{T}}^W = \sqrt{2 \cdot p_{\mathrm{T}}^{\nu} \cdot p_{\mathrm{T}}^{\ell} \cdot [1 - \cos\Delta\phi(\ell, \nu)]}$, where $\Delta\phi(\ell, \nu)$ is the angle between the lepton and the neutrino in the transverse plane, is required to be greater than 30 GeV. In addition, it is required that the angular distance ΔR between the charged leptons from W and Z decay is larger than 0.3, and that ΔR between the two leptons from the Z decay is larger than 0.2.

The integrated cross section, measured in the fiducial region of the detector, is extrapolated to a total phase space, defined by requiring that the invariant mass of the lepton pair associated with the Z boson decay is in the range $66 < m_Z < 116$ GeV, and extrapolating to all decay channels of the W and Z bosons.

In order to define the VBS fiducial region for the cross-section measurement, in addition to the inclusive fiducial criteria, at least two jets with a p_{T} greater than 30 GeV and an absolute value of the pseudorapidity η_j below 4.5 are required. These particle level jets are defined using the anti-k_t algorithm with a radius parameter $R = 0.4$. The angular distance between all selected leptons and jets, $\Delta R(j, \ell)$, is required to be greater than 0.3. If the $\Delta R(j, \ell)$ requirement is not satisfied, the jet is discarded. The invariant mass of the two leading jets, m_{jj}, must be above 500 GeV to enhance the sensitivity to VBS processes.

For setting limits on aQGC, the fiducial region definition was optimized to give the best expected limits. Therefore, in addition to the criteria used for the VBS fiducial cross-section measurement, it is required that the difference in azimuthal angle $\lvert\Delta\phi(W, Z)\rvert$ between the W and Z directions is greater than 2 rad. In addition, in order to increase the sensitivity to aQGC signals, the scalar sum of the transverse momenta of the three charged leptons associated with the W and Z bosons, $\sum \lvert p_{\mathrm{T}}^{\ell}\rvert$, is greater than 250 GeV.

A summary of the phase-space definition used in this paper is given in Table I.

IV. STANDARD MODEL PREDICTIONS FOR $W^{\pm}Z$ PRODUCTION

The measured integrated cross section is compared with the SM NLO prediction from the POWHEG event generator [17–20], interfaced with PYTHIA 8.175 [21] for parton showering (PS) and hadronization. The POWHEG MC event generator implements the next-to-leading order QCD

corrections to the production of electroweak vector boson pairs at hadron colliders, including the full spin and decay angle correlations [22]. This calculation is referred to as POWHEG+PYTHIA later on. At a center-of-mass energy of $\sqrt{s} = 8$ TeV, in proton-proton collisions, the SM NLO cross section for $W^{\pm}Z$ production in the fiducial phase space defined in Sec. III, estimated with POWHEG+PYTHIA using factorization and dynamic renormalization scales μ_{R} and μ_{F} equal to $m_{WZ}/2$, where m_{WZ} is the invariant mass of the WZ system, and the CT10 [23] PDF set, is

$$\sigma^{\mathrm{fid,th}}_{W^{\pm}Z\to\ell'\nu\ell\ell} = 30.0 \pm 0.8(\mathrm{PDF}) \pm 1.3(\mathrm{scale})\ \mathrm{fb}.$$

The predicted cross sections for $W^{+}Z$ and $W^{-}Z$ inclusive production are

$$\sigma^{\mathrm{fid,th}}_{W^{+}Z\to\ell'\nu\ell\ell} = 18.8 \pm 0.5(\mathrm{PDF}) \pm 0.8(\mathrm{scale})\ \mathrm{fb},$$

$$\sigma^{\mathrm{fid,th}}_{W^{-}Z\to\ell'\nu\ell\ell} = 11.1 \pm 0.5(\mathrm{PDF}) \pm 0.5(\mathrm{scale})\ \mathrm{fb}.$$

In these estimates, the W and Z decays in a single leptonic channel with muons or electrons are considered. The uncertainty due to the PDF is computed using the eigenvectors of the CT10 PDF set scaled to 68% confidence level (C.L.) and the envelope of the differences between the results obtained with CT10, MSTW 2008 [24], NNPDF 3.0 [25], and ATLAS-epWZ12 NLO [26] PDF sets. The QCD scale uncertainty is estimated conventionally by varying μ_{R} and μ_{F} by factors of 2 around the nominal scale $m_{WZ}/2$ with the constraint $0.5 \le \mu_{\mathrm{R}}/\mu_{\mathrm{F}} \le 2$. A maximum variation of the cross section of 4% is found. However, the SM prediction, which is at NLO accuracy in perturbative QCD, is highly sensitive to the choice of renormalization scale μ_{R}. For example, choosing a fixed renormalization scale of $\mu_{\mathrm{R}} = (m_W + m_Z)/2$ instead of a dynamic scale $\mu_{\mathrm{R}} = m_{WZ}$ increases the SM predicted cross section by 7%. The total uncertainty on the theoretical prediction is estimated as the linear sum of the PDF and QCD scale uncertainties, following the recommendations in Ref. [27].

The differential distributions are compared to the predictions of the POWHEG+PYTHIA, MC@NLO 4.0 [28], interfaced with HERWIG [29] for PS and hadronization, and SHERPA 1.4.5 [30,31] event generators. The SHERPA predictions used in this paper are computed at LO and take into account the real emission of up to three partons in the matrix element calculations. They are therefore expected to describe the jet multiplicity distribution and the event kinematics at higher jet multiplicity better than POWHEG +PYTHIA where only the real emission of at most one parton is directly calculated at NLO.

The uncertainties on predicted differential cross sections arising from the PDF and the QCD scale uncertainties are estimated as described above. Recently, approximate next-to-next-to-leading-order ($\bar{n}$NLO) corrections have been computed and presented as K-factors for differential cross-section distributions [9]. For a number of commonly used observables these corrections are sizable, of the order of 30% to 100%. The $\bar{n}$NLO correction to the m_{T}^{WZ} distribution is smaller ($< 10\%$) indicating that this observable is less sensitive to higher order perturbative contributions to the transition amplitude that appear at next-to-next-to-leading order (NNLO). The approximate $\bar{n}$NLO calculation can only account for the dominant part of the NNLO QCD corrections and in certain regions of the phase space.

Electroweak quantum corrections at NLO to the $W^{\pm}Z$ cross sections, including photon-quark-induced processes, have been computed [10,11]. These corrections have an impact mainly on differential cross sections. The complete calculation is done in the zero-width approximation, and the decays of vector bosons are not included. It is therefore not included in the available Monte Carlo (MC) generators. For this reason, the uncertainty on the differential distributions arising from missing higher orders in the EW theory is included by taking the existing EW corrections at NLO as an additional theory uncertainty on the predictions from POWHEG+PYTHIA. The effect increases with increasing p_{T}^{Z} and m_{T}^{WZ}. At a center-of-mass energy of 8 TeV, they range from -0.3% to a value of 3.2% in the highest p_{T}^{Z} bin considered in this analysis and from 0.12% to a value of 1.1% in the highest m_{T}^{WZ} bin considered in this analysis [11]. The total uncertainty on the differential theoretical predictions is estimated as the linear sum of the PDF, QCD scale, and EW correction uncertainties [27].

The SM cross section of the VBS process is calculated at NLO in QCD with the Monte Carlo generator VBFNLO [32–36]. In proton-proton collisions with a center-of-mass energy of 8 TeV this cross section in the VBS fiducial phase space defined in Sec. III is 0.13 ± 0.01 fb. This calculated cross section is for one single leptonic decay channel of the W and Z in muons or electrons. The total uncertainty on the VBS theoretical prediction is estimated as the linear sum of the PDF and QCD scale uncertainties, each determined as described above.

V. SIMULATED EVENT SAMPLES

Simulated event samples are used for estimates of the irreducible background, for the correction of the signal yield for detector effects, for the extrapolation from the fiducial to the total phase space, for the extraction of the gauge couplings, and for comparisons of the results to the theoretical expectations.

The simulated samples are overlaid with additional proton-proton interactions (pileup) generated with PYTHIA 8.1 using the MSTW2008 LO PDF set and the A2 [37] set of tuned parameters. The MC events are also reweighted to better reproduce the distribution of the mean number of interactions per bunch crossing and of the longitudinal position of the primary pp collision vertex

observed in the data. All generated events are passed through the ATLAS detector simulation [38] based on GEANT4 [39] and processed using the same reconstruction software as for data.

Scale factors are applied to the simulated events to correct for the small differences from data in the trigger, reconstruction, and identification efficiencies for electrons and muons [40–42]. Furthermore, in simulated events the electron energy and the muon momentum are smeared to account for the small differences in resolution between data and simulation [42,43].

A. Signal samples

The $W^{\pm}Z$ SM production processes and subsequent leptonic decays are generated at NLO in QCD using the POWHEG MC event generator [17–20], interfaced with PYTHIA 8.175 [21] for PS, hadronization and the underlying event (UE) simulation. This sample is used to correct for acceptance and detector effects.

Signal events with aTGC are generated at NLO with the MC@NLO 4.0 [28] Monte Carlo generator interfaced with HERWIG [29] and JIMMY [44] for the simulation of the PS, hadronization, and UE.

In all above-mentioned signal samples, the final-state radiation (FSR) resulting from the quantum electrodynamics (QED) interaction is modeled with PHOTOS [45].

For the VBS analysis, the $W^{\pm}Z$ production associated with at least two jets is generated at LO with SHERPA 1.4.5 [30,31], which uses the CKKW [46] matching scheme and an internal model for QED radiation based on the YFS method [47]. Signal events in the VBS analysis arise from the processes that occur at zero order in the strong coupling constant α_s and are labeled $WZjj$-EW. The remaining processes leading to $W^{\pm}Z$ final states, associated with at least two jets, are called $WZjj$-QCD processes.

Events with aQGC are generated at LO using the WHIZARD [48] MC generator. A K-matrix unitarization method [49,50] is employed in order to ensure the unitarity of the scattering amplitude, which would be violated for values of quartic gauge couplings different from the SM value.

The CT10 [23] PDF set is used for all signal samples.

B. Background samples

Backgrounds to the $W^{\pm}Z$ signal come from events with two or more electroweak gauge bosons, top quarks, and gauge bosons associated with jets ($V + j$, $V = W$, Z), and events from double parton scattering (DPS) processes where the $W^{\pm}Z$ signature results from collisions between two pairs of partons producing a single W and a single Z boson. In the VBS analysis the $WZjj$-QCD process is a background to the $WZjj$-EW production. Interference effects between $WZjj$-QCD and $WZjj$-EW processes are expected to be negligible and are therefore not considered.

Monte Carlo simulation is used to compute the contribution from processes with at least three prompt leptons and for comparison with the data-driven estimation of the contribution from background processes with at least one misidentified lepton.

The $q\bar{q} \to ZZ^{(*)}$ processes are generated at NLO with POWHEG interfaced with PYTHIA 8.175 or at LO with SHERPA 1.4.5, which includes up to three partons in the matrix element calculation. The first sample is used in the inclusive analysis, the second in the VBS analysis. The $gg \to ZZ^{(*)}$ process is simulated with GG2ZZ at LO [51] interfaced with HERWIG [29] for the simulation of the PS and of the hadronization and JIMMY [44] for the UE. Processes with three gauge bosons are simulated with MADGRAPH [52] interfaced with PYTHIA. The associated production of top pairs with a weak gauge boson is simulated with MADGRAPH interfaced with PYTHIA, and the associated production of a single top and a Z boson is simulated with SHERPA. The total predictions of these MC samples are rescaled to match NLO predictions from Refs. [53,54] and Ref. [55], respectively.

The contribution from DPS processes is estimated using PYTHIA MC samples generated with two hard scatterings with single-boson production processes (W, Z/γ^*). The cross section of the DPS samples is estimated using its factorization into the product of two single scattering cross sections [56] and the effective area parameter for hard double-parton interactions recently measured by ATLAS [57].

ALPGEN [58] interfaced with JIMMY [44] and SHERPA [30] samples are used to model the $W + j$ and $Z + j$ backgrounds, respectively. Top pair production is simulated with POWHEG+PYTHIA. The WW diboson production is modeled with POWHEG+PYTHIA and GG2WW+HERWIG. ALPGEN and SHERPA are used to model $W\gamma$ and $Z\gamma$ diboson production, respectively.

The set of PDF used to generate ALPGEN and MADGRAPH samples is CTEQ6L1 [59] while the CT10 [23] PDF set is used to generate all the other background samples.

VI. DATA SAMPLE AND SELECTIONS

The data set was collected in 2012 during pp collisions at $\sqrt{s} = 8$ TeV. It only includes data recorded with stable beam conditions and with all relevant subdetector systems operational, and corresponds to a total integrated luminosity of 20.3 fb^{-1}. The absolute luminosity scale is derived from beam-separation scans performed in November 2012. The uncertainty on the integrated luminosity is 1.9% [60].

Data events are selected by requiring at least one electron or muon candidate. The electron and muon triggers impose a p_{T} threshold of 24 GeV along with an isolation requirement on the lepton. In order to increase the efficiency for high-p_{T} leptons, the electron and muon triggers are complemented by single-electron or single-muon triggers with no isolation requirement and with a threshold of

60 GeV or 36 GeV, respectively. Events are required to have at least one primary vertex reconstructed from at least three tracks, where the tracks must have a p_{T} greater than 400 MeV.

All final states with electrons, muons, and $E_{\mathrm{T}}^{\mathrm{miss}}$ from $W^{\pm}Z$ leptonic decays are considered. In the following, the different final states are referred to as $\mu^{\pm}\mu^{+}\mu^{-}$, $e^{\pm}\mu^{+}\mu^{-}$, $\mu^{\pm}e^{+}e^{-}$, and $e^{\pm}e^{+}e^{-}$. No requirement on the number of jets is applied in the inclusive analysis, while jets are explicitly required in the dedicated analysis in order to enhance the contribution from the VBS process.

A. Object reconstruction and selection

Muon candidates are identified by tracks or track segments reconstructed in the muon spectrometer system and matched to tracks reconstructed in the inner detector [42]. The p_{T} of the muon must be greater than 15 GeV and its $|\eta|$ less than 2.5. The ratio between the transverse impact parameter d_0 (with respect to the primary vertex) to its uncertainty (d_0 significance) must be smaller than 3, and the longitudinal impact parameter $|z_0 \cdot \sin(\theta)|$ must be less than 0.5 mm. Isolated muons are then selected with a requirement that the scalar sum of the p_{T} of the tracks within a cone of size $\Delta R = 0.2$ around the muon, excluding the muon itself, must be less than 15% of the muon p_{T}.

Electron candidates are reconstructed from energy clusters in the calorimeter and matched to an inner detector track [40]. The lateral and transverse shapes of the cluster must be consistent with those of an electromagnetic shower. The p_{T} of the electron must be greater than 15 GeV and the pseudorapidity of the cluster must be in the ranges $|\eta| < 1.37$ or $1.52 < |\eta| < 2.47$. The d_0 significance of the electron candidate must be smaller than 6 and the longitudinal impact parameter $|z_0 \cdot \sin(\theta)|$ must be less than 0.5 mm. To ensure that the electron candidate is isolated, the total transverse energy E_{T}, corrected for pileup effects, in an isolation cone of $\Delta R = 0.2$ around the electron candidate and excluding the electron itself must be less than 14% of the electron E_{T}. The scalar sum of the p_{T} of all tracks excluding the electron track itself within the isolation cone must be less than 13% of the electron p_{T}. If an electron overlaps with a muon candidate within $\Delta R = 0.1$, the electron is rejected. This criterion mainly removes photons from final-state radiation and jets misidentified as electrons.

Jets are reconstructed using the anti-k_t algorithm [61] with a radius parameter $R = 0.4$ using topological clusters of energy deposition in the calorimeter. Jets arising from detector noise or noncollision events are rejected [62]. Jets are calibrated and corrected for detector effects using a combination of simulated events and *in situ* methods [62–64]. The jet energies are also corrected to account for energy arising from pileup [65]. In order to reject jets from pileup, the summed scalar p_{T} of tracks associated with both the jet and the primary vertex is required to be greater than 50% of the summed scalar p_{T} of all the tracks associated with the jet [65]. This criterion is applied to jets with p_{T} smaller than 50 GeV and within $|\eta| < 2.4$. The presence of jets with $p_{\mathrm{T}} > 30$ GeV and a pseudorapidity $|\eta_j| < 4.5$ is explicitly required only in the VBS analysis. Jets overlapping with an electron or muon candidate within $\Delta R = 0.3$ are rejected.

The missing transverse momentum, $E_{\mathrm{T}}^{\mathrm{miss}}$ in the event is calculated as the negative vector sum of the transverse momentum of calibrated leptons, photons, and jets, and additional low-energy deposits in the calorimeter [66,67]. The contribution of the low-energy deposits from soft particles to the $E_{\mathrm{T}}^{\mathrm{miss}}$ is further corrected to mitigate the effect of pileup on the $E_{\mathrm{T}}^{\mathrm{miss}}$ reconstruction performance [68].

B. Event selection

Events are required to contain at least three lepton candidates satisfying the selection criteria described above.

In order to decrease the background from ZZ processes, events containing four or more candidate leptons satisfying a looser p_{T} requirement of $p_{\mathrm{T}} > 7$ GeV are discarded.

To ensure that the trigger efficiency is well determined, at least one of the candidate leptons is required to have $p_{\mathrm{T}} > 25$ GeV and to be geometrically matched to a lepton that triggered the event.

The event must have at least one pair of leptons of the same flavor and opposite charge, with an invariant mass that is consistent with the nominal Z boson mass [16] within 10 GeV. This pair is considered as a Z boson candidate. If more than one pair is found, the pair whose invariant mass is closest to the nominal Z boson mass is taken as the Z boson candidate. The third lepton is assigned to the W boson.

To reduce the $Z + j$ background, the lepton assigned to the W boson is required to satisfy more stringent criteria than those required for the leptons attributed to the Z boson. The p_{T} threshold for this lepton is increased to 20 GeV. In addition, electrons must satisfy tighter identification criteria that include requirements on the transverse impact parameter with respect to the primary vertex and on the number of hits in the innermost pixel layer in order to reject photon conversions. In addition, the size of the lepton isolation cones is increased to $\Delta R = 0.3$ and the sum of the p_{T} of the tracks in the isolation cone of the lepton must be less than 10% of the lepton p_{T}. Finally, the transverse mass of the W candidate computed using the $E_{\mathrm{T}}^{\mathrm{miss}}$ and the p_{T} of the third lepton is required to be above 30 GeV.

To select VBS event candidates, in addition to the above-mentioned selection criteria, the presence of at least two jets with p_{T} greater than 30 GeV with an absolute value of η less than 4.5 is required. The invariant mass of the two leading jets must be above 500 GeV, and the angular distance between all selected leptons and jets is required to be greater than 0.3.

For the search of aQGC, in addition to the selection criteria applied in the VBS analysis, it is required that the difference in the azimuthal angle between the reconstructed W and Z directions is greater than 2 rad and that the scalar sum of the transverse momenta of the three charged leptons associated with the W and Z bosons is greater than 250 GeV.

VII. BACKGROUND ESTIMATION

The background sources are classified into two groups: events where at least one of the candidate leptons is not a prompt lepton (reducible background) and events where all candidates are prompt leptons (irreducible background). Candidates that are not prompt leptons are also called "misidentified" or "fake" leptons.

Events in the first group originate from $Z+j$, $Z\gamma$, $t\bar{t}$, and WW production processes. This background is estimated with a data-driven method based on the inversion of a global matrix containing the efficiencies and the misidentification probabilities for prompt and fake leptons (see Sec. VII A). In the inclusive analysis, this contribution represents about half of the total backgrounds. About 2% of this background contribution arises from events with two fake leptons. The background from events with three fake leptons, e.g., from multijet processes, is negligible.

The events contributing to the second group originate from ZZ, $t\bar{t}+V$, VVV (where $V=Z$ or W), $tZ(j)$ events, and DPS processes. The amount of irreducible background is estimated using MC simulations due to the low cross sections of the corresponding processes and the statistical limitations of estimates using data-driven methods. In the inclusive analysis the dominant contribution in this second group is from ZZ production and represents about 70% of the irreducible background. The MC-based estimation of the ZZ background is validated by comparing data and MC simulation in properly defined control regions (see Sec. VII B).

The main background in the VBS analysis originates from the processes defined as $WZjj$-QCD in Sec. V A and amounts to ∼70% of the total backgrounds. The second most important background contribution arises from the tZj process and amounts to ∼10% of the total estimated background.

Interference effects between the $WZjj$-QCD and tZj background processes and the VBS signal ($WZjj$-EW) are expected to be negligible. The treatment of the tZj background is further discussed in Sec. XI C. In the VBS analysis, background events due to misidentified leptons and due to ZZ events amount to about 9% and 7% of the total background, respectively.

A. Background from misidentified leptons ($Z+j$, $Z\gamma$, $t\bar{t}$, WW)

The matrix method [69] is a data-driven method for the calculation of the reducible background which exploits the classification of the leptons as loose (L) or tight (T) candidates and the probability that a fake lepton is misidentified as a loose or tight lepton.

Three-lepton events in the WZ data sample, selected as explained in Sec. VI B, but relaxing some of the lepton identification criteria, are classified into eight categories. Each category contains a number of events, $N_{\alpha\beta\gamma}$, where the first index refers always to the W lepton, the second to the Z leading lepton, and the third to the Z trailing lepton. Each index can be L or T depending on whether the corresponding lepton met only the loose identification criteria or satisfied the tight ones. Loose leptons are leptons that survive the overlap removal criteria (as described in Sec. VI A) but do not meet the isolation criteria, while tight leptons are signal leptons as defined in Secs. VI A and VI B. These eight categories are called *identification categories* here. The number of events in each category, $N_{\alpha\beta\gamma}$, is measured directly in data.

The same WZ data sample of three-lepton events can be decomposed in eight *true categories* according to the nature of each lepton as prompt or nonprompt. Each category contains a number of events, N_{ijk}, where each index, ordered as described above, can be R or F depending on the kind of corresponding lepton (prompt, R, or nonprompt, F). The number of events in each category N_{ijk} is the result of the matrix method calculation.

The number of events, $N_{\alpha\beta\gamma}$, in each identification category is related to the number of events N_{ijk} of the true categories by an 8×8 matrix expressed in terms of the probability that a prompt lepton is identified as a tight (loose) lepton, denoted here by e ($\bar{e}=1-e$), and the probability that a fake lepton is misidentified as a tight (loose) lepton, denoted here by f ($\bar{f}=1-f$). The matrix reduces to a 7×7 matrix since the category N_{FFF} can be neglected, the number of events with three misidentified leptons being more than 2 orders of magnitude smaller than the number of those with only one misidentified lepton. The value of f is small; therefore terms with order higher than two in f can be neglected. It has been verified that these simplifications do not change the final result.

The matrix is inverted to obtain the number of events with at least one misidentified lepton, which represents the amount of reducible background in the WZ sample, $N_{\mathrm{reducible}}$,

$$N_{\mathrm{reducible}} = N^{\mathrm{red}}_{\mathrm{TTL}}F_3 + N^{\mathrm{red}}_{\mathrm{TLT}}F_2 + N^{\mathrm{red}}_{\mathrm{LTT}}F_1 - N^{\mathrm{red}}_{\mathrm{TLL}}F_2F_3 - N^{\mathrm{red}}_{\mathrm{LTL}}F_1F_3 - N^{\mathrm{red}}_{\mathrm{LLT}}F_1F_2, \quad (2)$$

where $N^{\mathrm{red}}_{\alpha\beta\gamma} = N_{\alpha\beta\gamma} - N^{\mathrm{irr}}_{\alpha\beta\gamma}$, $F_i = \frac{f_i}{\bar{f}_i}$, and the index $i=1,2,3$ refers to the W lepton, the Z leading lepton, and the Z trailing lepton, respectively. The value of $N_{\alpha\beta\gamma}$ is obtained by counting the number of WZ events in the selected data sample with leptons satisfying the loose or tight criteria. The variable $N^{\mathrm{irr}}_{\alpha\beta\gamma}$ represents the number of events with

three prompt leptons in the corresponding identification category $\alpha\beta\gamma$ and is estimated using MC simulation. The values of F_i are measured differentially as a function of the lepton transverse momentum, using $W+j$ or $Z+j$ control samples taken from data for F_1 or for F_2 and F_3, respectively. The efficiencies $e(\bar{e})$ do not appear in Eq. (2) since they are included in the $N^{\mathrm{irr}}_{\alpha\beta\gamma}$ term.

The control samples and the reducible background in the WZ sample are composed of events with misidentified leptons from light- or heavy-flavor jets and from photon conversions. The data-driven estimates of the F_i factors correspond to an average value weighted by the abundance of each kind of background and may vary depending on the composition of the sample used to extract them. For this reason, data samples enriched in the different types of background have been used to verify that the background composition in the above-defined $W+j$ and $Z+j$ control samples is the same, within uncertainties, as in the signal region.

Other methods to assess the reducible background have been considered and provide results in good agreement with the matrix method estimation.

B. Background from ZZ processes

The ZZ background is estimated using MC simulation, as explained in Sec. V B. The number of expected ZZ events from POWHEG is scaled by 1.05 to account for NNLO QCD and NLO EW corrections [10,11,70]. In the VBS analysis, the scale factor used for SHERPA is taken to be 1.0 since SHERPA incorporates matrix element calculations up to three partons.

These estimations are validated by comparing the MC expectations with the event yield and several kinematic distributions of a data sample enriched in ZZ events. The ZZ control sample is selected by requiring a Z candidate meeting all the analysis selection criteria accompanied by two additional leptons of the same flavor and opposite charge, satisfying the lepton criteria described in Sec. VI A. The comparisons are performed in the above-defined control region and in a subregion where at least two jets are present in addition. In the first case, the data are compared with the predictions from POWHEG and GG2ZZ Monte Carlo simulations, while in the second case SHERPA and GG2ZZ Monte Carlo samples are used. Overall the agreement between the data and the expectations is within 1 standard deviation of the experimental uncertainty. The shapes of main kinematic variables are also found to be well described by the MC expectations.

VIII. DETECTOR-LEVEL RESULTS

Table II summarizes the numbers of expected and observed events together with the estimated background contributions in the inclusive analysis. Only statistical uncertainties are quoted. Systematic uncertainties affecting the predicted yields include the theoretical uncertainty on the cross sections as discussed in Sec. IV, and experimental uncertainties discussed in Sec. X. Figure 1 shows, at detector level, the momentum and the invariant mass of the Z candidate, the transverse mass of the W candidate and a transverse masslike variable of the WZ system, m_{T}^{WZ}, after applying all selection criteria. The variable m_{T}^{WZ} is reconstructed as

$$m_{\mathrm{T}}^{WZ}=\sqrt{\left(\sum_{\ell=1}^{3}p_{\mathrm{T}}^{\ell}+E_{\mathrm{T}}^{\mathrm{miss}}\right)^{2}-\left[\left(\sum_{\ell=1}^{3}p_{x}^{\ell}+E_{x}^{\mathrm{miss}}\right)^{2}+\left(\sum_{\ell=1}^{3}p_{y}^{\ell}+E_{y}^{\mathrm{miss}}\right)^{2}\right]}. \tag{3}$$

TABLE II. Numbers of observed and expected events after the $W^{\pm}Z$ inclusive selection described in Sec. VI B in each of the considered channels and for the sum of all channels. The expected number of $W^{\pm}Z$ events from POWHEG+PYTHIA and the estimated number of background events from other processes are detailed. The sum of background events containing misidentified leptons is labeled "Misid. leptons." Only statistical uncertainties are quoted.

Channel	eee	μee	$e\mu\mu$	$\mu\mu\mu$	All
Data	406	483	539	663	2091
Total expected	336.7 ± 2.2	410.8 ± 2.4	469.1 ± 2.1	608.2 ± 3.5	1824.8 ± 7.0
WZ	255.7 ± 1.1	337.2 ± 1.0	367.0 ± 1.1	495.9 ± 2.3	1455.7 ± 5.5
Misid. leptons	43.7 ± 1.9	32.2 ± 2.1	50.2 ± 1.7	52.8 ± 2.6	178.9 ± 4.2
ZZ	25.9 ± 0.2	26.7 ± 0.3	36.1 ± 0.3	39.5 ± 0.3	128.2 ± 0.6
$t\bar{t}+V$	5.5 ± 0.2	6.7 ± 0.2	7.2 ± 0.3	9.1 ± 0.3	28.5 ± 0.5
tZ	4.2 ± 0.1	5.5 ± 0.2	6.0 ± 0.2	7.7 ± 0.2	23.3 ± 0.3
DPS	1.2 ± 0.1	1.9 ± 0.1	1.8 ± 0.1	2.3 ± 0.2	7.2 ± 0.3
VVV	0.5 ± 0.0	0.7 ± 0.0	0.8 ± 0.0	0.9 ± 0.0	3.0 ± 0.1

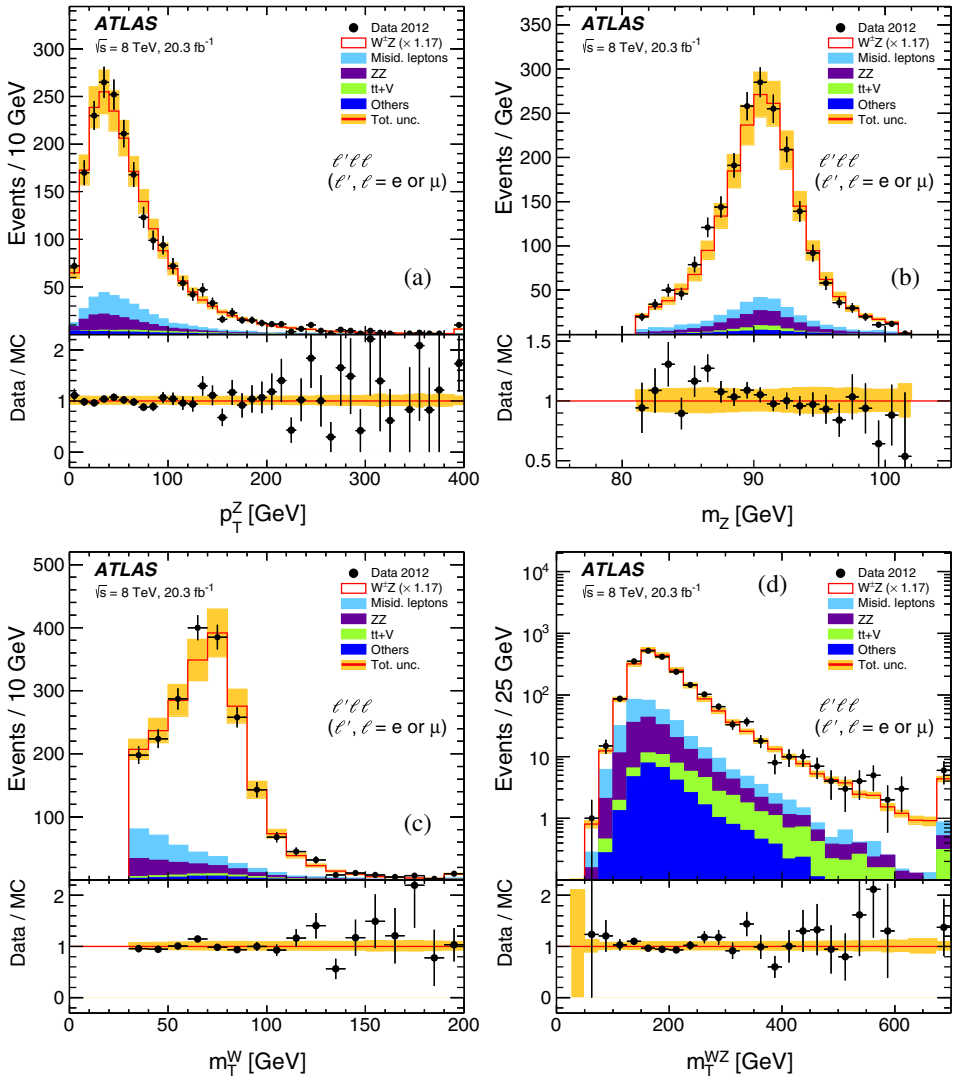

FIG. 1. Distributions, summed over all channels, of the following kinematic variables: (a) the transverse momentum of the reconstructed Z boson p_{T}^{Z}, (b) the mass of the Z m_Z, (c) the transverse mass of the reconstructed W boson m_{T}^{W}, and (d) the transverse-masslike variable for the WZ system m_{T}^{WZ}. The points correspond to the data and the histograms to the expectations of the different SM processes. All Monte Carlo expectations are scaled to the integrated luminosity of the data using the predicted MC cross sections of each sample. The sum of background events containing misidentified leptons is labeled "Misid. leptons." The POWHEG+PYTHIA MC prediction is used for the $W^{\pm}Z$ signal contribution. It is scaled by a global factor of 1.17 to match the measured inclusive $W^{\pm}Z$ cross section. The open red histogram shows the total prediction and the shaded orange band its estimated total uncertainty. The last bin contains the overflow.

The expectations based on MC simulation are scaled to the integrated luminosity of the data using the predicted cross sections of each sample. The POWHEG +PYTHIA MC prediction is used for the $W^{\pm}Z$ signal contribution. In Fig. 1 it is scaled by a global factor of 1.17 to match the measured inclusive $W^{\pm}Z$ cross section of Sec. XI A. This scaling is only used for an illustrative purpose in this figure and does not affect the measurements. Table III shows the number of expected and observed events together with the estimated background contributions for the VBS and aQGC analyses, respectively. Figure 1 indicates that the MC predictions provide a fair description of the shapes of the data distributions.

IX. CORRECTIONS FOR DETECTOR EFFECTS AND ACCEPTANCE

For a given channel $W^{\pm}Z \to \ell'^{\pm}\nu\ell^{+}\ell^{-}$, where ℓ and ℓ' are either an electron or a muon, the integrated fiducial cross section that includes the leptonic branching fractions of the W and Z is calculated as

TABLE III. Numbers of observed and expected events for the sum of all channels after the $W^{\pm}Z$ VBS and aQGC selections described in Sec. VI B. The expected number of $WZjj$-EW events from SHERPA and the estimated number of background events from other processes are detailed. The sum of background events containing misidentified leptons is labeled "Misid. leptons." Only statistical uncertainties are quoted.

Selection	VBS	aQGC
Data	45	9
Total expected	37.2 ± 1.1	4.9 ± 0.3
$WZjj$-EW	7.4 ± 0.2	1.1 ± 0.1
$WZjj$-QCD	20.8 ± 0.8	2.8 ± 0.3
tZ	3.0 ± 0.1	0.3 ± 0.0
Misid. leptons	2.5 ± 0.6	0.1 ± 0.1
ZZ	1.9 ± 0.3	0.2 ± 0.1
$t\bar{t} + V$	1.6 ± 0.1	0.3 ± 0.0

$$\sigma^{\text{fid}}_{W^{\pm}Z\to\ell'\nu\ell\ell} = \frac{N_{\text{data}} - N_{\text{bkg}}}{\mathcal{L}\cdot C_{WZ}} \times \left(1 - \frac{N_{\tau}}{N_{\text{all}}}\right), \tag{4}$$

where N_{data} and N_{bkg} are the number of observed events and the estimated number of background events, respectively, $\mathcal{L}$ is the integrated luminosity, and C_{WZ}, obtained from simulation, is the ratio of the number of selected signal events at detector level to the number of events at particle level in the fiducial phase space. This factor corrects for detector efficiencies and for QED final-state radiation effects. The contribution from τ lepton decays, amounting approximately to 4%, is removed from the cross-section definition by introducing the term in parentheses. This term is computed using simulation, where N_{τ} is the number of selected events in which at least one of the bosons decays into a τ lepton and N_{all} is the number of selected WZ events with decays into any lepton.

The C_{WZ} factors for $W^{-}Z$, $W^{+}Z$, and $W^{\pm}Z$ inclusive processes computed with POWHEG+PYTHIA for each of the four leptonic channels are shown in Table IV.

The total cross section is calculated as

$$\sigma^{\text{tot}}_{W^{\pm}Z} = \frac{\sigma^{\text{fid}}_{W^{\pm}Z\to\ell'\nu\ell\ell}}{\mathcal{B}_W \mathcal{B}_Z A_{WZ}}, \tag{5}$$

TABLE IV. The C_{WZ} factors for each of the eee, μee, $e\mu\mu$, and $\mu\mu\mu$ inclusive channels. The POWHEG+PYTHIA MC event sample with the "resonant shape" lepton assignment algorithm at particle level is used. Only statistical uncertainties are reported.

Channel	C_{W^-Z}	C_{W^+Z}	$C_{W^{\pm}Z}$
eee	0.412 ± 0.002	0.399 ± 0.002	0.404 ± 0.001
μee	0.532 ± 0.002	0.540 ± 0.002	0.537 ± 0.001
$e\mu\mu$	0.596 ± 0.002	0.572 ± 0.002	0.581 ± 0.001
$\mu\mu\mu$	0.786 ± 0.002	0.789 ± 0.002	0.788 ± 0.002

where $\mathcal{B}_W = 10.86 \pm 0.09\%$ and $\mathcal{B}_Z = 3.3658 \pm 0.0023\%$ are the W and Z leptonic branching fractions [16], respectively, and A_{WZ} is the acceptance factor calculated at particle level as the ratio of the number of events in the fiducial phase space to the number of events in the total phase space as defined in Sec. III.

A single acceptance factor of $A_{WZ} = 0.395 \pm 0.001(\text{stat})$, obtained by averaging the acceptance factors computed in the μee and $e\mu\mu$ channels, is used since it has been verified that interference effects related to the presence of identical leptons in the final state, as in the eee and $\mu\mu\mu$ channels, are below 1%. The use of the μee and $e\mu\mu$ channels for the computation of A_{WZ} avoids the ambiguity arising from the assignment at the particle level of final-state leptons to the W and Z bosons.

The differential detector-level distributions are corrected for detector resolution and for QED FSR effects using an iterative Bayesian unfolding method [71], as implemented in the ROOUNFOLD toolkit [72]. Three iterations were consistently used for the unfolding of each variable. The width of the bins in each distribution was chosen according to the experimental resolution and to the statistical significance of the expected number of events in each bin. For the data distributions used to extract the limits on anomalous gauge couplings, a dedicated bin optimization was performed using signal MC events, in order to reach the best sensitivity for the fitted parameters. The fraction of signal MC events reconstructed in each bin is always greater than 50% and around 60% on average.

Simulated signal events are used to obtain for each distribution a response matrix that accounts for bin-to-bin migration effects between the reconstructed-level and particle-level distributions. In the inclusive measurements, the POWHEG+PYTHIA signal sample is used since it provides a fair description of the data distributions. For the jet multiplicity differential measurement and in the VBS analysis, the SHERPA signal sample is used for the computation of the response matrix since this sample includes up to three partons in the matrix element calculation and therefore better describes the jet multiplicity of data. To build the response matrix for the unfolding of the jet multiplicity, the p_{T} threshold of the particle level jets, as defined in Sec. III, is set to 25 GeV. This threshold is similar to the one used in the recent measurement of the WW cross section by the ATLAS Collaboration [73]. A jet p_{T} threshold of 30 GeV, corresponding to the definition of the VBS phase space, is, however, used for the unfolding of the invariant mass spectrum of the two leading jets.

X. SYSTEMATIC UNCERTAINTIES

The systematic uncertainties on the integrated and differential cross sections are due to uncertainties of experimental and theoretical nature on the acceptance, on the correction procedure for detector effects, on the background estimation, and on the luminosity.

The systematic uncertainties on the A_{WZ} and C_{WZ} factors due to the theoretical modeling in the event generators are evaluated taking into account the uncertainties related to the choice of the PDF, of the QCD renormalization and factorization scales, and of the parton showering simulation. Uncertainties due to the choice of PDF are computed using the CT10 eigenvectors and the envelope of the differences among CT10, MSTW 2008, NNPDF 3.0, and ATLAS-epWZ12 PDF sets. QCD scale uncertainties are estimated by varying μ_R and μ_F by factors of 2 around the nominal scale $m_{WZ}/2$ with the constraint $0.5 \leq \mu_R/\mu_F \leq 2$. Uncertainties due to the choice of the parton showering model are estimated by interfacing POWHEG with either PYTHIA or HERWIG and comparing the results. These uncertainties of theoretical nature have no significant effect on the C_{WZ} factors but affect the A_{WZ} acceptance factor, where the dominant contribution originates from the PDF choice and is below 1.3%.

The uncertainty on the differential distributions arising from the theoretical modeling in the event generators and being propagated to the response matrix in the unfolding procedure is estimated by reweighting simulated events at particle level to the unfolded results obtained as described in Sec. IX. An alternative response matrix is defined using these reweighted MC events and is used to unfold POWHEG +PYTHIA reconstructed MC events. A systematic uncertainty is estimated by comparing this unfolded distribution to the original particle-level POWHEG+PYTHIA prediction.

The experimental systematic uncertainty on the C_{WZ} factors and on the response matrix includes uncertainties on the electron energy or muon momentum scale and resolution, on the E_T^{miss} scale and resolution, on the jet energy scale and resolution, as well as uncertainties on the scale factors applied to the simulation in order to reproduce the trigger, reconstruction, identification, and isolation efficiencies measured in data. The uncertainty associated with the pileup reweighting procedure is negligible. For the measurements of the W charge-dependent cross sections, an uncertainty arising from the charge misidentification of leptons is also considered. It affects only electrons and leads to uncertainties of ~0.1% on the integrated cross section combining all decay channels. The systematic uncertainties on the measured cross section are determined by repeating the analysis after applying appropriate variations for each source of systematic uncertainty to the simulated samples.

The lepton energy or momentum scale corrections are obtained from a comparison of the Z boson invariant mass distribution in data and simulations, while the uncertainties on the efficiency scale factors are derived from a comparison of tag-and-probe results in data and simulations [40–42]. Uncertainties on the jet energy scale are determined from a combination of methods based on simulation and *in situ* techniques [62,63]. The uncertainty on the jet energy resolution is derived from a comparison of the resolutions obtained in data and in simulated dijet events [64]. The uncertainty on the E_T^{miss} is estimated by propagating the uncertainties on the objects and by applying energy scale and resolution uncertainties to the calorimeter energy clusters that are not associated with a jet or an electron. The dominant contribution among the experimental systematic uncertainties in the eee and μee channels derives from the electron identification efficiency, being at most 2.9%, while in the $e\mu\mu$ and $\mu\mu\mu$ channels it originates from the muon reconstruction efficiency and is at most 2.1%.

The uncertainty on the amount of background from misidentified leptons is estimated taking into account the statistical uncertainties on the event yields in each identification category and on the F_i factors (see Sec. VII A). Uncertainties arising from the definition of the $W + j$ and $Z + j$ control samples and from their composition are also included. The former are evaluated by changing the control sample selection criteria and the latter by using a different way of computing the fake rate, which relies on a matrix method where the matrix is obtained using particle-level information.

An uncertainty of 7% on the amount of ZZ background is evaluated as the difference between the predicted and measured numbers of ZZ events in the defined control regions. The uncertainty arising from other kinds of irreducible backgrounds is evaluated by propagating the uncertainty on their MC cross section which are estimated to be 30%, 15%, and 50% for $t\bar{t} + V$, tZ, and DPS processes, respectively.

TABLE V. Summary of the relative uncertainties on the measured fiducial cross section $\sigma^{fid}_{W^{\pm}Z}$ for each channel and for their combination. Uncertainties are given in percent. The decomposition of the total systematic uncertainty into the main sources correlated between channels and a source uncorrelated between channels is indicated in the first rows.

	eee	μee	$e\mu\mu$	$\mu\mu\mu$	Combined
Source	Relative uncertainties [%]				
e energy scale	0.8	0.4	0.4	0.0	0.3
e id. efficiency	2.9	1.8	1.0	0.0	1.0
μ momentum scale	0.0	0.1	0.1	0.1	0.1
μ id. efficiency	0.0	0.7	1.3	2.0	1.4
E_T^{miss} and jets	0.3	0.2	0.2	0.1	0.3
Trigger	0.1	0.1	0.2	0.3	0.2
Pileup	0.3	0.2	0.2	0.1	0.2
Misid. leptons background	2.9	0.9	3.1	0.9	1.3
ZZ background	0.6	0.5	0.6	0.5	0.5
Other backgrounds	0.7	0.7	0.7	0.7	0.7
Uncorrelated	0.7	0.6	0.5	0.5	0.3
Total systematics	4.5	2.6	3.7	2.5	2.4
Luminosity	2.2	2.2	2.2	2.2	2.2
Statistics	6.2	5.4	5.3	4.7	2.7
Total	8.0	6.3	6.8	5.7	4.2

The uncertainty on the unfolding procedure arising from the limited number of events in the simulation is estimated using pseudoexperiments.

The uncertainty on the integrated luminosity [74] is applied to the signal normalization as well as to all background contributions that are estimated using MC simulations. It results in an effect of 2.2% on the measured cross sections.

The overall uncertainty on the single-channel $W^{\pm}Z$ fiducial cross section varies from approximately 6% to 8%. Table V shows the statistical and main systematic uncertainties on the $W^{\pm}Z$ fiducial cross section for each of the four channels and for their combination.

XI. CROSS-SECTION MEASUREMENTS

A. Integrated cross sections

The measured fiducial cross sections in the four channels are combined using the measured total event yields and statistical procedure based on the minimization of a negative log-likelihood function that accounts for correlations between the sources of systematic uncertainty affecting each channel [75]. The systematic uncertainties are included in the likelihood function as nuisance parameters. The combination of the $W^{\pm}Z$ cross sections in the fiducial phase space yields a p-value of 48%, and the combinations of $W^{+}Z$ and $W^{-}Z$ cross sections yield p-values of 15% and 26%, respectively.

The $W^{\pm}Z$ production cross section in the detector fiducial region resulting from the combination of the four channels including the W and Z branching ratio in a single leptonic channel with muons or electrons is

$$\sigma^{\mathrm{fid}}_{W^{\pm}Z\to\ell'\nu\ell\ell} = 35.1 \pm 0.9(\mathrm{stat}) \pm 0.8(\mathrm{sys}) \pm 0.8(\mathrm{lumi})\ \mathrm{fb}, \tag{6}$$

where the uncertainties correspond to statistical, systematic, and luminosity uncertainties, respectively. The measurement is to be compared to the SM expectation of 30.0 ± 2.1 fb from POWHEG+PYTHIA, as discussed in Sec. IV. The measured $W^{\pm}Z$ production cross sections are compared to the SM NLO prediction from POWHEG +PYTHIA in Fig. 2 and all results for $W^{\pm}Z$, $W^{+}Z$, and $W^{-}Z$ final states are reported in Table VI.

The measured cross section is larger than the quoted SM prediction. However, the SM prediction, which is at NLO accuracy in perturbative QCD, is highly sensitive to the choice of renormalization scale μ_{R}. In addition, new perturbative effects appearing at NNLO could enhance the SM prediction compared to the NLO calculation. Indeed, for the other diboson final states ZZ, WW, $Z\gamma$,

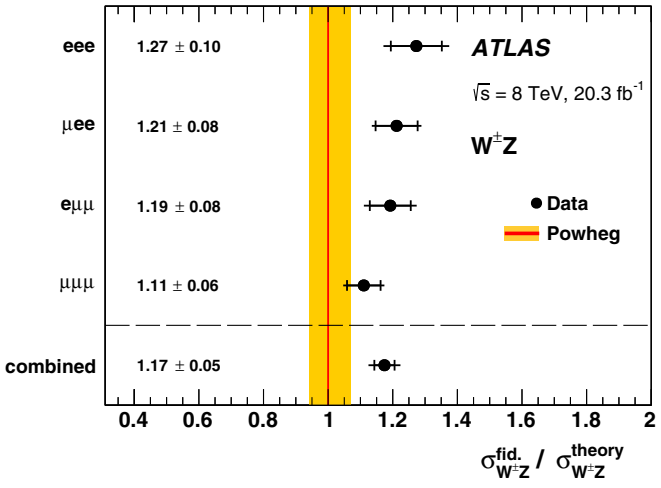

FIG. 2. Ratio of the measured $W^{\pm}Z$ integrated cross sections in the fiducial phase space to the NLO SM prediction from POWHEG +PYTHIA using the CT10 PDF set and renormalization and factorization scales $\mu_R = \mu_F = m_{WZ}/2$, in each of the four channels and for their combination. The inner and outer error bars on the data points represent the statistical and total uncertainties, respectively. The shaded orange band represents the uncertainty associated with the SM prediction.

TABLE VI. Fiducial integrated cross section in fb, for $W^{\pm}Z$, $W^{+}Z$, and $W^{-}Z$ production, measured in each of the eee, μee, $e\mu\mu$, and $\mu\mu\mu$ channels and all four channels combined. The statistical (δ_{stat}), total systematic (δ_{sys}), luminosity (δ_{lumi}), and total (δ_{tot}) uncertainties are given in percent.

Channel	σ^{fid} [fb]	δ_{stat} [%]	δ_{sys} [%]	δ_{lumi} [%]	δ_{tot} [%]
	$\sigma^{\mathrm{fid}}_{W^{\pm}Z\to\ell'\nu\ell\ell}$				
$e^{\pm}ee$	38.1	6.2	4.5	2.2	8.0
$\mu^{\pm}ee$	36.3	5.4	2.6	2.2	6.3
$e^{\pm}\mu\mu$	35.7	5.3	3.7	2.2	6.8
$\mu^{\pm}\mu\mu$	33.3	4.7	2.5	2.2	5.7
Combined	35.1	2.7	2.4	2.2	4.2
SM expectation	30.0	···	···	···	7.0
	$\sigma^{\mathrm{fid}}_{W^{+}Z\to\ell'\nu\ell\ell}$				
$e^{+}ee$	22.6	8.0	4.4	2.2	9.4
$\mu^{+}ee$	23.9	6.5	2.5	2.2	7.3
$e^{+}\mu\mu$	19.9	7.2	3.5	2.2	8.3
$\mu^{+}\mu\mu$	19.8	6.0	2.5	2.2	6.8
Combined	21.2	3.4	2.3	2.2	4.6
SM expectation	18.8	···	···	···	6.8
	$\sigma^{\mathrm{fid}}_{W^{-}Z\to\ell'\nu\ell\ell}$				
$e^{-}ee$	15.4	9.8	5.0	2.3	11.2
$\mu^{-}ee$	12.4	9.5	3.1	2.3	10.3
$e^{-}\mu\mu$	15.7	8.0	4.2	2.3	9.2
$\mu^{-}\mu\mu$	13.4	7.5	2.8	2.3	8.3
Combined	14.0	4.3	2.8	2.3	5.6
SM expectation	11.1	···	···	···	8.9

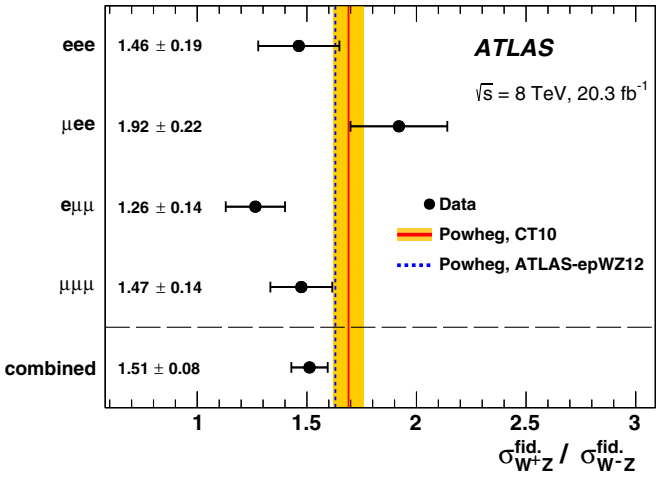

FIG. 3. Measured ratios $\sigma^{\mathrm{fid}}_{W^+Z}/\sigma^{\mathrm{fid}}_{W^-Z}$ of W^+Z and W^-Z integrated cross sections in the fiducial phase space in each of the four channels and for their combination. The error bars on the data points represent the total uncertainties, dominated by statistical uncertainties. The NLO SM prediction from POWHEG+PYTHIA using the CT10 PDF set and renormalization and factorization scales $\mu_R = \mu_F = m_{WZ}/2$ is represented by the red line and the shaded orange band for the associated uncertainty. The POWHEG+PYTHIA prediction using the ATLAS-epWZ12 PDF set is also displayed as the dashed line.

and $W\gamma$ NNLO calculations have recently become available [70,76–78], and in all cases the NNLO corrections were found to be positive and larger than the uncertainty on the NLO calculation estimated by the conventional independent up and down variations of μ_{R} and μ_{F} by a factor of 2.

The ratio of W^+Z to W^-Z production cross sections is also measured in the fiducial phase space and yields

$$\frac{\sigma^{\mathrm{fid}}_{W^+Z\to\ell'\nu\ell\ell}}{\sigma^{\mathrm{fid}}_{W^-Z\to\ell'\nu\ell\ell}} = 1.51 \pm 0.08(\mathrm{stat}) \pm 0.01(\mathrm{sys}) \pm 0.01(\mathrm{lumi}).$$

Most of the systematic uncertainties cancel in the ratio, and the measurement is dominated by the statistical uncertainty. The measured cross-section ratios, for each channel and for their combination, are compared in Fig. 3 to the SM expectation of 1.69 ± 0.07, calculated with POWHEG +PYTHIA and the CT10 PDF set. The use of the ATLAS-epWZ12 PDF set instead of CT10 changes the SM prediction to 1.63, indicating the sensitivity of the ratio $\sigma^{\mathrm{fid}}_{W^+Z}/\sigma^{\mathrm{fid}}_{W^-Z}$ to the PDFs. The total uncertainty of the present measurement is of the same order of magnitude as the estimated uncertainties in the PDF and the SM prediction.

Finally, the combined fiducial cross section is extrapolated to a total phase space, defined by requiring that the invariant mass of the lepton pairs associated with the Z boson decay be in the range $66 < m_Z < 116$ GeV. The result is

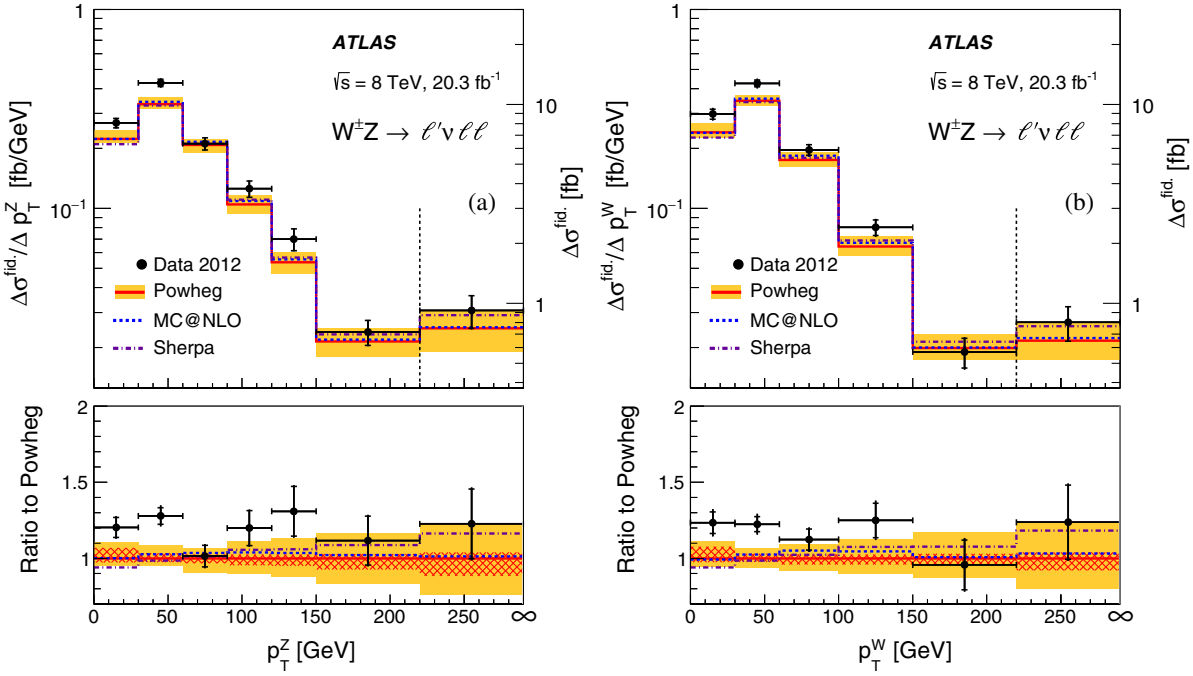

FIG. 4. The measured $W^{\pm}Z$ differential cross section in the fiducial phase space as a function of (a) p^Z_{T} and (b) p^W_{T}. The inner and outer error bars on the data points represent the statistical and total uncertainties, respectively. The measurements are compared to the prediction from POWHEG+PYTHIA (red line, see text for details). The orange band represents its total theoretical uncertainty and the hatched red area the part of the theoretical uncertainty arising from the PDF and parton shower uncertainties. The predictions from the MC@NLO and SHERPA MC generators are also indicated by dashed and dot-dashed lines, respectively. The SHERPA prediction is rescaled to the integrated cross section predicted by POWHEG+PYTHIA. The right y axis refers to the last cross-section point, separated from the others by a vertical dashed line, as this last bin is integrated up to the maximum value reached in the phase space.

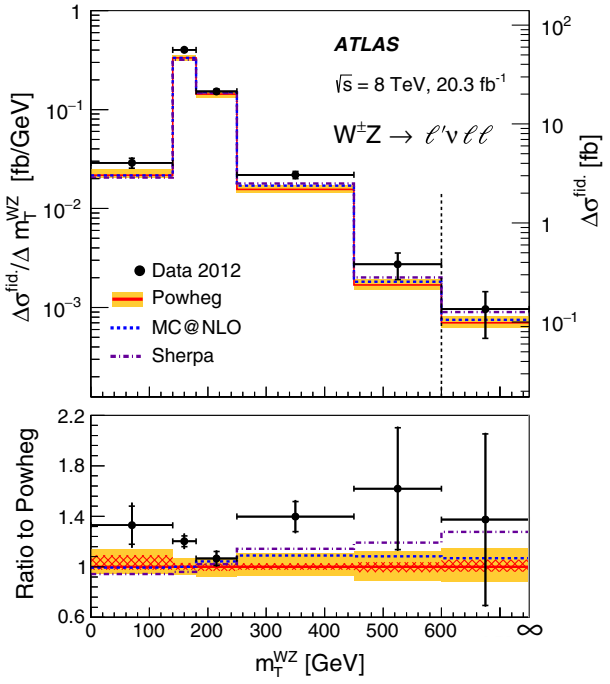

FIG. 5. The measured $W^{\pm}Z$ differential cross section in the fiducial phase space as a function of m_{T}^{WZ}. The inner and outer error bars on the data points represent the statistical and total uncertainties, respectively. The measurements are compared to the prediction from POWHEG+PYTHIA (red line, see text for details). The orange band represents its total theoretical uncertainty and the hatched red area the part of the theoretical uncertainty arising from the PDF and shower uncertainties. The predictions from the MC@NLO and SHERPA MC generators are also indicated by dashed and dot-dashed lines, respectively. The SHERPA prediction is rescaled to the integrated cross section predicted by POWHEG+PYTHIA. The right y axis refers to the last cross-section point, separated from the others by a vertical dashed line, as this last bin is integrated up to the maximum value reached in the phase space.

$$\sigma^{\mathrm{tot}}_{W^{\pm}Z} = 24.3 \pm 0.6(\mathrm{stat}) \pm 0.6(\mathrm{sys}) \pm 0.4(\mathrm{th}) \pm 0.5(\mathrm{lumi})\ \mathrm{pb},$$

where besides the statistical and systematic uncertainties a theory uncertainty (th) has been included from the propagation of the theoretical uncertainty on A_{WZ} to the total cross section. The measurement is to be compared to the SM expectation calculated with POWHEG+PYTHIA of 21.0 ± 1.6 pb.

B. Differential cross sections

For the measurements of the differential distributions, all four decay channels, eee, $e\mu\mu$, μee, and $\mu\mu\mu$, are added together. The resulting distributions are unfolded with a response matrix computed using a POWHEG+PYTHIA MC signal sample that includes all four topologies and divided by four such that cross sections refer to final states where the W and Z decay in a single leptonic channel with muons or electrons.

The $W^{\pm}Z$ production cross section is measured as a function of the transverse momentum of the Z and W boson, p_{T}^{Z} and p_{T}^{W} (Fig. 4), as a function of the transverse mass of the $W^{\pm}Z$ system m_{T}^{WZ} (Fig. 5), as a function of the p_{T} of the neutrino associated with the decay of the W boson, p_{T}^{ν}, and as a function of the absolute difference between the rapidities of the Z boson and the lepton from the decay of the W boson, $|y_Z - y_{\ell,W}|$ (Fig. 6).

The differential cross sections as a function of the transverse momenta of the neutrino or of the lepton from the W decay are interesting because of their sensitivity to the polarization of the W boson. Experimentally, given the fiducial phase space of the measurement, the p_{T}^{ν} observable has the advantage of probing lower transverse momenta than the transverse momentum of the lepton from the W boson decay, $p_{\mathrm{T}}^{\ell,W}$, which is restricted to values above 20 GeV. Therefore, despite the worse experimental resolution for the reconstruction of p_{T}^{ν} compared to $p_{\mathrm{T}}^{\ell,W}$, p_{T}^{ν} could be more sensitive to polarization effects.

In order to derive the p_{T}^{ν} from data events, the assumption is made that the whole $E_{\mathrm{T}}^{\mathrm{miss}}$ of events arises from the neutrino of the W boson decay. Using MC samples, this assumption was verified to be valid for SM WZ events. The observed $E_{\mathrm{T}}^{\mathrm{miss}}$ distribution is therefore unfolded to p_{T}^{ν} using WZ MC events.

Previously, no observable related to decay angles of final-state particles had been measured for WZ events. The rapidity correlations between the W and Z decay products have been found to be useful tools in searching for the approximately zero WZ helicity amplitudes expected at LO in the SM or for aTGC [7,8]. These rapidity correlations are also sensitive to QCD corrections, PDF effects, and polarization effects of the W and Z bosons. The rapidity difference between the W and Z bosons, $|y_Z - y_W|$, is a boost-invariant substitute for the center-of-mass scattering angle θ of the W with respect to the direction of the incoming quark. Since the rapidity of the W boson cannot be uniquely reconstructed due to the presence of the neutrino, the rapidity of the lepton from the W boson decay is used. Therefore the rapidity difference $|y_Z - y_{\ell,W}|$ is measured instead of $|y_Z - y_W|$.

The W^+Z/W^-Z ratio of the production cross sections is also measured as a function of p_{T}^{Z}, p_{T}^{W}, m_{T}^{WZ}, p_{T}^{ν}, and $|y_Z - y_{\ell,W}|$ and presented in Figs. 7, 8, and 9.

The measured differential cross sections are compared to the predictions from the POWHEG+PYTHIA MC generator, which uses the CT10 PDF set and dynamic QCD scales of $\mu_{\mathrm{F}} = \mu_{\mathrm{R}} = m_{WZ}/2$. The theoretical uncertainties on the differential predictions from POWHEG+PYTHIA arise from the choice of PDF set and QCD scales and are evaluated as explained in Sec. IV. The total uncertainty on the theoretical predictions is estimated as the linear sum of the PDF, parton shower, QCD scale, and EW correction uncertainties, following the recommendations of Ref. [27]. The measured

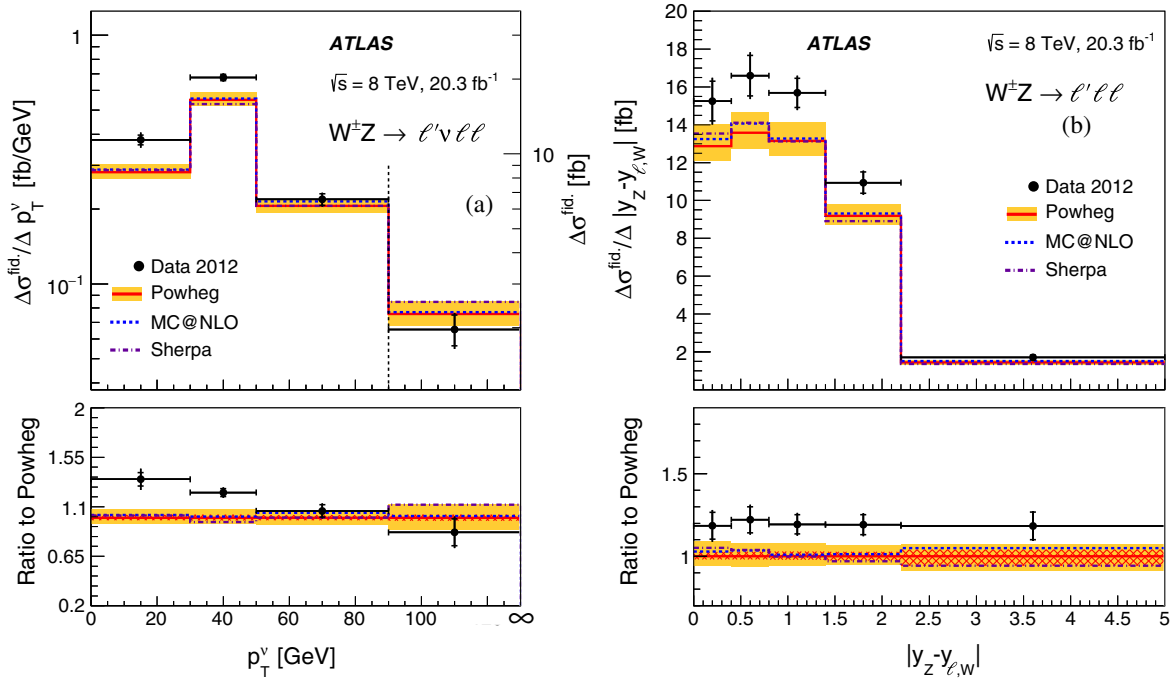

FIG. 6. The measured $W^{\pm}Z$ differential cross section in the fiducial phase space as a function of (a) p_{T}^{ν} and (b) $|y_Z - y_{\ell,W}|$. The inner and outer error bars on the data points represent the statistical and total uncertainties, respectively. The measurements are compared to the prediction from POWHEG+PYTHIA (red line, see text for details). The orange band represents its total theoretical uncertainty and the hatched red area the part of the theoretical uncertainty arising from the PDF and shower uncertainties. The predictions from the MC@NLO and SHERPA MC generators are also indicated by dashed and dot-dashed lines, respectively. The SHERPA prediction is rescaled to the integrated cross section predicted by POWHEG+PYTHIA. The right y axis in (a) refers to the last cross-section point, separated from the others by a vertical dashed line, as this last bin is integrated up to the maximum value reached in the phase space.

cross-section distributions are also compared to predictions from the MC@NLO and SHERPA MC event generators.

Fair agreement of the shapes of measured distributions of inclusive cross sections and W^+Z/W^-Z cross section ratios with the different MC predictions is observed. However, the precision of SM predictions of $W^{\pm}Z$ production is limited to NLO and LO accuracy for perturbative QCD and EW effects, respectively. New effects of higher perturbative orders could therefore potentially affect the present SM predictions, beyond the presently estimated theoretical

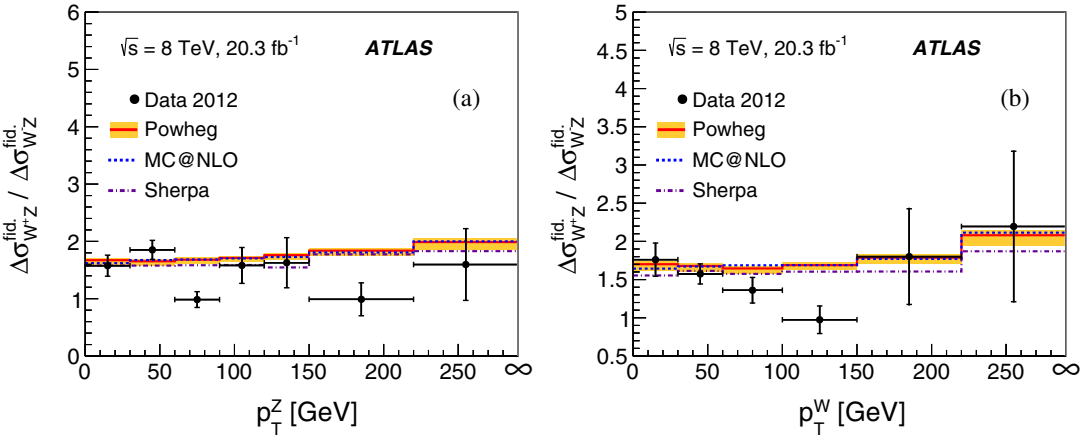

FIG. 7. The ratio of the W^+Z and W^-Z differential cross sections in the fiducial phase space as a function of (a) p_{T}^{Z} and (b) p_{T}^{W}. The inner and outer error bars on the data points represent the statistical and total uncertainties, respectively. The measurements are compared to the prediction from POWHEG+PYTHIA (red line; see text for details). The orange band represents its total theoretical uncertainty, which is dominated by the PDF uncertainty. The predictions from the MC@NLO and SHERPA MC generators are also indicated by dashed and dot-dashed lines, respectively.

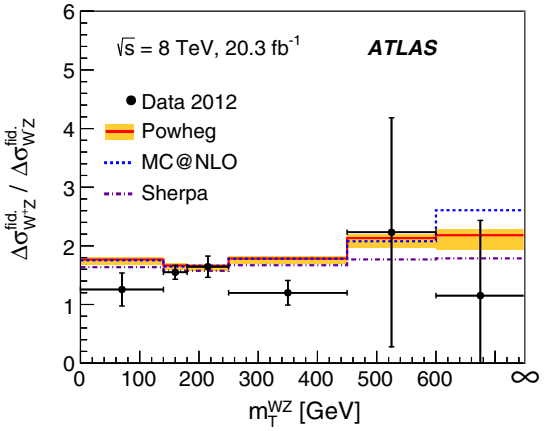

FIG. 8. The ratio of the W^+Z and W^-Z differential cross sections in the fiducial phase space as a function of m_T^{WZ}. The inner and outer error bars on the data points represent the statistical and total uncertainties, respectively. The measurements are compared to the prediction from POWHEG+PYTHIA (red line, see text for details). The orange band represents its total theoretical uncertainty, which is dominated by the PDF uncertainty. The predictions from the MC@NLO and SHERPA MC generators are also indicated by dashed and dot-dashed lines, respectively.

uncertainties. From the p_T^ν differential cross section in Fig. 6(a) we observe that the global excess of the measured integrated cross section compared to the POWHEG+PYTHIA prediction seems to be related to the region with $p_T^\nu < 50$ GeV, this difference being more pronounced for $p_T^\nu < 30$ GeV for W^-Z events as seen in the first bin of Fig. 9(a).

The exclusive multiplicity of jets unfolded at particle level is presented in Fig. 10. This distribution uses the same jet definition as for the VBS analysis (see Sec. VI A) but with a lower jet p_T threshold of 25 GeV at detector and at particle level. The measurement is compared with predictions from SHERPA and POWHEG+PYTHIA. The SHERPA prediction provides a good description of the measured jet multiplicity while this is not the case for POWHEG +PYTHIA and MC@NLO. Moreover, the ratio of 0-jet to 1-jet event cross sections predicted by POWHEG+PYTHIA is lower than predicted by SHERPA and than measured in data. Finally, the measured $W^\pm Z$ differential cross section as a function of the invariant mass, m_{jj}, of the two leading jets with $p_T > 30$ GeV is presented in Fig. 11. The measurement is better described by the SHERPA prediction, which includes the sum of $WZjj$-QCD and $WZjj$-EW contributions. The contribution of $WZjj$-EW events, which is increasing at higher m_{jj} is exemplified in the figure.

C. Limits on vector boson scattering production

This part of the analysis aims to study $WZjj$-EW production, which includes VBS and tZj processes. The latter process results from a t-channel exchange of a W boson between a b and a u quark giving a final state with a t quark, a Z boson, and a light quark jet, but does not exhibit diagrams with gauge boson couplings. Its contribution in the SHERPA $WZjj$-EW sample is disentangled from the VBS part, considered in this paper as the signal, with a splitting procedure relying on the presence of b quarks at generator level. Interference effects between the signal and the tZj process are expected to be negligible. Since the b-tagged sample, enriched in tZj events, still contains a small fraction (∼5%) of signal events from the scattering of the initial-state b quark, two results with or without subtraction of the tZj contribution, are provided.

Given a too-low expected statistical significance for a cross-section measurement, the experimental result is

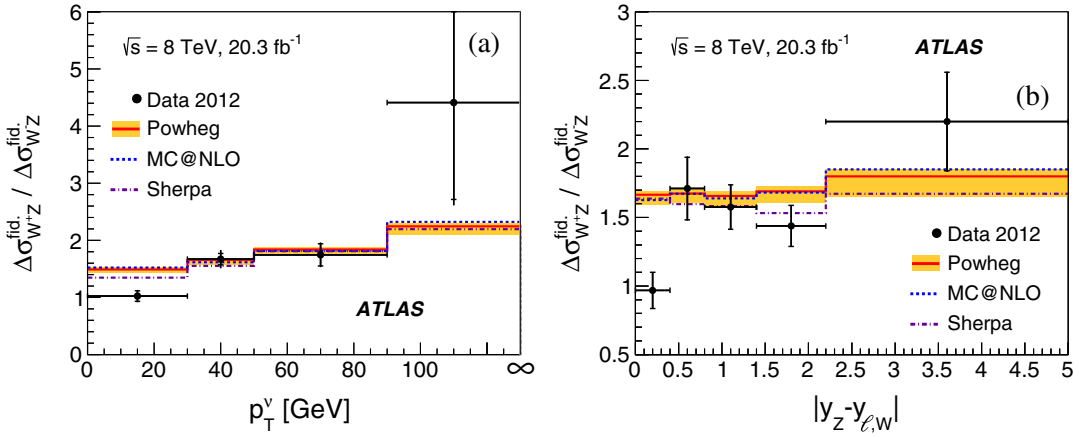

FIG. 9. The ratio of the W^+Z and W^-Z differential cross sections in the fiducial phase space as a function of (a) p_T^ν and (b) $|y_Z - y_{\ell,W}|$. The inner and outer error bars on the data points represent the statistical and total uncertainties, respectively. The measurements are compared to the prediction from POWHEG+PYTHIA (red line; see text for details). The orange band represents its total theoretical uncertainty, which is dominated by the PDF uncertainty. The predictions from the MC@NLO and SHERPA MC generators are also indicated by dashed and dot-dashed lines, respectively.

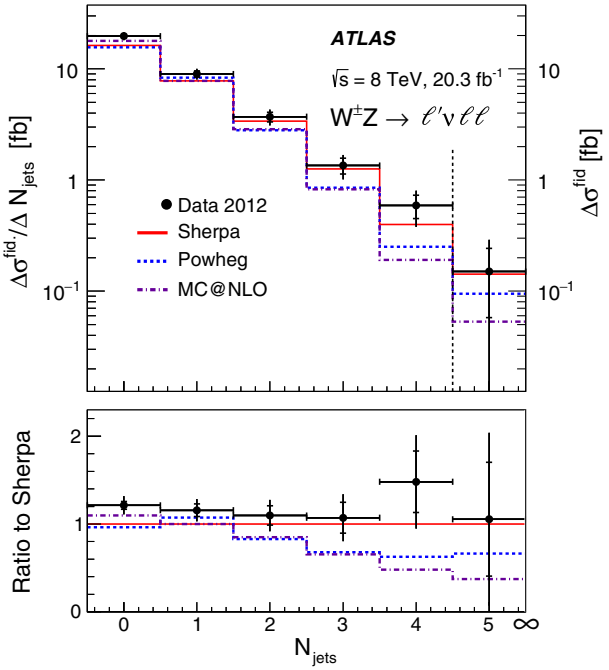

FIG. 10. The measured $W^{\pm}Z$ differential cross section in the fiducial phase space as a function of the exclusive jet multiplicity of jets with $p_{\mathrm{T}} > 25$ GeV. The inner and outer error bars on the data points represent the statistical and total uncertainties, respectively. The measurements are compared to the prediction from SHERPA (red line), POWHEG+PYTHIA (dashed blue line), and MC@NLO (dot-dashed violet line). The SHERPA prediction is rescaled to the integrated cross section predicted by POWHEG +PYTHIA. The right y axis refers to the last cross section point, separated from the others by a vertical dashed line, as this last bin is integrated up to the maximum value reached in the phase space.

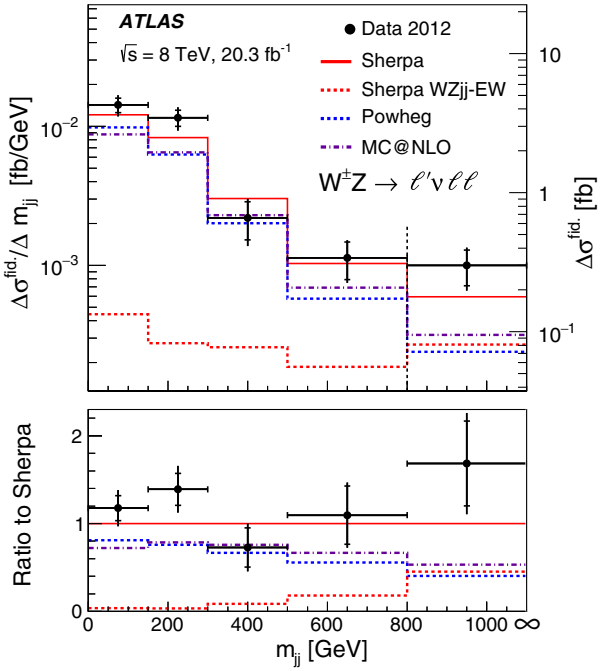

FIG. 11. The measured $W^{\pm}Z$ differential cross section as a function of the invariant mass of the two leading jets with $p_{\mathrm{T}} > 30$ GeV. The inner and outer error bars on the data points represent the statistical and total uncertainties, respectively. The measurements are compared to the prediction from SHERPA (red line), which includes both the $WZjj$-QCD and $WZjj$-EW processes, POWHEG+PYTHIA (dashed blue line) and MC@NLO (dot-dashed violet line). The part of the SHERPA prediction corresponding to $WZjj$-EW events is also represented by a dashed red line. In the bottom panel the dashed red line therefore corresponds to the $WZjj$-EW fraction of the total SHERPA prediction. The right y axis refers to the last cross section point, separated from the others by a vertical dashed line, as this last bin is integrated up to the maximum value reached in the phase space.

reported as an upper limit at 95% C.L. on the fiducial cross section multiplied by the W and Z branching ratios in a single leptonic channel with muons or electrons. Observed and expected upper limits are calculated using the numbers of observed and expected events, the estimated number of background events (see Table III), the luminosity of the data sample, and the detector and reconstruction efficiencies of ~67%, and are presented in Table VII. Similar upper limits on the $\sigma^{\mathrm{fid}}_{W^{\pm}Zjj\text{-EW}\to\ell'\nu\ell\ell}$ production cross section are measured in the aQGC phase space and shown in Table VII. The measured upper cross-section limits are within 1σ and 2σ uncertainty on the expected limit for the VBS and aQGC phase-space measurements, respectively. In the VBS phase space, the number of observed data events corresponds to a cross section for $WZjj$-EW production of $0.29^{+0.14}_{-0.12}(\mathrm{stat})\,^{+0.09}_{-0.1}(\mathrm{sys})$ fb, to be compared to the SM expectation of 0.13 ± 0.01 fb from VBFNLO.

XII. ANOMALOUS TRIPLE GAUGE COUPLINGS

To extract the aTGC, two model-independent parametrizations of possible effects beyond the SM are followed. The first makes use of an effective Lagrangian describing the WWZ vertex and includes only terms that separately conserve the charge conjugation (C) and parity (P) quantum numbers [79,80]. The deviation of the vector boson WWZ couplings from the SM predicted values are introduced as dimensionless anomalous couplings $\Delta\kappa^Z$, Δg_1^Z, and λ^Z.

Without effects not described by the SM, the anomalous terms cause a violation of the unitarity bound in the interaction amplitudes. To prevent this violation, the anomalous couplings are introduced as form factors dependent on the partonic center-of-mass energy, $\hat{s}$: $\alpha(\hat{s}) = \alpha(0)/(1 + \hat{s}/\Lambda_{\mathrm{co}}^2)^2$, where $\alpha(0)$ is the generic anomalous coupling value at low energy and Λ_{co} is a cutoff scale at which physics effects beyond the SM should manifest.

The second parametrization is based on an effective field theory (EFT) in which the particle content of the SM is not changed and the theory is extended by adding to the SM Lagrangian a linear combination of operators of mass

TABLE VII. Observed and expected upper limits at 95% C.L. in fb on the fiducial cross section $\sigma^{\text{fid}}_{W^\pm Zjj\text{-EW}\to\ell'\nu\ell\ell}$, multiplied by the W and Z branching ratios in a single leptonic channel with muons or electrons in the VBS and aQGC fiducial phase space. Values obtained with or without subtraction of the tZj contribution are presented. The 1σ and 2σ uncertainty intervals around the expected limits are also indicated.

95% C.L. upper limit on $\sigma^{\text{fid}}_{W^\pm Zjj\text{-EW}\to\ell'\nu\ell\ell}$ [fb]		
	VBS only	VBS + tZj
VBS phase space		
Observed	0.63	0.67
Expected	0.45	0.49
$\pm1\sigma$ Expected	[0.28;0.62]	[0.33;0.67]
$\pm2\sigma$ Expected	[0.08;0.80]	[0.19;0.84]
aQGC phase space		
Observed	0.25	0.25
Expected	0.13	0.13
$\pm1\sigma$ Expected	[0.08;0.20]	[0.08;0.20]
$\pm2\sigma$ Expected	[0.04;0.28]	[0.06;0.28]

dimension higher than four [81,82]. The dimension-six operators are expected to be dominant. There are three independent dimension-six C- and P-conserving operators that affect the electroweak vector boson self-interactions and that can lead to anomalous triple vector boson couplings. The corresponding new terms in the Lagrangian are

$$\mathcal{O}_{WWW} = \frac{c_{WWW}}{\Lambda^2}\text{Tr}[W_{\mu\nu}W^{\nu\rho}W^{\mu}_{\rho}],$$
$$\mathcal{O}_{W} = \frac{c_{W}}{\Lambda^2}(D_\mu\Phi)^\dagger W^{\mu\nu}(D_\nu\Phi),$$
$$\mathcal{O}_{B} = \frac{c_{B}}{\Lambda^2}(D_\mu\Phi)B^{\mu\nu}(D_\nu\Phi), \quad (7)$$

where $W_{ij}, W^{ij}, W^i_j (i=\mu,\nu, j=\nu,\rho)$, and $B^{\mu\nu}$ are built from the SM electroweak gauge boson fields, $D_i (i=\mu,\nu)$ are the covariant derivatives as introduced in the SM, and Φ is the Higgs doublet field. The dimensionless coefficients $c_i (i = WWW, W, B)$ and Λ represent the strength of the new couplings and the energy scale of new physics, respectively. This approach does not require the introduction of arbitrary form factors to restore unitarity.

The effective field theory allows the anomalous couplings to be reinterpreted in terms of the EFT parameters, $c_i/\Lambda^2 (i = WWW, W, B)$ [83]. For this reason the two parametrizations can be considered equivalent. They are both used in this analysis because the first allows a comparison with previous analyses and the second is a flexible way of parametrizing effects beyond the SM in a model-independent way. Therefore, the free parameters considered in this analysis are $\Delta\kappa^Z$, Δg_1^Z, and λ^Z or $c_i/\Lambda^2 (i = WWW, W, B)$.

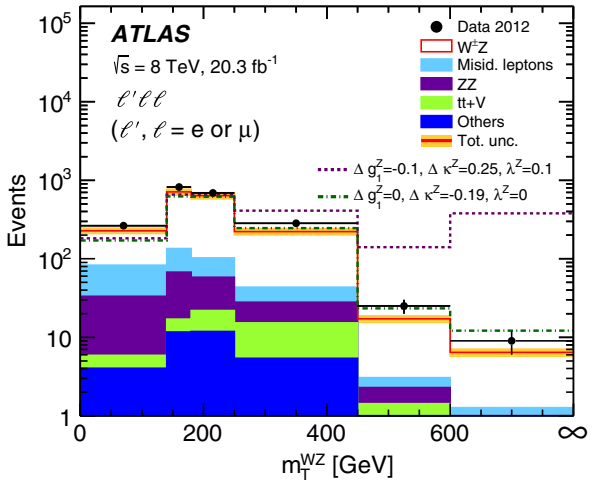

FIG. 12. Distribution of m_{T}^{WZ} in the sum of all channels with the same binning as used for the calculation of limits on aTGC. The points correspond to the data and the histograms to the expectations of the different SM processes. All Monte Carlo expectations are scaled to the integrated luminosity of the data using the predicted MC cross sections of each sample. The POWHEG +PYTHIA MC prediction is used for the SM $W^\pm Z$ signal contribution. The open red histogram shows the total prediction and the shaded orange band its estimated total uncertainty. The last bin contains the overflow. Two predictions with nonzero values of some of the anomalous coupling parameters are also represented by the dashed and dot-dashed lines, respectively.

The presence of aTGC would affect the $W^\pm Z$ integrated cross section and manifest itself as an increased yield of events at high values of p_{T}^Z or m_{T}^{WZ}. Limits on the aTGC are extracted from the m_{T}^{WZ} differential distribution at detector level, as presented in Fig. 12. The m_{T}^{WZ} distribution is expected to be less sensitive to higher-order QCD and EW effects in perturbation theory (as discussed in Sec. IV). For this reason it has smaller theoretical uncertainties than the p_{T}^Z distribution at high values and provides more stringent expected limits, as proven by a dedicated MC study.

The MC event generator MC@NLO is used to generate $W^\pm Z$ events and to compute, for each event, a set of

TABLE VIII. Expected and observed one-dimensional 95% C.L. intervals on the anomalous coupling parameters.

Λ_{co}	Coupling	Expected	Observed
2 TeV	Δg_1^Z	[−0.023; 0.055]	[−0.029; 0.050]
	$\Delta\kappa^Z$	[−0.22; 0.36]	[−0.23; 0.46]
	λ^Z	[−0.026; 0.026]	[−0.028; 0.028]
15 TeV	Δg_1^Z	[−0.016; 0.033]	[−0.019; 0.029]
	$\Delta\kappa^Z$	[−0.17; 0.25]	[−0.19; 0.30]
	λ^Z	[−0.016; 0.016]	[−0.017; 0.017]
∞	Δg_1^Z	[−0.016; 0.032]	[−0.019; 0.029]
	$\Delta\kappa^Z$	[−0.17; 0.25]	[−0.19; 0.30]
	λ^Z	[−0.016; 0.016]	[−0.016; 0.016]

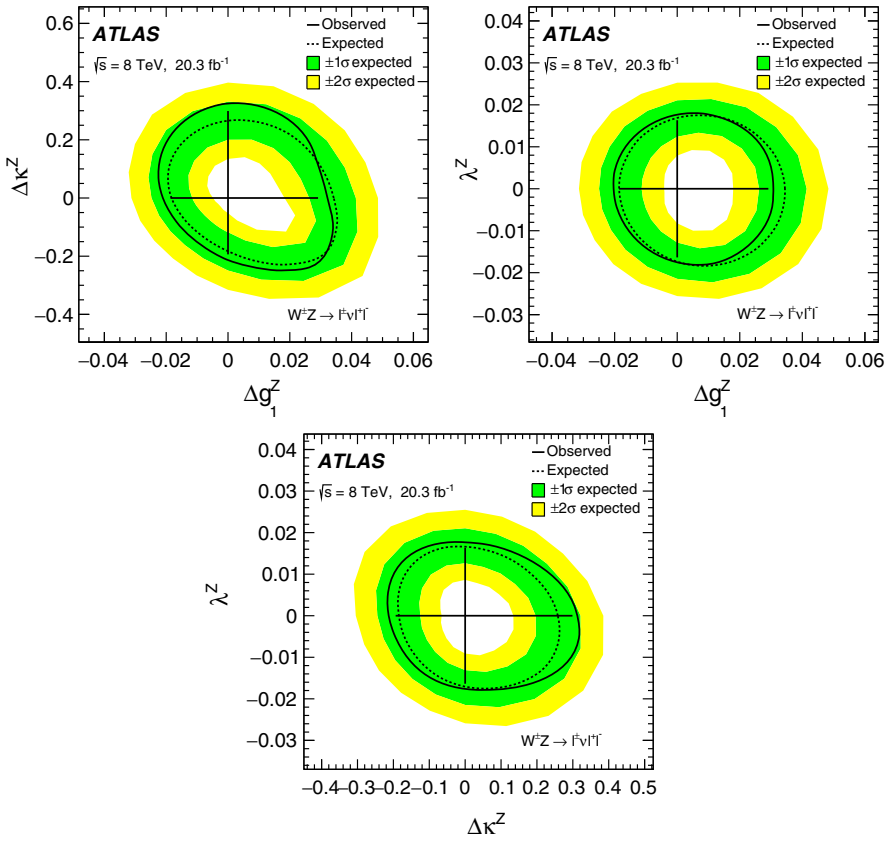

FIG. 13. Expected and observed 95% C.L. limit contours for $\Lambda_{co} \to \infty$ in the planes $(\Delta\kappa^Z, \Delta g_1^Z)$, $(\Delta g_1^Z, \lambda^Z)$, and $(\Delta\kappa^Z, \lambda^Z)$. The solid and dashed lines in the figures represent the observed and expected limits, respectively. The regions outside the black contours are excluded. The green and yellow bands correspond to the 1σ and 2σ uncertainty on the expected limit, respectively. The vertical and horizontal lines represent the 95% C.L. one-dimensional limits calculated separately.

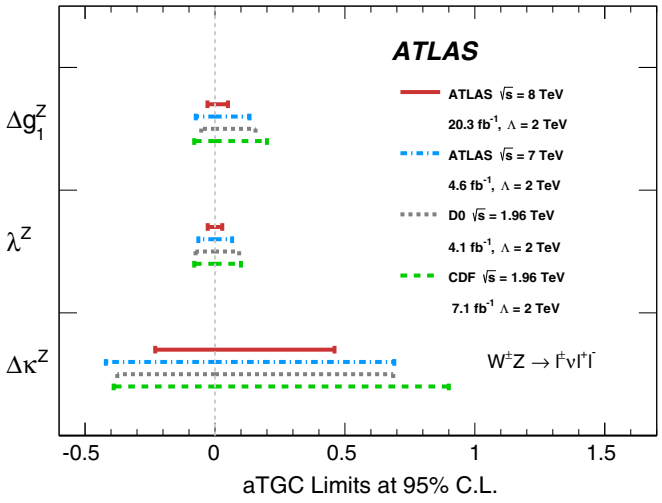

FIG. 14. Comparison of one-dimensional limits at 95% C.L. on the anomalous coupling parameters using a cutoff scale of $\Lambda_{co} =$ 2 TeV and obtained from the analysis of $W^{\pm}Z$ events by the ATLAS [3], D0 [84], and CDF experiments [1].

weights that are employed to reweight the SM sample to any chosen value of the anomalous couplings, or EFT coefficients. With this procedure, expected m_T^{WZ} distributions are obtained for different values of the anomalous couplings, or EFT coefficients. This reweighting procedure is validated by comparing the SM sample reweighted to a given set of aTGC values with a sample generated using the same set of aTGC values. A global systematic uncertainty of 10% across all m_T^{WZ} bins was included in the aTGC limit extraction procedure to account for the reweighting method.

Frequentist confidence intervals on the anomalous coupling are computed by forming a profile likelihood test that incorporates the observed and expected numbers of signal events in each bin of the m_T^{WZ} distribution for different values of the anomalous couplings. The systematic uncertainties are included in the likelihood function as nuisance parameters.

Table VIII presents the observed and expected one-dimensional intervals at 95% C.L. on $\Delta\kappa^Z$, Δg_1^Z, and λ^Z with the cutoff scale $\Lambda_{co} = 2$ TeV, $\Lambda_{co} = 15$ TeV, and $\Lambda_{co} = \infty$ (no cutoff). Each limit is obtained by setting the other two couplings to the SM value. The Λ_{co} value of

TABLE IX. One-dimensional intervals at 95% C.L. on the EFT parameters expected and observed in data.

EFT coupling	Expected [TeV^{-2}]	Observed [TeV^{-2}]
c_W/Λ^2	[−3.7; 7.6]	[−4.3; 6.8]
c_B/Λ^2	[−270; 180]	[−320; 210]
c_{WWW}/Λ^2	[−3.9; 3.8]	[−3.9; 4.0]

15 TeV is the largest form factor scale that can preserve unitarity for all aTGC in this analysis.

Expected and observed 95% C.L. limit contours in the planes $(\Delta\kappa^Z, \Delta g_1^Z)$, $(\Delta g_1^Z, \lambda^Z)$, and $(\Delta\kappa^Z, \lambda^Z)$ are shown in Fig. 13. For each of the contours, the third parameter is set to the SM value and the limits are derived without any cutoff.

In Fig. 14 the present observed limits are compared to limits previously obtained using WZ events produced in $p\bar{p}$ collisions at the Tevatron [1,84] and by ATLAS with $\sqrt{s} = 7$ TeV pp collisions [3]. The new limits improve previous constraints by factors of 1.5 to 2.5 and are now the most stringent model-independent limits on WWZ anomalous couplings.

Table IX presents the observed and expected one-dimensional intervals at 95% C.L. on c_{WWW}/Λ^2, c_B/Λ^2, and c_W/Λ^2. The sensitivity of the $W^{\pm}Z$ final state to the EFT parameter c_B/Λ^2 is much weaker.

XIII. ANOMALOUS QUARTIC GAUGE COUPLINGS

To extract limits on aQGC, the EFT approach introduced in the previous section is used. Several ways of parametrizing possible deviations with respect to the SM exist. In this analysis, the choice is to express the deviation using two parameters α_4 and α_5 following existing notations [49,85–87]. They are the coefficients of the two linearly independent dimension-four operators contributing to the quartic gauge couplings beyond the SM.

The WHIZARD event generator is used to compute the ratio in the aQGC fiducial phase space, at particle level, of the expected fiducial cross section for different values of α_4 and α_5, to the SM cross section. WHIZARD includes a unitarization scheme in order to ensure the unitary of the scattering amplitude, which would be violated for values of the quartic gauge couplings different from the SM value.

These ratios are multiplied by the SM fiducial cross section estimated with SHERPA to obtain the predicted fiducial cross sections as a function of α_4 and α_5. The SHERPA MC generator is used as the reference SM generator for the sake of consistency with the VBS cross-section limit measurement of Sec. XI C and with a previous search for aQGC using $W^{\pm}W^{\pm}jj$ events [88]. The expected fiducial cross sections include only the VBS part of the $WZjj$-EW process.

Distributions for the variables $|\Delta\phi(W,Z)|$ and $\sum |p_{\mathrm{T}}^{\ell}|$ that are used to select events in the aQGC fiducial phase space are shown in Fig. 15 for events passing the VBS phase space selection. The change of the shape of these distributions when one of the aQGC parameters has a nonzero value is also shown. After correcting for the selection efficiency, the measured fiducial cross section in the aQGC phase space is used to set limits on the aQGC. The selection efficiency is estimated to be ≈70% and found to be constant over the considered α_4 and α_5 values, within the MC statistical uncertainties. Limits are obtained as for the aTGC limits of Sec. XII from a profile likelihood method that incorporates the systematic uncertainties. The expected and observed two-dimensional limit contours at 95% C.L. on α_4 and α_5 are shown in Fig. 16. The present

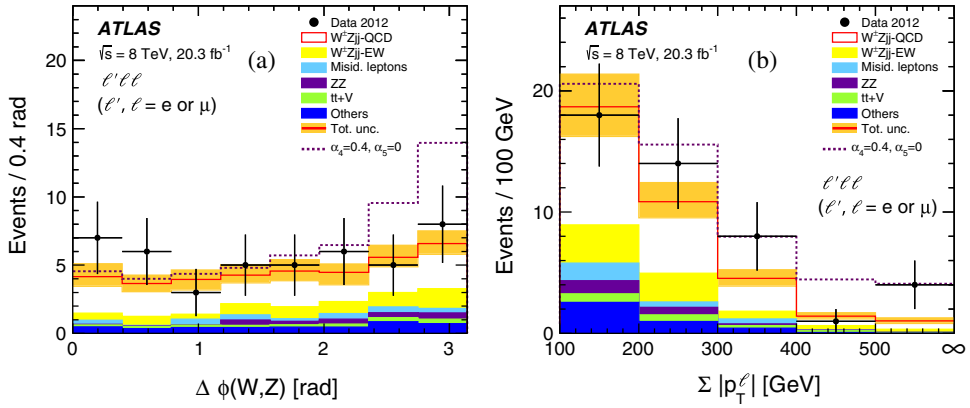

FIG. 15. Distribution of the difference in azimuthal angle between the reconstructed W and Z bosons, (a) $|\Delta\phi(W,Z)|$, and of the scalar sum of the transverse momenta of the three charged leptons associated with the W and Z bosons, (b) $\sum |p_{\mathrm{T}}^{\ell}|$, for the sum of all channels, in the VBS phase space. All Monte Carlo expectations are scaled to the integrated luminosity of the data using the predicted MC cross sections of each sample. The SHERPA MC prediction is used for the SM $WZjj$-QCD and $WZjj$-EW predictions. The open red histogram shows the total prediction and the shaded orange band its estimated total uncertainty. The prediction with nonzero values of one of the aQGC parameters is also represented by the dashed line.

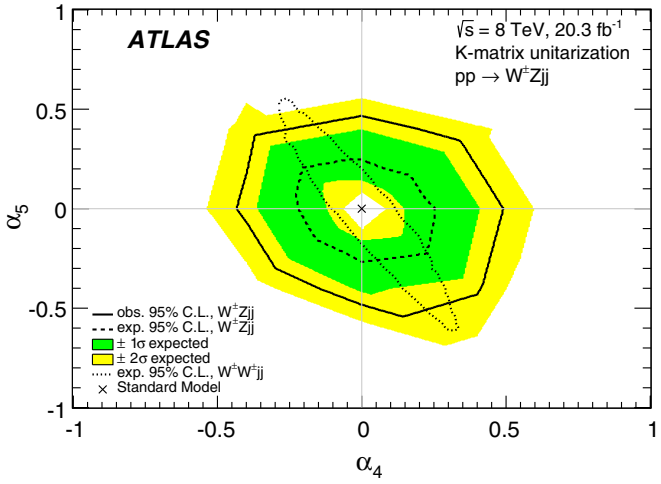

FIG. 16. Expected and observed 95% C.L. limit contours on aQGC parameters α_4 and α_5. The solid and dashed lines in the figures represent the observed and expected limits, respectively. The regions outside the black contours are excluded. The green and yellow bands correspond to the 1σ and 2σ uncertainty on the expected limit, respectively. The expected exclusion contour from an analysis by the ATLAS Collaboration using $W^{\pm}W^{\pm}jj$ events [88] is indicated by the dotted line.

limit is compared to the expected limit obtained by the ATLAS Collaboration using $W^{\pm}W^{\pm}jj$ events [88]. This analysis of $W^{\pm}Zjj$ events probes a domain of the (α_4, α_5) parameter space that could not be excluded by the analysis of $W^{\pm}W^{\pm}jj$ events.

The limits on (α_4, α_5) coefficients used in WHIZARD can be translated to limits on the $(f_{S,0}/\Lambda^4, f_{S,1}/\Lambda^4)$ coefficients of the $\mathcal{O}_{S,0}$ and $\mathcal{O}_{S,1}$ operators of Ref. [89] using the following conversion for the $WWZZ$ vertex [90]:

$$\frac{f_{S,0(1)}}{\Lambda^4} = \alpha_{4(5)} \times \frac{16}{v^4}, \tag{8}$$

where $v = 246.22$ GeV is the Higgs vacuum expectation value. Assuming $\Lambda = 1$ TeV and that this conversion also holds for the K-matrix unitarization, a value of $\alpha_{4(5)} = 0.5$ corresponds to $f_{S,0(1)} = 2177$ for $W^{\pm}Zjj$ events.

XIV. CONCLUSION

Measurements of $W^{\pm}Z$ production using $\sqrt{s} = 8$ TeV pp collisions at the LHC are presented. The data were collected with the ATLAS detector and correspond to an integrated luminosity of 20.3 fb^{-1}. The measurements use leptonic decay modes of the gauge bosons to electrons or muons and are performed in a fiducial phase space approximating the detector acceptance. The measured inclusive cross section in the fiducial region for one leptonic decay channel is $\sigma_{WZ^{\pm}\to\ell'\nu\ell\ell} = 35.1 \pm 0.9(\text{stat}) \pm 0.8(\text{sys}) \pm 0.8(\text{lumi})$ fb, to be compared to the next-to-leading-order Standard Model expectation of 30.0 ± 2.1 fb. With a total experimental relative uncertainty of 4.2%, a precision better than presently available from theoretical predictions is reached. The measured cross section is found to be slightly larger than the NLO SM prediction. A comparison to a prediction incorporating full NNLO QCD effects would therefore be very interesting.

Furthermore, the $W^{\pm}Z$ production cross section is measured as a function of each of several kinematic variables and compared to SM predictions of the POWHEG+PYTHIA, MC@NLO, and SHERPA Monte Carlo event generators.

The ratio of the cross sections for W^+Z and W^-Z production is measured. Integrated over the detector fiducial phase space it is $\sigma^{\text{fid}}_{W^+Z\to\ell'\nu\ell\ell}/\sigma^{\text{fid}}_{W^-Z\to\ell'\nu\ell\ell} = 1.51 \pm 0.11$ to be compared to the NLO SM expectation of 1.69 ± 0.07. The differential evolution of this cross-section ratio as a function of each of a few kinematic variables is also measured and compared to available SM predictions.

The transverse mass spectrum of the $W^{\pm}Z$ system is used to search for anomalous triple gauge boson couplings and limits on Δk^Z, Δg_1^Z, and λ^Z are derived. With an improvement by a factor of about 2 compared to previously existing constraints, these are the most stringent model-independent limits on WWZ anomalous couplings to date. Results are also interpreted as limits on the c_W/Λ^2, c_B/Λ^2, and c_{WWW}/Λ^2 coefficients of the EFT parametrization.

Finally, events with a W and a Z boson associated with two or more forward jets have been analyzed and an upper limit at 95% C.L. on the $W^{\pm}Z$ scattering cross section of 0.63 fb for one leptonic decay channel has been established. Limits on anomalous quartic gauge boson couplings have also been extracted.

For $W^{\pm}Z$ production, the measurements presented here are the most precise and complete to date and have the potential to further constrain existing Standard Model theoretical predictions, which are presently only available at next-to-leading order in QCD.

ACKNOWLEDGMENTS

We thank CERN for the very successful operation of the LHC, as well as the support staff from our institutions without whom ATLAS could not be operated efficiently. We acknowledge the support of ANPCyT, Argentina; YerPhI, Armenia; ARC, Australia; BMWFW and FWF, Austria; ANAS, Azerbaijan; SSTC, Belarus; CNPq and FAPESP, Brazil; NSERC, NRC and CFI, Canada; CERN; CONICYT, Chile; CAS, MOST and NSFC, China; COLCIENCIAS, Colombia; MSMT CR, MPO CR and VSC CR, Czech Republic; DNRF and DNSRC, Denmark; IN2P3-CNRS, CEA-DSM/IRFU, France; GNSF, Georgia; BMBF, HGF, and MPG, Germany; GSRT, Greece; RGC, Hong Kong SAR, China; ISF, I-CORE and Benoziyo Center, Israel; INFN, Italy; MEXT and JSPS, Japan; CNRST, Morocco; FOM and NWO, Netherlands; RCN, Norway; MNiSW and NCN, Poland; FCT, Portugal;

MNE/IFA, Romania; MES of Russia and NRC KI, Russian Federation; JINR; MESTD, Serbia; MSSR, Slovakia; ARRS and MIZŠ, Slovenia; DST/NRF, South Africa; MINECO, Spain; SRC and Wallenberg Foundation, Sweden; SERI, SNSF and Cantons of Bern and Geneva, Switzerland; MOST, Taiwan; TAEK, Turkey; STFC, United Kingdom; DOE and NSF, United States of America. In addition, individual groups and members have received support from BCKDF, the Canada Council, CANARIE, CRC, Compute Canada, FQRNT, and the Ontario Innovation Trust, Canada; EPLANET, ERC, FP7, Horizon 2020 and Marie Skłodowska-Curie Actions, European Union; Investissements d'Avenir Labex and Idex, ANR, Région Auvergne and Fondation Partager le Savoir, France; DFG and AvH Foundation, Germany; Herakleitos, Thales and Aristeia programmes co-financed by EU-ESF and the Greek NSRF; BSF, GIF and Minerva, Israel; BRF, Norway; the Royal Society and Leverhulme Trust, United Kingdom. The crucial computing support from all WLCG partners is acknowledged gratefully, in particular from CERN and the ATLAS Tier-1 facilities at TRIUMF (Canada), NDGF (Denmark, Norway, Sweden), CC-IN2P3 (France), KIT/GridKA (Germany), INFN-CNAF (Italy), NL-T1 (Netherlands), PIC (Spain), ASGC (Taiwan), RAL (UK) and BNL (USA) and in the Tier-2 facilities worldwide.

National Research Centre Kurchatov Institute, Russian Federation

[1] T. Aaltonen *et al.* (CDF Collaboration), Phys. Rev. D **86**, 031104 (2012).
[2] V. M. Abazov *et al.* (D0 Collaboration), Phys. Rev. D **85**, 112005 (2012).
[3] G. Aad *et al.* (ATLAS Collaboration), Eur. Phys. J. C **72**, 2173 (2012).
[4] S. Schael *et al.* (ALEPH, DELPHI, L3, and OPAL Collaborations), Phys. Rep. **532**, 119 (2013).
[5] V. M. Abazov *et al.* (D0 Collaboration), Phys. Lett. B **718**, 451 (2012).
[6] S. Chatrchyan *et al.* (CMS Collaboration), Eur. Phys. J. C **73**, 2283 (2013).
[7] U. Baur, T. Han, and J. Ohnemus, Phys. Rev. D **51**, 3381 (1995).
[8] E. Accomando and A. Kaiser, Phys. Rev. D **73**, 093006 (2006).
[9] F. Campanario and S. Sapeta, Phys. Lett. B **718**, 100 (2012).
[10] A. Bierweiler, T. Kasprzik, and J. H. Kühn, J. High Energy Phys. 12 (2013) 071.
[11] J. Baglio, L. D. Ninh, and M. M. Weber, Phys. Rev. D **88**, 113005 (2013). (We would like to thank Le Duc Ninh for providing us with the NLO electroweak corrections to WZ production at $\sqrt{s} = 8$ TeV at the LHC).
[12] J. Ohnemus, Phys. Rev. D **44**, 3477 (1991).
[13] S. Frixione, P. Nason, and G. Ridolfi, Nucl. Phys. **B383**, 3 (1992).
[14] G. Aad *et al.* (ATLAS Collaboration), J. Instrum. **3**, S08003 (2008).
[15] G. Aad *et al.* (ATLAS Collaboration), CERN Technical Report No. ATL-PHYS-PUB-2015-013, 2015, https://cds.cern.ch/record/2022743.
[16] K. A. Olive *et al.*, Chin. Phys. C **38**, 090001 (2014).
[17] P. Nason, J. High Energy Phys. 11 (2004) 040.
[18] S. Frixione, P. Nason, and C. Oleari, J. High Energy Phys. 11 (2007) 070.
[19] S. Alioli, P. Nason, C. Oleari, and E. Re, J. High Energy Phys. 06 (2010) 043.
[20] T. Melia, P. Nason, R. Röntsch, and G. Zanderighi, J. High Energy Phys. 11 (2011) 078.
[21] T. Sjöstrand, S. Mrenna, and P. Z. Skands, Comput. Phys. Commun. **178**, 852 (2008).
[22] L. J. Dixon, Z. Kunszt, and A. Signer, Nucl. Phys. **B531**, 3 (1998).
[23] H.-L. Lai, M. Guzzi, J. Huston, Z. Li, P. M. Nadolsky, J. Pumplin, and C.-P. Yuan, Phys. Rev. D **82**, 074024 (2010).
[24] A. D. Martin, W. J. Stirling, R. S. Thorne, and G. Watt, Eur. Phys. J. C **63**, 189 (2009).
[25] R. D. Ball *et al.*, J. High Energy Phys. 04 (2015) 040.
[26] G. Aad *et al.* (ATLAS Collaboration), Phys. Rev. Lett. **109**, 012001 (2012).
[27] S. Dittmaier *et al.* (LHC Higgs Cross Section Working Group), arXiv:1101.0593.
[28] S. Frixione and B. R. Webber, J. High Energy Phys. 06 (2002) 029.
[29] S. Gieseke, A. Ribon, M. H. Seymour, P. Stephens, and B. Webber, J. High Energy Phys. 02 (2004) 005.
[30] T. Gleisberg, S. Höche, F. Krauss, M. Schönherr, S. Schumann, F. Siegert, and J. Winter, J. High Energy Phys. 02 (2009) 007.
[31] S. Hoeche, F. Krauss, M. Schönherr, and F. Siegert, J. High Energy Phys. 04 (2013) 027.
[32] K. Arnold *et al.*, Comput. Phys. Commun. **180**, 1661 (2009).
[33] K. Arnold *et al.*, arXiv:1107.4038.
[34] J. Baglio *et al.*, arXiv:1404.3940.
[35] F. Campanario, C. Englert, S. Kallweit, M. Spannowsky, and D. Zeppenfeld, J. High Energy Phys. 07 (2010) 076.
[36] F. Campanario, C. Englert, and M. Spannowsky, Phys. Rev. D **82**, 054015 (2010).
[37] G. Aad *et al.* (ATLAS Collaboration), CERN Technical Report No. ATL-PHYS-PUB-2012-003, 2012, https://cds.cern.ch/record/1474107.
[38] G. Aad *et al.* (ATLAS Collaboration), Eur. Phys. J. C **70**, 823 (2010).
[39] S. Agostinelli *et al.* (GEANT4 Collaboration), Nucl. Instrum. Methods Phys. Res., Sect. A **506**, 250 (2003).

[40] G. Aad *et al.* (ATLAS Collaboration), Eur. Phys. J. C **74**, 2941 (2014).
[41] G. Aad *et al.* (ATLAS Collaboration), CERN Technical Report No. ATLAS-CONF-2014-032, 2014, https://cds.cern.ch/record/1706245.
[42] G. Aad *et al.* (ATLAS Collaboration), Eur. Phys. J. C **74**, 3130 (2014).
[43] G. Aad *et al.* (ATLAS Collaboration), Eur. Phys. J. C **74**, 3071 (2014).
[44] J. M. Butterworth, J. R. Forshaw, and M. H. Seymour, Z. Phys. C **72**, 637 (1996).
[45] P. Golonka and Z. Was, Eur. Phys. J. C **45**, 97 (2006).
[46] S. Catani, F. Krauss, B. R. Webber, and R. Kuhn, J. High Energy Phys. 11 (2001) 063.
[47] D. R. Yennie, S. C. Frautschi, and H. Suura, Ann. Phys. (N.Y.) **13**, 379 (1961).
[48] W. Kilian, T. Ohl, and J. Reuter, Eur. Phys. J. C **71**, 1742 (2011).
[49] A. Alboteanu, W. Kilian, and J. Reuter, J. High Energy Phys. 11 (2008) 010.
[50] S. U. Chung *et al.*, Ann. Phys. (Berlin) **4**, 404 (1995).
[51] T. Binoth, N. Kauer, and P. Mertsch, in *Proceedings of the 16th International Workshop on Deep Inelastic Scattering and Related Subjects (DIS 2008)* (Wiley, New York, 2008), p. 142.
[52] J. Alwall, M. Herquet, F. Maltoni, O. Mattelaer, and T. Stelzer, J. High Energy Phys. 06 (2011) 128.
[53] J. M. Campbell and R. K. Ellis, J. High Energy Phys. 07 (2012) 052.
[54] M. V. Garzelli, A. Kardos, C. G. Papadopoulos, and Z. Trócsányi, J. High Energy Phys. 11 (2012) 056.
[55] J. Campbell, R. K. Ellis, and R. Rötsch, Phys. Rev. D **87**, 114006 (2013).
[56] J. R. Gaunt, C.-H. Kom, A. Kulesza, and W. James Stirling, Eur. Phys. J. C **69**, 53 (2010).
[57] G. Aad *et al.* (ATLAS Collaboration), New J. Phys. **15**, 033038 (2013).
[58] M. L. Mangano, F. Piccinini, A. D. Polosa, M. Moretti, and R. Pittau, J. High Energy Phys. 07 (2003) 001.
[59] J. Pumplin, D. R. Stump, J. Huston, H.-L. Lai, P. Nadolsky, and Wu-Ki Tung, J. High Energy Phys. 07 (2002) 012.
[60] ATLAS Collaboration (to be published).
[61] M. Cacciari, G. P. Salam, and G. Soyez, J. High Energy Phys. 04 (2008) 063.
[62] G. Aad *et al.* (ATLAS Collaboration), Eur. Phys. J. C **73**, 2304 (2013).
[63] G. Aad *et al.* (ATLAS Collaboration), CERN Technical Report No. ATLAS-CONF-2015-002, 2015, https://cds.cern.ch/record/2001682.
[64] G. Aad *et al.* (ATLAS Collaboration), CERN Technical Report No. ATLAS-CONF-2015-017, 2015, https://cds.cern.ch/record/2008678.
[65] G. Aad *et al.* (ATLAS Collaboration), arXiv:1510.03823.
[66] G. Aad *et al.* (ATLAS Collaboration), Eur. Phys. J. C **72**, 1844 (2012).
[67] G. Aad *et al.* (ATLAS Collaboration), CERN Technical Report No. ATLAS-CONF-2013-082, 2013, https://cds.cern.ch/record/1570993.
[68] G. Aad *et al.* (ATLAS Collaboration), CERN Technical Report No. ATLAS-CONF-2014-019, 2014, https://cds.cern.ch/record/1702055.
[69] G. Aad *et al.* (ATLAS Collaboration), J. High Energy Phys. 06 (2014) 035.
[70] F. Cascioli, T. Gehrmann, M. Grazzini, S. Kallweit, P. Maierhöfer, A. von Manteuffel, S. Pozzorini, D. Rathlev, L. Tancredi, and E. Weihs, Phys. Lett. B **735**, 311 (2014).
[71] G. D'Agostini, Nucl. Instrum. Methods Phys. Res., Sect. A **362**, 487 (1995).
[72] T. Adye, in *Proceedings of the PHYSTAT 2011 Workshop, CERN, Geneva, Switzerland* (CERN, Geneva, Switzerland, 2011), pp. 313–318.
[73] G. Aad *et al.* (ATLAS Collaboration), arXiv:1603.01702.
[74] G. Aad *et al.* (ATLAS Collaboration), Eur. Phys. J. C **73**, 2518 (2013).
[75] G. Aad *et al.* (ATLAS Collaboration), Phys. Lett. B **753**, 552 (2016).
[76] M. Grazzini, S. Kallweit, and D. Rathlev, Phys. Lett. B **750**, 407 (2015).
[77] T. Gehrmann, M. Grazzini, S. Kallweit, P. Maierhöfer, A. von Manteuffel, S. Pozzorini, D. Rathlev, and L. Tancredi, Phys. Rev. Lett. **113**, 212001 (2014).
[78] M. Grazzini, S. Kallweit, and D. Rathlev, J. High Energy Phys. 07 (2015) 085.
[79] K. Hagiwara, R. D. Peccei, D. Zeppenfeld, and K. Hikasa, Nucl. Phys. **B282**, 253 (1987).
[80] J. Ellison and J. Wudka, Annu. Rev. Nucl. Part. Sci. **48**, 33 (1998).
[81] W. Buchmuller and D. Wyler, Nucl. Phys. **B268**, 621 (1986).
[82] C. Degrande, N. Greiner, W. Kilian, O. Mattelaer, H. Mebane, T. Stelzer, S. Willenbrock, and C. Zhang, Ann. Phys. (Amsterdam) **335**, 21 (2013).
[83] K. Hagiwara, S. Ishihara, R. Szalapski, and D. Zeppenfeld, Phys. Rev. D **48**, 2182 (1993).
[84] V. M. Abazov *et al.* (D0 Collaboration), Phys. Lett. B **695**, 67 (2011).
[85] T. Appelquist and C. W. Bernard, Phys. Rev. D **22**, 200 (1980).
[86] A. C. Longhitano, Phys. Rev. D **22**, 1166 (1980).
[87] A. C. Longhitano, Nucl. Phys. **B188**, 118 (1981).
[88] G. Aad *et al.* (ATLAS Collaboration), Phys. Rev. Lett. **113**, 141803 (2014).
[89] O. Eboli, M. Gonzalez-Garcia, and J. Mizukoshi, Phys. Rev. D **74**, 073005 (2006).
[90] C. Degrande *et al.*, arXiv:1309.7890.

G. Aad,[86] B. Abbott,[113] J. Abdallah,[151] O. Abdinov,[11] B. Abeloos,[117] R. Aben,[107] M. Abolins,[91] O. S. AbouZeid,[137] H. Abramowicz,[153] H. Abreu,[152] R. Abreu,[116] Y. Abulaiti,[146a,146b] B. S. Acharya,[163a,163b,b] L. Adamczyk,[39a] D. L. Adams,[26] J. Adelman,[108] S. Adomeit,[100] T. Adye,[131] A. A. Affolder,[75] T. Agatonovic-Jovin,[13] J. Agricola,[55]

J. A. Aguilar-Saavedra,[126a,126f] S. P. Ahlen,[23] F. Ahmadov,[66,c] G. Aielli,[133a,133b] H. Akerstedt,[146a,146b] T. P. A. Åkesson,[82] A. V. Akimov,[96] G. L. Alberghi,[21a,21b] J. Albert,[168] S. Albrand,[56] M. J. Alconada Verzini,[72] M. Aleksa,[31] I. N. Aleksandrov,[66] C. Alexa,[27b] G. Alexander,[153] T. Alexopoulos,[10] M. Alhroob,[113] G. Alimonti,[92a] J. Alison,[32] S. P. Alkire,[36] B. M. M. Allbrooke,[149] B. W. Allen,[116] P. P. Allport,[18] A. Aloisio,[104a,104b] A. Alonso,[37] F. Alonso,[72] C. Alpigiani,[138] B. Alvarez Gonzalez,[31] D. Álvarez Piqueras,[166] M. G. Alviggi,[104a,104b] B. T. Amadio,[15] K. Amako,[67] Y. Amaral Coutinho,[25a] C. Amelung,[24] D. Amidei,[90] S. P. Amor Dos Santos,[126a,126c] A. Amorim,[126a,126b] S. Amoroso,[31] N. Amram,[153] G. Amundsen,[24] C. Anastopoulos,[139] L. S. Ancu,[50] N. Andari,[108] T. Andeen,[32] C. F. Anders,[59b] G. Anders,[31] J. K. Anders,[75] K. J. Anderson,[32] A. Andreazza,[92a,92b] V. Andrei,[59a] S. Angelidakis,[9] I. Angelozzi,[107] P. Anger,[45] A. Angerami,[36] F. Anghinolfi,[31] A. V. Anisenkov,[109,d] N. Anjos,[12] A. Annovi,[124a,124b] M. Antonelli,[48] A. Antonov,[98] J. Antos,[144b] F. Anulli,[132a] M. Aoki,[67] L. Aperio Bella,[18] G. Arabidze,[91] Y. Arai,[67] J. P. Araque,[126a] A. T. H. Arce,[46] F. A. Arduh,[72] J-F. Arguin,[95] S. Argyropoulos,[64] M. Arik,[19a] A. J. Armbruster,[31] L. J. Armitage,[77] O. Arnaez,[31] H. Arnold,[49] M. Arratia,[29] O. Arslan,[22] A. Artamonov,[97] G. Artoni,[120] S. Artz,[84] S. Asai,[155] N. Asbah,[43] A. Ashkenazi,[153] B. Åsman,[146a,146b] L. Asquith,[149] K. Assamagan,[26] R. Astalos,[144a] M. Atkinson,[165] N. B. Atlay,[141] K. Augsten,[128] G. Avolio,[31] B. Axen,[15] M. K. Ayoub,[117] G. Azuelos,[95,e] M. A. Baak,[31] A. E. Baas,[59a] M. J. Baca,[18] H. Bachacou,[136] K. Bachas,[74a,74b] M. Backes,[31] M. Backhaus,[31] P. Bagiacchi,[132a,132b] P. Bagnaia,[132a,132b] Y. Bai,[34a] J. T. Baines,[131] O. K. Baker,[175] E. M. Baldin,[109,d] P. Balek,[129] T. Balestri,[148] F. Balli,[136] W. K. Balunas,[122] E. Banas,[40] Sw. Banerjee,[172,f] A. A. E. Bannoura,[174] L. Barak,[31] E. L. Barberio,[89] D. Barberis,[51a,51b] M. Barbero,[86] T. Barillari,[101] M. Barisonzi,[163a,163b] T. Barklow,[143] N. Barlow,[29] S. L. Barnes,[85] B. M. Barnett,[131] R. M. Barnett,[15] Z. Barnovska,[5] A. Baroncelli,[134a] G. Barone,[24] A. J. Barr,[120] L. Barranco Navarro,[166] F. Barreiro,[83] J. Barreiro Guimarães da Costa,[34a] R. Bartoldus,[143] A. E. Barton,[73] P. Bartos,[144a] A. Basalaev,[123] A. Bassalat,[117] A. Basye,[165] R. L. Bates,[54] S. J. Batista,[158] J. R. Batley,[29] M. Battaglia,[137] M. Bauce,[132a,132b] F. Bauer,[136] H. S. Bawa,[143,g] J. B. Beacham,[111] M. D. Beattie,[73] T. Beau,[81] P. H. Beauchemin,[161] R. Beccherle,[124a,124b] P. Bechtle,[22] H. P. Beck,[17,h] K. Becker,[120] M. Becker,[84] M. Beckingham,[169] C. Becot,[110] A. J. Beddall,[19d] A. Beddall,[19b] V. A. Bednyakov,[66] M. Bedognetti,[107] C. P. Bee,[148] L. J. Beemster,[107] T. A. Beermann,[31] M. Begel,[26] J. K. Behr,[120] C. Belanger-Champagne,[88] A. S. Bell,[79] W. H. Bell,[50] G. Bella,[153] L. Bellagamba,[21a] A. Bellerive,[30] M. Bellomo,[87] K. Belotskiy,[98] O. Beltramello,[31] N. L. Belyaev,[98] O. Benary,[153] D. Benchekroun,[135a] M. Bender,[100] K. Bendtz,[146a,146b] N. Benekos,[10] Y. Benhammou,[153] E. Benhar Noccioli,[175] J. Benitez,[64] J. A. Benitez Garcia,[159b] D. P. Benjamin,[46] J. R. Bensinger,[24] S. Bentvelsen,[107] L. Beresford,[120] M. Beretta,[48] D. Berge,[107] E. Bergeaas Kuutmann,[164] N. Berger,[5] F. Berghaus,[168] J. Beringer,[15] S. Berlendis,[56] C. Bernard,[23] N. R. Bernard,[87] C. Bernius,[110] F. U. Bernlochner,[22] T. Berry,[78] P. Berta,[129] C. Bertella,[84] G. Bertoli,[146a,146b] F. Bertolucci,[124a,124b] I. A. Bertram,[73] C. Bertsche,[113] D. Bertsche,[113] G. J. Besjes,[37] O. Bessidskaia Bylund,[146a,146b] M. Bessner,[43] N. Besson,[136] C. Betancourt,[49] S. Bethke,[101] A. J. Bevan,[77] W. Bhimji,[15] R. M. Bianchi,[125] L. Bianchini,[24] M. Bianco,[31] O. Biebel,[100] D. Biedermann,[16] R. Bielski,[85] N. V. Biesuz,[124a,124b] M. Biglietti,[134a] J. Bilbao De Mendizabal,[50] H. Bilokon,[48] M. Bindi,[55] S. Binet,[117] A. Bingul,[19b] C. Bini,[132a,132b] S. Biondi,[21a,21b] D. M. Bjergaard,[46] C. W. Black,[150] J. E. Black,[143] K. M. Black,[23] D. Blackburn,[138] R. E. Blair,[6] J.-B. Blanchard,[136] J. E. Blanco,[78] T. Blazek,[144a] I. Bloch,[43] C. Blocker,[24] W. Blum,[84,a] U. Blumenschein,[55] S. Blunier,[33a] G. J. Bobbink,[107] V. S. Bobrovnikov,[109,d] S. S. Bocchetta,[82] A. Bocci,[46] C. Bock,[100] M. Boehler,[49] D. Boerner,[174] J. A. Bogaerts,[31] D. Bogavac,[13] A. G. Bogdanchikov,[109] C. Bohm,[146a] V. Boisvert,[78] T. Bold,[39a] V. Boldea,[27b] A. S. Boldyrev,[163a,163c] M. Bomben,[81] M. Bona,[77] M. Boonekamp,[136] A. Borisov,[130] G. Borissov,[73] J. Bortfeldt,[100] D. Bortoletto,[120] V. Bortolotto,[61a,61b,61c] K. Bos,[107] D. Boscherini,[21a] M. Bosman,[12] J. D. Bossio Sola,[28] J. Boudreau,[125] J. Bouffard,[2] E. V. Bouhova-Thacker,[73] D. Boumediene,[35] C. Bourdarios,[117] N. Bousson,[114] S. K. Boutle,[54] A. Boveia,[31] J. Boyd,[31] I. R. Boyko,[66] J. Bracinik,[18] A. Brandt,[8] G. Brandt,[55] O. Brandt,[59a] U. Bratzler,[156] B. Brau,[87] J. E. Brau,[116] H. M. Braun,[174,a] W. D. Breaden Madden,[54] K. Brendlinger,[122] A. J. Brennan,[89] L. Brenner,[107] R. Brenner,[164] S. Bressler,[171] T. M. Bristow,[47] D. Britton,[54] D. Britzger,[43] F. M. Brochu,[29] I. Brock,[22] R. Brock,[91] G. Brooijmans,[36] T. Brooks,[78] W. K. Brooks,[33b] J. Brosamer,[15] E. Brost,[116] J. H. Broughton,[18] P. A. Bruckman de Renstrom,[40] D. Bruncko,[144b] R. Bruneliere,[49] A. Bruni,[21a] G. Bruni,[21a] BH Brunt,[29] M. Bruschi,[21a] N. Bruscino,[22] P. Bryant,[32] L. Bryngemark,[82] T. Buanes,[14] Q. Buat,[142] P. Buchholz,[141] A. G. Buckley,[54] I. A. Budagov,[66] F. Buehrer,[49] M. K. Bugge,[119] O. Bulekov,[98] D. Bullock,[8] H. Burckhart,[31] S. Burdin,[75] C. D. Burgard,[49] B. Burghgrave,[108] K. Burka,[40] S. Burke,[131] I. Burmeister,[44] E. Busato,[35] D. Büscher,[49] V. Büscher,[84] P. Bussey,[54] J. M. Butler,[23] A. I. Butt,[3] C. M. Buttar,[54] J. M. Butterworth,[79] P. Butti,[107] W. Buttinger,[26] A. Buzatu,[54] A. R. Buzykaev,[109,d] S. Cabrera Urbán,[166] D. Caforio,[128] V. M. Cairo,[38a,38b] O. Cakir,[4a] N. Calace,[50] P. Calafiura,[15] A. Calandri,[86] G. Calderini,[81] P. Calfayan,[100] L. P. Caloba,[25a] D. Calvet,[35] S. Calvet,[35]

T. P. Calvet,[86] R. Camacho Toro,[32] S. Camarda,[43] P. Camarri,[133a,133b] D. Cameron,[119] R. Caminal Armadans,[165] C. Camincher,[56] S. Campana,[31] M. Campanelli,[79] A. Campoverde,[148] V. Canale,[104a,104b] A. Canepa,[159a] M. Cano Bret,[34e] J. Cantero,[83] R. Cantrill,[126a] T. Cao,[41] M. D. M. Capeans Garrido,[31] I. Caprini,[27b] M. Caprini,[27b] M. Capua,[38a,38b] R. Caputo,[84] R. M. Carbone,[36] R. Cardarelli,[133a] F. Cardillo,[49] T. Carli,[31] G. Carlino,[104a] L. Carminati,[92a,92b] S. Caron,[106] E. Carquin,[33a] G. D. Carrillo-Montoya,[31] J. R. Carter,[29] J. Carvalho,[126a,126c] D. Casadei,[79] M. P. Casado,[12,i] M. Casolino,[12] D. W. Casper,[162] E. Castaneda-Miranda,[145a] A. Castelli,[107] V. Castillo Gimenez,[166] N. F. Castro,[126a,j] A. Catinaccio,[31] J. R. Catmore,[119] A. Cattai,[31] J. Caudron,[84] V. Cavaliere,[165] D. Cavalli,[92a] M. Cavalli-Sforza,[12] V. Cavasinni,[124a,124b] F. Ceradini,[134a,134b] L. Cerda Alberich,[166] B. C. Cerio,[46] A. S. Cerqueira,[25b] A. Cerri,[149] L. Cerrito,[77] F. Cerutti,[15] M. Cerv,[31] A. Cervelli,[17] S. A. Cetin,[19c] A. Chafaq,[135a] D. Chakraborty,[108] I. Chalupkova,[129] S. K. Chan,[58] Y. L. Chan,[61a] P. Chang,[165] J. D. Chapman,[29] D. G. Charlton,[18] A. Chatterjee,[50] C. C. Chau,[158] C. A. Chavez Barajas,[149] S. Che,[111] S. Cheatham,[73] A. Chegwidden,[91] S. Chekanov,[6] S. V. Chekulaev,[159a] G. A. Chelkov,[66,k] M. A. Chelstowska,[90] C. Chen,[65] H. Chen,[26] K. Chen,[148] S. Chen,[34c] S. Chen,[155] X. Chen,[34f] Y. Chen,[68] H. C. Cheng,[90] H. J. Cheng,[34a] Y. Cheng,[32] A. Cheplakov,[66] E. Cheremushkina,[130] R. Cherkaoui El Moursli,[135e] V. Chernyatin,[26,a] E. Cheu,[7] L. Chevalier,[136] V. Chiarella,[48] G. Chiarelli,[124a,124b] G. Chiodini,[74a] A. S. Chisholm,[18] A. Chitan,[27b] M. V. Chizhov,[66] K. Choi,[62] A. R. Chomont,[35] S. Chouridou,[9] B. K. B. Chow,[100] V. Christodoulou,[79] D. Chromek-Burckhart,[31] J. Chudoba,[127] A. J. Chuinard,[88] J. J. Chwastowski,[40] L. Chytka,[115] G. Ciapetti,[132a,132b] A. K. Ciftci,[4a] D. Cinca,[54] V. Cindro,[76] I. A. Cioara,[22] A. Ciocio,[15] F. Cirotto,[104a,104b] Z. H. Citron,[171] M. Ciubancan,[27b] A. Clark,[50] B. L. Clark,[58] P. J. Clark,[47] R. N. Clarke,[15] C. Clement,[146a,146b] Y. Coadou,[86] M. Cobal,[163a,163c] A. Coccaro,[50] J. Cochran,[65] L. Coffey,[24] L. Colasurdo,[106] B. Cole,[36] S. Cole,[108] A. P. Colijn,[107] J. Collot,[56] T. Colombo,[31] G. Compostella,[101] P. Conde Muiño,[126a,126b] E. Coniavitis,[49] S. H. Connell,[145b] I. A. Connelly,[78] V. Consorti,[49] S. Constantinescu,[27b] C. Conta,[121a,121b] G. Conti,[31] F. Conventi,[104a,l] M. Cooke,[15] B. D. Cooper,[79] A. M. Cooper-Sarkar,[120] T. Cornelissen,[174] M. Corradi,[132a,132b] F. Corriveau,[88,m] A. Corso-Radu,[162] A. Cortes-Gonzalez,[12] G. Cortiana,[101] G. Costa,[92a] M. J. Costa,[166] D. Costanzo,[139] G. Cottin,[29] G. Cowan,[78] B. E. Cox,[85] K. Cranmer,[110] S. J. Crawley,[54] G. Cree,[30] S. Crépé-Renaudin,[56] F. Crescioli,[81] W. A. Cribbs,[146a,146b] M. Crispin Ortuzar,[120] M. Cristinziani,[22] V. Croft,[106] G. Crosetti,[38a,38b] T. Cuhadar Donszelmann,[139] J. Cummings,[175] M. Curatolo,[48] J. Cúth,[84] C. Cuthbert,[150] H. Czirr,[141] P. Czodrowski,[3] S. D'Auria,[54] M. D'Onofrio,[75] M. J. Da Cunha Sargedas De Sousa,[126a,126b] C. Da Via,[85] W. Dabrowski,[39a] T. Dai,[90] O. Dale,[14] F. Dallaire,[95] C. Dallapiccola,[87] M. Dam,[37] J. R. Dandoy,[32] N. P. Dang,[49] A. C. Daniells,[18] N. S. Dann,[85] M. Danninger,[167] M. Dano Hoffmann,[136] V. Dao,[49] G. Darbo,[51a] S. Darmora,[8] J. Dassoulas,[3] A. Dattagupta,[62] W. Davey,[22] C. David,[168] T. Davidek,[129] M. Davies,[153] P. Davison,[79] Y. Davygora,[59a] E. Dawe,[89] I. Dawson,[139] R. K. Daya-Ishmukhametova,[87] K. De,[8] R. de Asmundis,[104a] A. De Benedetti,[113] S. De Castro,[21a,21b] S. De Cecco,[81] N. De Groot,[106] P. de Jong,[107] H. De la Torre,[83] F. De Lorenzi,[65] D. De Pedis,[132a] A. De Salvo,[132a] U. De Sanctis,[149] A. De Santo,[149] J. B. De Vivie De Regie,[117] W. J. Dearnaley,[73] R. Debbe,[26] C. Debenedetti,[137] D. V. Dedovich,[66] I. Deigaard,[107] J. Del Peso,[83] T. Del Prete,[124a,124b] D. Delgove,[117] F. Deliot,[136] C. M. Delitzsch,[50] M. Deliyergiyev,[76] A. Dell'Acqua,[31] L. Dell'Asta,[23] M. Dell'Orso,[124a,124b] M. Della Pietra,[104a,l] D. della Volpe,[50] M. Delmastro,[5] P. A. Delsart,[56] C. Deluca,[107] D. A. DeMarco,[158] S. Demers,[175] M. Demichev,[66] A. Demilly,[81] S. P. Denisov,[130] D. Denysiuk,[136] D. Derendarz,[40] J. E. Derkaoui,[135d] F. Derue,[81] P. Dervan,[75] K. Desch,[22] C. Deterre,[43] K. Dette,[44] P. O. Deviveiros,[31] A. Dewhurst,[131] S. Dhaliwal,[24] A. Di Ciaccio,[133a,133b] L. Di Ciaccio,[5] W. K. Di Clemente,[122] A. Di Domenico,[132a,132b] C. Di Donato,[132a,132b] A. Di Girolamo,[31] B. Di Girolamo,[31] A. Di Mattia,[152] B. Di Micco,[134a,134b] R. Di Nardo,[48] A. Di Simone,[49] R. Di Sipio,[158] D. Di Valentino,[30] C. Diaconu,[86] M. Diamond,[158] F. A. Dias,[47] M. A. Diaz,[33a] E. B. Diehl,[90] J. Dietrich,[16] S. Diglio,[86] A. Dimitrievska,[13] J. Dingfelder,[22] P. Dita,[27b] S. Dita,[27b] F. Dittus,[31] F. Djama,[86] T. Djobava,[52b] J. I. Djuvsland,[59a] M. A. B. do Vale,[25c] D. Dobos,[31] M. Dobre,[27b] C. Doglioni,[82] T. Dohmae,[155] J. Dolejsi,[129] Z. Dolezal,[129] B. A. Dolgoshein,[98,a] M. Donadelli,[25d] S. Donati,[124a,124b] P. Dondero,[121a,121b] J. Donini,[35] J. Dopke,[131] A. Doria,[104a] M. T. Dova,[72] A. T. Doyle,[54] E. Drechsler,[55] M. Dris,[10] Y. Du,[34d] J. Duarte-Campderros,[153] E. Duchovni,[171] G. Duckeck,[100] O. A. Ducu,[27b] D. Duda,[107] A. Dudarev,[31] L. Duflot,[117] L. Duguid,[78] M. Dührssen,[31] M. Dunford,[59a] H. Duran Yildiz,[4a] M. Düren,[53] A. Durglishvili,[52b] D. Duschinger,[45] B. Dutta,[43] M. Dyndal,[39a] C. Eckardt,[43] K. M. Ecker,[101] R. C. Edgar,[90] W. Edson,[2] N. C. Edwards,[47] T. Eifert,[31] G. Eigen,[14] K. Einsweiler,[15] T. Ekelof,[164] M. El Kacimi,[135c] V. Ellajosyula,[86] M. Ellert,[164] S. Elles,[5] F. Ellinghaus,[174] A. A. Elliot,[168] N. Ellis,[31] J. Elmsheuser,[100] M. Elsing,[31] D. Emeliyanov,[131] Y. Enari,[155] O. C. Endner,[84] M. Endo,[118] J. S. Ennis,[169] J. Erdmann,[44] A. Ereditato,[17] G. Ernis,[174] J. Ernst,[2] M. Ernst,[26] S. Errede,[165] E. Ertel,[84] M. Escalier,[117] H. Esch,[44] C. Escobar,[125] B. Esposito,[48] A. I. Etienvre,[136] E. Etzion,[153] H. Evans,[62]

A. Ezhilov,[123] F. Fabbri,[21a,21b] L. Fabbri,[21a,21b] G. Facini,[32] R. M. Fakhrutdinov,[130] S. Falciano,[132a] R. J. Falla,[79] J. Faltova,[129] Y. Fang,[34a] M. Fanti,[92a,92b] A. Farbin,[8] A. Farilla,[134a] C. Farina,[125] T. Farooque,[12] S. Farrell,[15] S. M. Farrington,[169] P. Farthouat,[31] F. Fassi,[135e] P. Fassnacht,[31] D. Fassouliotis,[9] M. Faucci Giannelli,[78] A. Favareto,[51a,51b] L. Fayard,[117] O. L. Fedin,[123,n] W. Fedorko,[167] S. Feigl,[119] L. Feligioni,[86] C. Feng,[34d] E. J. Feng,[31] H. Feng,[90] A. B. Fenyuk,[130] L. Feremenga,[8] P. Fernandez Martinez,[166] S. Fernandez Perez,[12] J. Ferrando,[54] A. Ferrari,[164] P. Ferrari,[107] R. Ferrari,[121a] D. E. Ferreira de Lima,[54] A. Ferrer,[166] D. Ferrere,[50] C. Ferretti,[90] A. Ferretto Parodi,[51a,51b] F. Fiedler,[84] A. Filipčič,[76] M. Filipuzzi,[43] F. Filthaut,[106] M. Fincke-Keeler,[168] K. D. Finelli,[150] M. C. N. Fiolhais,[126a,126c] L. Fiorini,[166] A. Firan,[41] A. Fischer,[2] C. Fischer,[12] J. Fischer,[174] W. C. Fisher,[91] N. Flaschel,[43] I. Fleck,[141] P. Fleischmann,[90] G. T. Fletcher,[139] G. Fletcher,[77] R. R. M. Fletcher,[122] T. Flick,[174] A. Floderus,[82] L. R. Flores Castillo,[61a] M. J. Flowerdew,[101] G. T. Forcolin,[85] A. Formica,[136] A. Forti,[85] A. G. Foster,[18] D. Fournier,[117] H. Fox,[73] S. Fracchia,[12] P. Francavilla,[81] M. Franchini,[21a,21b] D. Francis,[31] L. Franconi,[119] M. Franklin,[58] M. Frate,[162] M. Fraternali,[121a,121b] D. Freeborn,[79] S. M. Fressard-Batraneanu,[31] F. Friedrich,[45] D. Froidevaux,[31] J. A. Frost,[120] C. Fukunaga,[156] E. Fullana Torregrosa,[84] T. Fusayasu,[102] J. Fuster,[166] C. Gabaldon,[56] O. Gabizon,[174] A. Gabrielli,[21a,21b] A. Gabrielli,[15] G. P. Gach,[39a] S. Gadatsch,[31] S. Gadomski,[50] G. Gagliardi,[51a,51b] L. G. Gagnon,[95] P. Gagnon,[62] C. Galea,[106] B. Galhardo,[126a,126c] E. J. Gallas,[120] B. J. Gallop,[131] P. Gallus,[128] G. Galster,[37] K. K. Gan,[111] J. Gao,[34b,86] Y. Gao,[47] Y. S. Gao,[143,g] F. M. Garay Walls,[47] C. García,[166] J. E. García Navarro,[166] M. Garcia-Sciveres,[15] R. W. Gardner,[32] N. Garelli,[143] V. Garonne,[119] A. Gascon Bravo,[43] C. Gatti,[48] A. Gaudiello,[51a,51b] G. Gaudio,[121a] B. Gaur,[141] L. Gauthier,[95] I. L. Gavrilenko,[96] C. Gay,[167] G. Gaycken,[22] E. N. Gazis,[10] Z. Gecse,[167] C. N. P. Gee,[131] Ch. Geich-Gimbel,[22] M. P. Geisler,[59a] C. Gemme,[51a] M. H. Genest,[56] C. Geng,[34b,o] S. Gentile,[132a,132b] S. George,[78] D. Gerbaudo,[162] A. Gershon,[153] S. Ghasemi,[141] H. Ghazlane,[135b] B. Giacobbe,[21a] S. Giagu,[132a,132b] P. Giannetti,[124a,124b] B. Gibbard,[26] S. M. Gibson,[78] M. Gignac,[167] M. Gilchriese,[15] T. P. S. Gillam,[29] D. Gillberg,[30] G. Gilles,[174] D. M. Gingrich,[3,e] N. Giokaris,[9] M. P. Giordani,[163a,163c] F. M. Giorgi,[21a] F. M. Giorgi,[16] P. F. Giraud,[136] P. Giromini,[58] D. Giugni,[92a] C. Giuliani,[101] M. Giulini,[59b] B. K. Gjelsten,[119] S. Gkaitatzis,[154] I. Gkialas,[154] E. L. Gkougkousis,[117] L. K. Gladilin,[99] C. Glasman,[83] J. Glatzer,[31] P. C. F. Glaysher,[47] A. Glazov,[43] M. Goblirsch-Kolb,[101] J. Godlewski,[40] S. Goldfarb,[90] T. Golling,[50] D. Golubkov,[130] A. Gomes,[126a,126b,126d] R. Gonçalo,[126a] J. Goncalves Pinto Firmino Da Costa,[136] L. Gonella,[18] A. Gongadze,[66] S. González de la Hoz,[166] G. Gonzalez Parra,[12] S. Gonzalez-Sevilla,[50] L. Goossens,[31] P. A. Gorbounov,[97] H. A. Gordon,[26] I. Gorelov,[105] B. Gorini,[31] E. Gorini,[74a,74b] A. Gorišek,[76] E. Gornicki,[40] A. T. Goshaw,[46] C. Gössling,[44] M. I. Gostkin,[66] C. R. Goudet,[117] D. Goujdami,[135c] A. G. Goussiou,[138] N. Govender,[145b] E. Gozani,[152] L. Graber,[55] I. Grabowska-Bold,[39a] P. O. J. Gradin,[164] P. Grafström,[21a,21b] J. Gramling,[50] E. Gramstad,[119] S. Grancagnolo,[16] V. Gratchev,[123] H. M. Gray,[31] E. Graziani,[134a] Z. D. Greenwood,[80,p] C. Grefe,[22] K. Gregersen,[79] I. M. Gregor,[43] P. Grenier,[143] K. Grevtsov,[5] J. Griffiths,[8] A. A. Grillo,[137] K. Grimm,[73] S. Grinstein,[12,q] Ph. Gris,[35] J.-F. Grivaz,[117] S. Groh,[84] J. P. Grohs,[45] E. Gross,[171] J. Grosse-Knetter,[55] G. C. Grossi,[80] Z. J. Grout,[149] L. Guan,[90] W. Guan,[172] J. Guenther,[128] F. Guescini,[50] D. Guest,[162] O. Gueta,[153] E. Guido,[51a,51b] T. Guillemin,[5] S. Guindon,[2] U. Gul,[54] C. Gumpert,[31] J. Guo,[34e] Y. Guo,[34b,o] S. Gupta,[120] G. Gustavino,[132a,132b] P. Gutierrez,[113] N. G. Gutierrez Ortiz,[79] C. Gutschow,[45] C. Guyot,[136] C. Gwenlan,[120] C. B. Gwilliam,[75] A. Haas,[110] C. Haber,[15] H. K. Hadavand,[8] N. Haddad,[135e] A. Hadef,[86] P. Haefner,[22] S. Hageböck,[22] Z. Hajduk,[40] H. Hakobyan,[176,a] M. Haleem,[43] J. Haley,[114] D. Hall,[120] G. Halladjian,[91] G. D. Hallewell,[86] K. Hamacher,[174] P. Hamal,[115] K. Hamano,[168] A. Hamilton,[145a] G. N. Hamity,[139] P. G. Hamnett,[43] L. Han,[34b] K. Hanagaki,[67,r] K. Hanawa,[155] M. Hance,[137] B. Haney,[122] P. Hanke,[59a] R. Hanna,[136] J. B. Hansen,[37] J. D. Hansen,[37] M. C. Hansen,[22] P. H. Hansen,[37] K. Hara,[160] A. S. Hard,[172] T. Harenberg,[174] F. Hariri,[117] S. Harkusha,[93] R. D. Harrington,[47] P. F. Harrison,[169] F. Hartjes,[107] M. Hasegawa,[68] Y. Hasegawa,[140] A. Hasib,[113] S. Hassani,[136] S. Haug,[17] R. Hauser,[91] L. Hauswald,[45] M. Havranek,[127] C. M. Hawkes,[18] R. J. Hawkings,[31] A. D. Hawkins,[82] D. Hayden,[91] C. P. Hays,[120] J. M. Hays,[77] H. S. Hayward,[75] S. J. Haywood,[131] S. J. Head,[18] T. Heck,[84] V. Hedberg,[82] L. Heelan,[8] S. Heim,[122] T. Heim,[15] B. Heinemann,[15] J. J. Heinrich,[100] L. Heinrich,[110] C. Heinz,[53] J. Hejbal,[127] L. Helary,[23] S. Hellman,[146a,146b] C. Helsens,[31] J. Henderson,[120] R. C. W. Henderson,[73] Y. Heng,[172] S. Henkelmann,[167] A. M. Henriques Correia,[31] S. Henrot-Versille,[117] G. H. Herbert,[16] Y. Hernández Jiménez,[166] G. Herten,[49] R. Hertenberger,[100] L. Hervas,[31] G. G. Hesketh,[79] N. P. Hessey,[107] J. W. Hetherly,[41] R. Hickling,[77] E. Higón-Rodriguez,[166] E. Hill,[168] J. C. Hill,[29] K. H. Hiller,[43] S. J. Hillier,[18] I. Hinchliffe,[15] E. Hines,[122] R. R. Hinman,[15] M. Hirose,[157] D. Hirschbuehl,[174] J. Hobbs,[148] N. Hod,[107] M. C. Hodgkinson,[139] P. Hodgson,[139] A. Hoecker,[31] M. R. Hoeferkamp,[105] F. Hoenig,[100] M. Hohlfeld,[84] D. Hohn,[22] T. R. Holmes,[15] M. Homann,[44] T. M. Hong,[125] B. H. Hooberman,[165] W. H. Hopkins,[116] Y. Horii,[103] A. J. Horton,[142] J-Y. Hostachy,[56] S. Hou,[151] A. Hoummada,[135a] J. Howard,[120] J. Howarth,[43]

M. Hrabovsky,[115] I. Hristova,[16] J. Hrivnac,[117] T. Hryn'ova,[5] A. Hrynevich,[94] C. Hsu,[145c] P. J. Hsu,[151,s] S.-C. Hsu,[138] D. Hu,[36] Q. Hu,[34b] Y. Huang,[43] Z. Hubacek,[128] F. Hubaut,[86] F. Huegging,[22] T. B. Huffman,[120] E. W. Hughes,[36] G. Hughes,[73] M. Huhtinen,[31] T. A. Hülsing,[84] N. Huseynov,[66,c] J. Huston,[91] J. Huth,[58] G. Iacobucci,[50] G. Iakovidis,[26] I. Ibragimov,[141] L. Iconomidou-Fayard,[117] E. Ideal,[175] Z. Idrissi,[135e] P. Iengo,[31] O. Igonkina,[107] T. Iizawa,[170] Y. Ikegami,[67] M. Ikeno,[67] Y. Ilchenko,[32,t] D. Iliadis,[154] N. Ilic,[143] T. Ince,[101] G. Introzzi,[121a,121b] P. Ioannou,[9,a] M. Iodice,[134a] K. Iordanidou,[36] V. Ippolito,[58] A. Irles Quiles,[166] C. Isaksson,[164] M. Ishino,[69] M. Ishitsuka,[157] R. Ishmukhametov,[111] C. Issever,[120] S. Istin,[19a] F. Ito,[160] J. M. Iturbe Ponce,[85] R. Iuppa,[133a,133b] J. Ivarsson,[82] W. Iwanski,[40] H. Iwasaki,[67] J. M. Izen,[42] V. Izzo,[104a] S. Jabbar,[3] B. Jackson,[122] M. Jackson,[75] P. Jackson,[1] V. Jain,[2] K. B. Jakobi,[84] K. Jakobs,[49] S. Jakobsen,[31] T. Jakoubek,[127] D. O. Jamin,[114] D. K. Jana,[80] E. Jansen,[79] R. Jansky,[63] J. Janssen,[22] M. Janus,[55] G. Jarlskog,[82] N. Javadov,[66,c] T. Javůrek,[49] F. Jeanneau,[136] L. Jeanty,[15] J. Jejelava,[52a,u] G.-Y. Jeng,[150] D. Jennens,[89] P. Jenni,[49,v] J. Jentzsch,[44] C. Jeske,[169] S. Jézéquel,[5] H. Ji,[172] J. Jia,[148] H. Jiang,[65] Y. Jiang,[34b] S. Jiggins,[79] J. Jimenez Pena,[166] S. Jin,[34a] A. Jinaru,[27b] O. Jinnouchi,[157] P. Johansson,[139] K. A. Johns,[7] W. J. Johnson,[138] K. Jon-And,[146a,146b] G. Jones,[169] R. W. L. Jones,[73] S. Jones,[7] T. J. Jones,[75] J. Jongmanns,[59a] P. M. Jorge,[126a,126b] J. Jovicevic,[159a] X. Ju,[172] A. Juste Rozas,[12,q] M. K. Köhler,[171] A. Kaczmarska,[40] M. Kado,[117] H. Kagan,[111] M. Kagan,[143] S. J. Kahn,[86] E. Kajomovitz,[46] C. W. Kalderon,[120] A. Kaluza,[84] S. Kama,[41] A. Kamenshchikov,[130] N. Kanaya,[155] S. Kaneti,[29] V. A. Kantserov,[98] J. Kanzaki,[67] B. Kaplan,[110] L. S. Kaplan,[172] A. Kapliy,[32] D. Kar,[145c] K. Karakostas,[10] A. Karamaoun,[3] N. Karastathis,[10] M. J. Kareem,[55] E. Karentzos,[10] M. Karnevskiy,[84] S. N. Karpov,[66] Z. M. Karpova,[66] K. Karthik,[110] V. Kartvelishvili,[73] A. N. Karyukhin,[130] K. Kasahara,[160] L. Kashif,[172] R. D. Kass,[111] A. Kastanas,[14] Y. Kataoka,[155] C. Kato,[155] A. Katre,[50] J. Katzy,[43] K. Kawade,[103] K. Kawagoe,[71] T. Kawamoto,[155] G. Kawamura,[55] S. Kazama,[155] V. F. Kazanin,[109,d] R. Keeler,[168] R. Kehoe,[41] J. S. Keller,[43] J. J. Kempster,[78] H. Keoshkerian,[85] O. Kepka,[127] B. P. Kerševan,[76] S. Kersten,[174] R. A. Keyes,[88] F. Khalil-zada,[11] H. Khandanyan,[146a,146b] A. Khanov,[114] A. G. Kharlamov,[109,d] T. J. Khoo,[29] V. Khovanskiy,[97] E. Khramov,[66] J. Khubua,[52b,w] S. Kido,[68] H. Y. Kim,[8] S. H. Kim,[160] Y. K. Kim,[32] N. Kimura,[154] O. M. Kind,[16] B. T. King,[75] M. King,[166] S. B. King,[167] J. Kirk,[131] A. E. Kiryunin,[101] T. Kishimoto,[68] D. Kisielewska,[39a] F. Kiss,[49] K. Kiuchi,[160] O. Kivernyk,[136] E. Kladiva,[144b] M. H. Klein,[36] M. Klein,[75] U. Klein,[75] K. Kleinknecht,[84] P. Klimek,[146a,146b] A. Klimentov,[26] R. Klingenberg,[44] J. A. Klinger,[139] T. Klioutchnikova,[31] E.-E. Kluge,[59a] P. Kluit,[107] S. Kluth,[101] J. Knapik,[40] E. Kneringer,[63] E.B.F.G. Knoops,[86] A. Knue,[54] A. Kobayashi,[155] D. Kobayashi,[157] T. Kobayashi,[155] M. Kobel,[45] M. Kocian,[143] P. Kodys,[129] T. Koffas,[30] E. Koffeman,[107] L. A. Kogan,[120] T. Kohriki,[67] T. Koi,[143] H. Kolanoski,[16] M. Kolb,[59b] I. Koletsou,[5] A. A. Komar,[96,a] Y. Komori,[155] T. Kondo,[67] N. Kondrashova,[43] K. Köneke,[49] A. C. König,[106] T. Kono,[67,x] R. Konoplich,[110,y] N. Konstantinidis,[79] R. Kopeliansky,[62] S. Koperny,[39a] L. Köpke,[84] A. K. Kopp,[49] K. Korcyl,[40] K. Kordas,[154] A. Korn,[79] A. A. Korol,[109,d] I. Korolkov,[12] E. V. Korolkova,[139] O. Kortner,[101] S. Kortner,[101] T. Kosek,[129] V. V. Kostyukhin,[22] V. M. Kotov,[66] A. Kotwal,[46] A. Kourkoumeli-Charalampidi,[154] C. Kourkoumelis,[9] V. Kouskoura,[26] A. Koutsman,[159a] A. B. Kowalewska,[40] R. Kowalewski,[168] T. Z. Kowalski,[39a] W. Kozanecki,[136] A. S. Kozhin,[130] V. A. Kramarenko,[99] G. Kramberger,[76] D. Krasnopevtsev,[98] M. W. Krasny,[81] A. Krasznahorkay,[31] J. K. Kraus,[22] A. Kravchenko,[26] M. Kretz,[59c] J. Kretzschmar,[75] K. Kreutzfeldt,[53] P. Krieger,[158] K. Krizka,[32] K. Kroeninger,[44] H. Kroha,[101] J. Kroll,[122] J. Kroseberg,[22] J. Krstic,[13] U. Kruchonak,[66] H. Krüger,[22] N. Krumnack,[65] A. Kruse,[172] M. C. Kruse,[46] M. Kruskal,[23] T. Kubota,[89] H. Kucuk,[79] S. Kuday,[4b] J. T. Kuechler,[174] S. Kuehn,[49] A. Kugel,[59c] F. Kuger,[173] A. Kuhl,[137] T. Kuhl,[43] V. Kukhtin,[66] R. Kukla,[136] Y. Kulchitsky,[93] S. Kuleshov,[33b] M. Kuna,[132a,132b] T. Kunigo,[69] A. Kupco,[127] H. Kurashige,[68] Y. A. Kurochkin,[93] V. Kus,[127] E. S. Kuwertz,[168] M. Kuze,[157] J. Kvita,[115] T. Kwan,[168] D. Kyriazopoulos,[139] A. La Rosa,[101] J. L. La Rosa Navarro,[25d] L. La Rotonda,[38a,38b] C. Lacasta,[166] F. Lacava,[132a,132b] J. Lacey,[30] H. Lacker,[16] D. Lacour,[81] V. R. Lacuesta,[166] E. Ladygin,[66] R. Lafaye,[5] B. Laforge,[81] T. Lagouri,[175] S. Lai,[55] S. Lammers,[62] W. Lampl,[7] E. Lançon,[136] U. Landgraf,[49] M. P. J. Landon,[77] V. S. Lang,[59a] J. C. Lange,[12] A. J. Lankford,[162] F. Lanni,[26] K. Lantzsch,[22] A. Lanza,[121a] S. Laplace,[81] C. Lapoire,[31] J. F. Laporte,[136] T. Lari,[92a] F. Lasagni Manghi,[21a,21b] M. Lassnig,[31] P. Laurelli,[48] W. Lavrijsen,[15] A. T. Law,[137] P. Laycock,[75] T. Lazovich,[58] M. Lazzaroni,[92a,92b] O. Le Dortz,[81] E. Le Guirriec,[86] E. Le Menedeu,[12] E. P. Le Quilleuc,[136] M. LeBlanc,[168] T. LeCompte,[6] F. Ledroit-Guillon,[56] C. A. Lee,[26] S. C. Lee,[151] L. Lee,[1] G. Lefebvre,[81] M. Lefebvre,[168] F. Legger,[100] C. Leggett,[15] A. Lehan,[75] G. Lehmann Miotto,[31] X. Lei,[7] W. A. Leight,[30] A. Leisos,[154,z] A. G. Leister,[175] M. A. L. Leite,[25d] R. Leitner,[129] D. Lellouch,[171] B. Lemmer,[55] K. J. C. Leney,[79] T. Lenz,[22] B. Lenzi,[31] R. Leone,[7] S. Leone,[124a,124b] C. Leonidopoulos,[47] S. Leontsinis,[10] G. Lerner,[149] C. Leroy,[95] A. A. J. Lesage,[136] C. G. Lester,[29] M. Levchenko,[123] J. Levêque,[5] D. Levin,[90] L. J. Levinson,[171] M. Levy,[18] A. M. Leyko,[22] M. Leyton,[42] B. Li,[34b,aa] H. Li,[148] H. L. Li,[32] L. Li,[46] L. Li,[34e] Q. Li,[34a] S. Li,[46] X. Li,[85] Y. Li,[141] Z. Liang,[137] H. Liao,[35] B. Liberti,[133a] A. Liblong,[158] P. Lichard,[31] K. Lie,[165]

J. Liebal,[22] W. Liebig,[14] C. Limbach,[22] A. Limosani,[150] S. C. Lin,[151,bb] T. H. Lin,[84] B. E. Lindquist,[148] E. Lipeles,[122] A. Lipniacka,[14] M. Lisovyi,[59b] T. M. Liss,[165] D. Lissauer,[26] A. Lister,[167] A. M. Litke,[137] B. Liu,[151,cc] D. Liu,[151] H. Liu,[90] H. Liu,[26] J. Liu,[86] J. B. Liu,[34b] K. Liu,[86] L. Liu,[165] M. Liu,[46] M. Liu,[34b] Y. L. Liu,[34b] Y. Liu,[34b] M. Livan,[121a,121b] A. Lleres,[56] J. Llorente Merino,[83] S. L. Lloyd,[77] F. Lo Sterzo,[151] E. Lobodzinska,[43] P. Loch,[7] W. S. Lockman,[137] F. K. Loebinger,[85] A. E. Loevschall-Jensen,[37] K. M. Loew,[24] A. Loginov,[175] T. Lohse,[16] K. Lohwasser,[43] M. Lokajicek,[127] B. A. Long,[23] J. D. Long,[165] R. E. Long,[73] L. Longo,[74a,74b] K. A. Looper,[111] L. Lopes,[126a] D. Lopez Mateos,[58] B. Lopez Paredes,[139] I. Lopez Paz,[12] A. Lopez Solis,[81] J. Lorenz,[100] N. Lorenzo Martinez,[62] M. Losada,[20] P. J. Lösel,[100] X. Lou,[34a] A. Lounis,[117] J. Love,[6] P. A. Love,[73] H. Lu,[61a] N. Lu,[90] H. J. Lubatti,[138] C. Luci,[132a,132b] A. Lucotte,[56] C. Luedtke,[49] F. Luehring,[62] W. Lukas,[63] L. Luminari,[132a] O. Lundberg,[146a,146b] B. Lund-Jensen,[147] D. Lynn,[26] R. Lysak,[127] E. Lytken,[82] V. Lyubushkin,[66] H. Ma,[26] L. L. Ma,[34d] G. Maccarrone,[48] A. Macchiolo,[101] C. M. Macdonald,[139] B. Maček,[76] J. Machado Miguens,[122,126b] D. Madaffari,[86] R. Madar,[35] H. J. Maddocks,[164] W. F. Mader,[45] A. Madsen,[43] J. Maeda,[68] S. Maeland,[14] T. Maeno,[26] A. Maevskiy,[99] E. Magradze,[55] J. Mahlstedt,[107] C. Maiani,[117] C. Maidantchik,[25a] A. A. Maier,[101] T. Maier,[100] A. Maio,[126a,126b,126d] S. Majewski,[116] Y. Makida,[67] N. Makovec,[117] B. Malaescu,[81] Pa. Malecki,[40] V. P. Maleev,[123] F. Malek,[56] U. Mallik,[64] D. Malon,[6] C. Malone,[143] S. Maltezos,[10] V. M. Malyshev,[109] S. Malyukov,[31] J. Mamuzic,[43] G. Mancini,[48] B. Mandelli,[31] L. Mandelli,[92a] I. Mandić,[76] J. Maneira,[126a,126b] L. Manhaes de Andrade Filho,[25b] J. Manjarres Ramos,[159b] A. Mann,[100] B. Mansoulie,[136] R. Mantifel,[88] M. Mantoani,[55] S. Manzoni,[92a,92b] L. Mapelli,[31] G. Marceca,[28] L. March,[50] G. Marchiori,[81] M. Marcisovsky,[127] M. Marjanovic,[13] D. E. Marley,[90] F. Marroquim,[25a] S. P. Marsden,[85] Z. Marshall,[15] L. F. Marti,[17] S. Marti-Garcia,[166] B. Martin,[91] T. A. Martin,[169] V. J. Martin,[47] B. Martin dit Latour,[14] M. Martinez,[12,q] S. Martin-Haugh,[131] V. S. Martoiu,[27b] A. C. Martyniuk,[79] M. Marx,[138] F. Marzano,[132a] A. Marzin,[31] L. Masetti,[84] T. Mashimo,[155] R. Mashinistov,[96] J. Masik,[85] A. L. Maslennikov,[109,d] I. Massa,[21a,21b] L. Massa,[21a,21b] P. Mastrandrea,[5] A. Mastroberardino,[38a,38b] T. Masubuchi,[155] P. Mättig,[174] J. Mattmann,[84] J. Maurer,[27b] S. J. Maxfield,[75] D. A. Maximov,[109,d] R. Mazini,[151] S. M. Mazza,[92a,92b] N. C. Mc Fadden,[105] G. Mc Goldrick,[158] S. P. Mc Kee,[90] A. McCarn,[90] R. L. McCarthy,[148] T. G. McCarthy,[30] L. I. McClymont,[79] K. W. McFarlane,[57,a] J. A. Mcfayden,[79] G. Mchedlidze,[55] S. J. McMahon,[131] R. A. McPherson,[168,m] M. Medinnis,[43] S. Meehan,[138] S. Mehlhase,[100] A. Mehta,[75] K. Meier,[59a] C. Meineck,[100] B. Meirose,[42] B. R. Mellado Garcia,[145c] F. Meloni,[17] A. Mengarelli,[21a,21b] S. Menke,[101] E. Meoni,[161] K. M. Mercurio,[58] S. Mergelmeyer,[16] P. Mermod,[50] L. Merola,[104a,104b] C. Meroni,[92a] F. S. Merritt,[32] A. Messina,[132a,132b] J. Metcalfe,[6] A. S. Mete,[162] C. Meyer,[84] C. Meyer,[122] J-P. Meyer,[136] J. Meyer,[107] H. Meyer Zu Theenhausen,[59a] R. P. Middleton,[131] S. Miglioranzi,[163a,163c] L. Mijović,[22] G. Mikenberg,[171] M. Mikestikova,[127] M. Mikuž,[76] M. Milesi,[89] A. Milic,[31] D. W. Miller,[32] C. Mills,[47] A. Milov,[171] D. A. Milstead,[146a,146b] A. A. Minaenko,[130] Y. Minami,[155] I. A. Minashvili,[66] A. I. Mincer,[110] B. Mindur,[39a] M. Mineev,[66] Y. Ming,[172] L. M. Mir,[12] K. P. Mistry,[122] T. Mitani,[170] J. Mitrevski,[100] V. A. Mitsou,[166] A. Miucci,[50] P. S. Miyagawa,[139] J. U. Mjörnmark,[82] T. Moa,[146a,146b] K. Mochizuki,[86] S. Mohapatra,[36] W. Mohr,[49] S. Molander,[146a,146b] R. Moles-Valls,[22] R. Monden,[69] M. C. Mondragon,[91] K. Mönig,[43] J. Monk,[37] E. Monnier,[86] A. Montalbano,[148] J. Montejo Berlingen,[31] F. Monticelli,[72] S. Monzani,[92a,92b] R. W. Moore,[3] N. Morange,[117] D. Moreno,[20] M. Moreno Llácer,[55] P. Morettini,[51a] D. Mori,[142] T. Mori,[155] M. Morii,[58] M. Morinaga,[155] V. Morisbak,[119] S. Moritz,[84] A. K. Morley,[150] G. Mornacchi,[31] J. D. Morris,[77] S. S. Mortensen,[37] L. Morvaj,[148] M. Mosidze,[52b] J. Moss,[143] K. Motohashi,[157] R. Mount,[143] E. Mountricha,[26] S. V. Mouraviev,[96,a] E. J. W. Moyse,[87] S. Muanza,[86] R. D. Mudd,[18] F. Mueller,[101] J. Mueller,[125] R. S. P. Mueller,[100] T. Mueller,[29] D. Muenstermann,[73] P. Mullen,[54] G. A. Mullier,[17] F. J. Munoz Sanchez,[85] J. A. Murillo Quijada,[18] W. J. Murray,[169,131] H. Musheghyan,[55] A. G. Myagkov,[130,dd] M. Myska,[128] B. P. Nachman,[143] O. Nackenhorst,[50] J. Nadal,[55] K. Nagai,[120] R. Nagai,[67,x] Y. Nagai,[86] K. Nagano,[67] Y. Nagasaka,[60] K. Nagata,[160] M. Nagel,[101] E. Nagy,[86] A. M. Nairz,[31] Y. Nakahama,[31] K. Nakamura,[67] T. Nakamura,[155] I. Nakano,[112] H. Namasivayam,[42] R. F. Naranjo Garcia,[43] R. Narayan,[32] D. I. Narrias Villar,[59a] I. Naryshkin,[123] T. Naumann,[43] G. Navarro,[20] R. Nayyar,[7] H. A. Neal,[90] P.Yu. Nechaeva,[96] T. J. Neep,[85] P. D. Nef,[143] A. Negri,[121a,121b] M. Negrini,[21a] S. Nektarijevic,[106] C. Nellist,[117] A. Nelson,[162] S. Nemecek,[127] P. Nemethy,[110] A. A. Nepomuceno,[25a] M. Nessi,[31,ee] M. S. Neubauer,[165] M. Neumann,[174] R. M. Neves,[110] P. Nevski,[26] P. R. Newman,[18] D. H. Nguyen,[6] R. B. Nickerson,[120] R. Nicolaidou,[136] B. Nicquevert,[31] J. Nielsen,[137] A. Nikiforov,[16] V. Nikolaenko,[130,dd] I. Nikolic-Audit,[81] K. Nikolopoulos,[18] J. K. Nilsen,[119] P. Nilsson,[26] Y. Ninomiya,[155] A. Nisati,[132a] R. Nisius,[101] T. Nobe,[155] L. Nodulman,[6] M. Nomachi,[118] I. Nomidis,[30] T. Nooney,[77] S. Norberg,[113] M. Nordberg,[31] N. Norjoharuddeen,[120] O. Novgorodova,[45] S. Nowak,[101] M. Nozaki,[67] L. Nozka,[115] K. Ntekas,[10] E. Nurse,[79] F. Nuti,[89] F. O'grady,[7] D. C. O'Neil,[142] A. A. O'Rourke,[43] V. O'Shea,[54] F. G. Oakham,[30,e] H. Oberlack,[101] T. Obermann,[22] J. Ocariz,[81] A. Ochi,[68] I. Ochoa,[36] J. P. Ochoa-Ricoux,[33a] S. Oda,[71] S. Odaka,[67] H. Ogren,[62]

A. Oh,[85] S. H. Oh,[46] C. C. Ohm,[15] H. Ohman,[164] H. Oide,[31] H. Okawa,[160] Y. Okumura,[32] T. Okuyama,[67] A. Olariu,[27b] L. F. Oleiro Seabra,[126a] S. A. Olivares Pino,[47] D. Oliveira Damazio,[26] A. Olszewski,[40] J. Olszowska,[40] A. Onofre,[126a,126e] K. Onogi,[103] P. U. E. Onyisi,[32,t] C. J. Oram,[159a] M. J. Oreglia,[32] Y. Oren,[153] D. Orestano,[134a,134b] N. Orlando,[61b] R. S. Orr,[158] B. Osculati,[51a,51b] R. Ospanov,[85] G. Otero y Garzon,[28] H. Otono,[71] M. Ouchrif,[135d] F. Ould-Saada,[119] A. Ouraou,[136] K. P. Oussoren,[107] Q. Ouyang,[34a] A. Ovcharova,[15] M. Owen,[54] R. E. Owen,[18] V. E. Ozcan,[19a] N. Ozturk,[8] K. Pachal,[142] A. Pacheco Pages,[12] C. Padilla Aranda,[12] M. Pagáčová,[49] S. Pagan Griso,[15] F. Paige,[26] P. Pais,[87] K. Pajchel,[119] G. Palacino,[159b] S. Palestini,[31] M. Palka,[39b] D. Pallin,[35] A. Palma,[126a,126b] E.St. Panagiotopoulou,[10] C. E. Pandini,[81] J. G. Panduro Vazquez,[78] P. Pani,[146a,146b] S. Panitkin,[26] D. Pantea,[27b] L. Paolozzi,[50] Th.D. Papadopoulou,[10] K. Papageorgiou,[154] A. Paramonov,[6] D. Paredes Hernandez,[175] M. A. Parker,[29] K. A. Parker,[139] F. Parodi,[51a,51b] J. A. Parsons,[36] U. Parzefall,[49] V. R. Pascuzzi,[158] E. Pasqualucci,[132a] S. Passaggio,[51a] F. Pastore,[134a,134b,a] Fr. Pastore,[78] G. Pásztor,[30] S. Pataraia,[174] N. D. Patel,[150] J. R. Pater,[85] T. Pauly,[31] J. Pearce,[168] B. Pearson,[113] L. E. Pedersen,[37] M. Pedersen,[119] S. Pedraza Lopez,[166] R. Pedro,[126a,126b] S. V. Peleganchuk,[109,d] D. Pelikan,[164] O. Penc,[127] C. Peng,[34a] H. Peng,[34b] J. Penwell,[62] B. S. Peralva,[25b] M. M. Perego,[136] D. V. Perepelitsa,[26] E. Perez Codina,[159a] L. Perini,[92a,92b] H. Pernegger,[31] S. Perrella,[104a,104b] R. Peschke,[43] V. D. Peshekhonov,[66] K. Peters,[31] R. F. Y. Peters,[85] B. A. Petersen,[31] T. C. Petersen,[37] E. Petit,[56] A. Petridis,[1] C. Petridou,[154] P. Petroff,[117] E. Petrolo,[132a] M. Petrov,[120] F. Petrucci,[134a,134b] N. E. Pettersson,[157] A. Peyaud,[136] R. Pezoa,[33b] P. W. Phillips,[131] G. Piacquadio,[143] E. Pianori,[169] A. Picazio,[87] E. Piccaro,[77] M. Piccinini,[21a,21b] M. A. Pickering,[120] R. Piegaia,[28] J. E. Pilcher,[32] A. D. Pilkington,[85] A. W. J. Pin,[85] J. Pina,[126a,126b,126d] M. Pinamonti,[163a,163c,ff] J. L. Pinfold,[3] A. Pingel,[37] S. Pires,[81] H. Pirumov,[43] M. Pitt,[171] L. Plazak,[144a] M.-A. Pleier,[26] V. Pleskot,[84] E. Plotnikova,[66] P. Plucinski,[146a,146b] D. Pluth,[65] R. Poettgen,[146a,146b] L. Poggioli,[117] D. Pohl,[22] G. Polesello,[121a] A. Poley,[43] A. Policicchio,[38a,38b] R. Polifka,[158] A. Polini,[21a] C. S. Pollard,[54] V. Polychronakos,[26] K. Pommès,[31] L. Pontecorvo,[132a] B. G. Pope,[91] G. A. Popeneciu,[27c] D. S. Popovic,[13] A. Poppleton,[31] S. Pospisil,[128] K. Potamianos,[15] I. N. Potrap,[66] C. J. Potter,[29] C. T. Potter,[116] G. Poulard,[31] J. Poveda,[31] V. Pozdnyakov,[66] M. E. Pozo Astigarraga,[31] P. Pralavorio,[86] A. Pranko,[15] S. Prell,[65] D. Price,[85] L. E. Price,[6] M. Primavera,[74a] S. Prince,[88] M. Proissl,[47] K. Prokofiev,[61c] F. Prokoshin,[33b] S. Protopopescu,[26] J. Proudfoot,[6] M. Przybycien,[39a] D. Puddu,[134a,134b] D. Puldon,[148] M. Purohit,[26,gg] P. Puzo,[117] J. Qian,[90] G. Qin,[54] Y. Qin,[85] A. Quadt,[55] D. R. Quarrie,[15] W. B. Quayle,[163a,163b] M. Queitsch-Maitland,[85] D. Quilty,[54] S. Raddum,[119] V. Radeka,[26] V. Radescu,[59b] S. K. Radhakrishnan,[148] P. Radloff,[116] P. Rados,[89] F. Ragusa,[92a,92b] G. Rahal,[177] S. Rajagopalan,[26] M. Rammensee,[31] C. Rangel-Smith,[164] M. G. Ratti,[92a,92b] F. Rauscher,[100] S. Rave,[84] T. Ravenscroft,[54] M. Raymond,[31] A. L. Read,[119] N. P. Readioff,[75] D. M. Rebuzzi,[121a,121b] A. Redelbach,[173] G. Redlinger,[26] R. Reece,[137] K. Reeves,[42] L. Rehnisch,[16] J. Reichert,[122] H. Reisin,[28] C. Rembser,[31] H. Ren,[34a] M. Rescigno,[132a] S. Resconi,[92a] O. L. Rezanova,[109,d] P. Reznicek,[129] R. Rezvani,[95] R. Richter,[101] S. Richter,[79] E. Richter-Was,[39b] O. Ricken,[22] M. Ridel,[81] P. Rieck,[16] C. J. Riegel,[174] J. Rieger,[55] O. Rifki,[113] M. Rijssenbeek,[148] A. Rimoldi,[121a,121b] L. Rinaldi,[21a] B. Ristić,[50] E. Ritsch,[31] I. Riu,[12] F. Rizatdinova,[114] E. Rizvi,[77] C. Rizzi,[12] S. H. Robertson,[88,m] A. Robichaud-Veronneau,[88] D. Robinson,[29] J. E. M. Robinson,[43] A. Robson,[54] C. Roda,[124a,124b] Y. Rodina,[86] A. Rodriguez Perez,[12] D. Rodriguez Rodriguez,[166] S. Roe,[31] C. S. Rogan,[58] O. Røhne,[119] A. Romaniouk,[98] M. Romano,[21a,21b] S. M. Romano Saez,[35] E. Romero Adam,[166] N. Rompotis,[138] M. Ronzani,[49] L. Roos,[81] E. Ros,[166] S. Rosati,[132a] K. Rosbach,[49] P. Rose,[137] O. Rosenthal,[141] V. Rossetti,[146a,146b] E. Rossi,[104a,104b] L. P. Rossi,[51a] J. H. N. Rosten,[29] R. Rosten,[138] M. Rotaru,[27b] I. Roth,[171] J. Rothberg,[138] D. Rousseau,[117] C. R. Royon,[136] A. Rozanov,[86] Y. Rozen,[152] X. Ruan,[145c] F. Rubbo,[143] I. Rubinskiy,[43] V. I. Rud,[99] M. S. Rudolph,[158] F. Rühr,[49] A. Ruiz-Martinez,[31] Z. Rurikova,[49] N. A. Rusakovich,[66] A. Ruschke,[100] H. L. Russell,[138] J. P. Rutherfoord,[7] N. Ruthmann,[31] Y. F. Ryabov,[123] M. Rybar,[165] G. Rybkin,[117] S. Ryu,[6] A. Ryzhov,[130] A. F. Saavedra,[150] G. Sabato,[107] S. Sacerdoti,[28] H.F-W. Sadrozinski,[137] R. Sadykov,[66] F. Safai Tehrani,[132a] P. Saha,[108] M. Sahinsoy,[59a] M. Saimpert,[136] T. Saito,[155] H. Sakamoto,[155] Y. Sakurai,[170] G. Salamanna,[134a,134b] A. Salamon,[133a,133b] J. E. Salazar Loyola,[33b] D. Salek,[107] P. H. Sales De Bruin,[138] D. Salihagic,[101] A. Salnikov,[143] J. Salt,[166] D. Salvatore,[38a,38b] F. Salvatore,[149] A. Salvucci,[61a] A. Salzburger,[31] D. Sammel,[49] D. Sampsonidis,[154] A. Sanchez,[104a,104b] J. Sánchez,[166] V. Sanchez Martinez,[166] H. Sandaker,[119] R. L. Sandbach,[77] H. G. Sander,[84] M. P. Sanders,[100] M. Sandhoff,[174] C. Sandoval,[20] R. Sandstroem,[101] D. P. C. Sankey,[131] M. Sannino,[51a,51b] A. Sansoni,[48] C. Santoni,[35] R. Santonico,[133a,133b] H. Santos,[126a] I. Santoyo Castillo,[149] K. Sapp,[125] A. Sapronov,[66] J. G. Saraiva,[126a,126d] B. Sarrazin,[22] O. Sasaki,[67] Y. Sasaki,[155] K. Sato,[160] G. Sauvage,[5,a] E. Sauvan,[5] G. Savage,[78] P. Savard,[158,e] C. Sawyer,[131] L. Sawyer,[80,p] J. Saxon,[32] C. Sbarra,[21a] A. Sbrizzi,[21a,21b] T. Scanlon,[79] D. A. Scannicchio,[162] M. Scarcella,[150] V. Scarfone,[38a,38b] J. Schaarschmidt,[171] P. Schacht,[101] D. Schaefer,[31] R. Schaefer,[43] J. Schaeffer,[84]

S. Schaepe,[22] S. Schaetzel,[59b] U. Schäfer,[84] A. C. Schaffer,[117] D. Schaile,[100] R. D. Schamberger,[148] V. Scharf,[59a] V. A. Schegelsky,[123] D. Scheirich,[129] M. Schernau,[162] C. Schiavi,[51a,51b] C. Schillo,[49] M. Schioppa,[38a,38b] S. Schlenker,[31] K. Schmieden,[31] C. Schmitt,[84] S. Schmitt,[43] S. Schmitz,[84] B. Schneider,[159a] Y. J. Schnellbach,[75] U. Schnoor,[49] L. Schoeffel,[136] A. Schoening,[59b] B. D. Schoenrock,[91] E. Schopf,[22] A. L. S. Schorlemmer,[44] M. Schott,[84] D. Schouten,[159a] J. Schovancova,[8] S. Schramm,[50] M. Schreyer,[173] N. Schuh,[84] M. J. Schultens,[22] H.-C. Schultz-Coulon,[59a] H. Schulz,[16] M. Schumacher,[49] B. A. Schumm,[137] Ph. Schune,[136] C. Schwanenberger,[85] A. Schwartzman,[143] T. A. Schwarz,[90] Ph. Schwegler,[101] H. Schweiger,[85] Ph. Schwemling,[136] R. Schwienhorst,[91] J. Schwindling,[136] T. Schwindt,[22] G. Sciolla,[24] F. Scuri,[124a,124b] F. Scutti,[89] J. Searcy,[90] P. Seema,[22] S. C. Seidel,[105] A. Seiden,[137] F. Seifert,[128] J. M. Seixas,[25a] G. Sekhniaidze,[104a] K. Sekhon,[90] S. J. Sekula,[41] D. M. Seliverstov,[123,a] N. Semprini-Cesari,[21a,21b] C. Serfon,[119] L. Serin,[117] L. Serkin,[163a,163b] M. Sessa,[134a,134b] R. Seuster,[159a] H. Severini,[113] T. Sfiligoj,[76] F. Sforza,[31] A. Sfyrla,[50] E. Shabalina,[55] N. W. Shaikh,[146a,146b] L. Y. Shan,[34a] R. Shang,[165] J. T. Shank,[23] M. Shapiro,[15] P. B. Shatalov,[97] K. Shaw,[163a,163b] S. M. Shaw,[85] A. Shcherbakova,[146a,146b] C. Y. Shehu,[149] P. Sherwood,[79] L. Shi,[151,hh] S. Shimizu,[68] C. O. Shimmin,[162] M. Shimojima,[102] M. Shiyakova,[66,ii] A. Shmeleva,[96] D. Shoaleh Saadi,[95] M. J. Shochet,[32] S. Shojaii,[92a,92b] S. Shrestha,[111] E. Shulga,[98] M. A. Shupe,[7] P. Sicho,[127] P. E. Sidebo,[147] O. Sidiropoulou,[173] D. Sidorov,[114] A. Sidoti,[21a,21b] F. Siegert,[45] Dj. Sijacki,[13] J. Silva,[126a,126d] S. B. Silverstein,[146a] V. Simak,[128] O. Simard,[5] Lj. Simic,[13] S. Simion,[117] E. Simioni,[84] B. Simmons,[79] D. Simon,[35] M. Simon,[84] P. Sinervo,[158] N. B. Sinev,[116] M. Sioli,[21a,21b] G. Siragusa,[173] S.Yu. Sivoklokov,[99] J. Sjölin,[146a,146b] T. B. Sjursen,[14] M. B. Skinner,[73] H. P. Skottowe,[58] P. Skubic,[113] M. Slater,[18] T. Slavicek,[128] M. Slawinska,[107] K. Sliwa,[161] R. Slovak,[129] V. Smakhtin,[171] B. H. Smart,[5] L. Smestad,[14] S.Yu. Smirnov,[98] Y. Smirnov,[98] L. N. Smirnova,[99,jj] O. Smirnova,[82] M. N. K. Smith,[36] R. W. Smith,[36] M. Smizanska,[73] K. Smolek,[128] A. A. Snesarev,[96] G. Snidero,[77] S. Snyder,[26] R. Sobie,[168,m] F. Socher,[45] A. Soffer,[153] D. A. Soh,[151,hh] G. Sokhrannyi,[76] C. A. Solans Sanchez,[31] M. Solar,[128] E.Yu. Soldatov,[98] U. Soldevila,[166] A. A. Solodkov,[130] A. Soloshenko,[66] O. V. Solovyanov,[130] V. Solovyev,[123] P. Sommer,[49] H. Son,[161] H. Y. Song,[34b,aa] N. Soni,[1] A. Sood,[15] A. Sopczak,[128] V. Sopko,[128] V. Sorin,[12] D. Sosa,[59b] C. L. Sotiropoulou,[124a,124b] R. Soualah,[163a,163c] A. M. Soukharev,[109,d] D. South,[43] B. C. Sowden,[78] S. Spagnolo,[74a,74b] M. Spalla,[124a,124b] M. Spangenberg,[169] F. Spanò,[78] D. Sperlich,[16] F. Spettel,[101] R. Spighi,[21a] G. Spigo,[31] L. A. Spiller,[89] M. Spousta,[129] R. D. St. Denis,[54,a] A. Stabile,[92a] S. Staerz,[31] J. Stahlman,[122] R. Stamen,[59a] S. Stamm,[16] E. Stanecka,[40] R. W. Stanek,[6] C. Stanescu,[134a] M. Stanescu-Bellu,[43] M. M. Stanitzki,[43] S. Stapnes,[119] E. A. Starchenko,[130] G. H. Stark,[32] J. Stark,[56] P. Staroba,[127] P. Starovoitov,[59a] R. Staszewski,[40] P. Steinberg,[26] B. Stelzer,[142] H. J. Stelzer,[31] O. Stelzer-Chilton,[159a] H. Stenzel,[53] G. A. Stewart,[54] J. A. Stillings,[22] M. C. Stockton,[88] M. Stoebe,[88] G. Stoicea,[27b] P. Stolte,[55] S. Stonjek,[101] A. R. Stradling,[8] A. Straessner,[45] M. E. Stramaglia,[17] J. Strandberg,[147] S. Strandberg,[146a,146b] A. Strandlie,[119] M. Strauss,[113] P. Strizenec,[144b] R. Ströhmer,[173] D. M. Strom,[116] R. Stroynowski,[41] A. Strubig,[106] S. A. Stucci,[17] B. Stugu,[14] N. A. Styles,[43] D. Su,[143] J. Su,[125] R. Subramaniam,[80] S. Suchek,[59a] Y. Sugaya,[118] M. Suk,[128] V. V. Sulin,[96] S. Sultansoy,[4c] T. Sumida,[69] S. Sun,[58] X. Sun,[34a] J. E. Sundermann,[49] K. Suruliz,[149] G. Susinno,[38a,38b] M. R. Sutton,[149] S. Suzuki,[67] M. Svatos,[127] M. Swiatlowski,[32] I. Sykora,[144a] T. Sykora,[129] D. Ta,[49] C. Taccini,[134a,134b] K. Tackmann,[43] J. Taenzer,[158] A. Taffard,[162] R. Tafirout,[159a] N. Taiblum,[153] H. Takai,[26] R. Takashima,[70] H. Takeda,[68] T. Takeshita,[140] Y. Takubo,[67] M. Talby,[86] A. A. Talyshev,[109,d] J. Y. C. Tam,[173] K. G. Tan,[89] J. Tanaka,[155] R. Tanaka,[117] S. Tanaka,[67] B. B. Tannenwald,[111] S. Tapia Araya,[33b] S. Tapprogge,[84] S. Tarem,[152] G. F. Tartarelli,[92a] P. Tas,[129] M. Tasevsky,[127] T. Tashiro,[69] E. Tassi,[38a,38b] A. Tavares Delgado,[126a,126b] Y. Tayalati,[135d] A. C. Taylor,[105] G. N. Taylor,[89] P. T. E. Taylor,[89] W. Taylor,[159b] F. A. Teischinger,[31] P. Teixeira-Dias,[78] K. K. Temming,[49] D. Temple,[142] H. Ten Kate,[31] P. K. Teng,[151] J. J. Teoh,[118] F. Tepel,[174] S. Terada,[67] K. Terashi,[155] J. Terron,[83] S. Terzo,[101] M. Testa,[48] R. J. Teuscher,[158,m] T. Theveneaux-Pelzer,[86] J. P. Thomas,[18] J. Thomas-Wilsker,[78] E. N. Thompson,[36] P. D. Thompson,[18] R. J. Thompson,[85] A. S. Thompson,[54] L. A. Thomsen,[175] E. Thomson,[122] M. Thomson,[29] M. J. Tibbetts,[15] R. E. Ticse Torres,[86] V. O. Tikhomirov,[96,kk] Yu.A. Tikhonov,[109,d] S. Timoshenko,[98] P. Tipton,[175] S. Tisserant,[86] K. Todome,[157] T. Todorov,[5,a] S. Todorova-Nova,[129] J. Tojo,[71] S. Tokár,[144a] K. Tokushuku,[67] E. Tolley,[58] L. Tomlinson,[85] M. Tomoto,[103] L. Tompkins,[143,ll] K. Toms,[105] B. Tong,[58] E. Torrence,[116] H. Torres,[142] E. Torró Pastor,[138] J. Toth,[86,mm] F. Touchard,[86] D. R. Tovey,[139] T. Trefzger,[173] L. Tremblet,[31] A. Tricoli,[31] I. M. Trigger,[159a] S. Trincaz-Duvoid,[81] M. F. Tripiana,[12] W. Trischuk,[158] B. Trocmé,[56] A. Trofymov,[43] C. Troncon,[92a] M. Trottier-McDonald,[15] M. Trovatelli,[168] L. Truong,[163a,163b] M. Trzebinski,[40] A. Trzupek,[40] J.C-L. Tseng,[120] P. V. Tsiareshka,[93] G. Tsipolitis,[10] N. Tsirintanis,[9] S. Tsiskaridze,[12] V. Tsiskaridze,[49] E. G. Tskhadadze,[52a] K. M. Tsui,[61a] I. I. Tsukerman,[97] V. Tsulaia,[15] S. Tsuno,[67] D. Tsybychev,[148] A. Tudorache,[27b] V. Tudorache,[27b] A. N. Tuna,[58] S. A. Tupputi,[21a,21b] S. Turchikhin,[99,jj] D. Turecek,[128] D. Turgeman,[171] R. Turra,[92a,92b]

A. J. Turvey,[41] P. M. Tuts,[36] M. Tylmad,[146a,146b] M. Tyndel,[131] G. Ucchielli,[21a,21b] I. Ueda,[155] R. Ueno,[30] M. Ughetto,[146a,146b] F. Ukegawa,[160] G. Unal,[31] A. Undrus,[26] G. Unel,[162] F. C. Ungaro,[89] Y. Unno,[67] C. Unverdorben,[100] J. Urban,[144b] P. Urquijo,[89] P. Urrejola,[84] G. Usai,[8] A. Usanova,[63] L. Vacavant,[86] V. Vacek,[128] B. Vachon,[88] C. Valderanis,[84] E. Valdes Santurio,[146a,146b] N. Valencic,[107] S. Valentinetti,[21a,21b] A. Valero,[166] L. Valery,[12] S. Valkar,[129] S. Vallecorsa,[50] J. A. Valls Ferrer,[166] W. Van Den Wollenberg,[107] P. C. Van Der Deijl,[107] R. van der Geer,[107] H. van der Graaf,[107] N. van Eldik,[152] P. van Gemmeren,[6] J. Van Nieuwkoop,[142] I. van Vulpen,[107] M. C. van Woerden,[31] M. Vanadia,[132a,132b] W. Vandelli,[31] R. Vanguri,[122] A. Vaniachine,[6] P. Vankov,[107] G. Vardanyan,[176] R. Vari,[132a] E. W. Varnes,[7] T. Varol,[41] D. Varouchas,[81] A. Vartapetian,[8] K. E. Varvell,[150] F. Vazeille,[35] T. Vazquez Schroeder,[88] J. Veatch,[7] L. M. Veloce,[158] F. Veloso,[126a,126c] S. Veneziano,[132a] A. Ventura,[74a,74b] M. Venturi,[168] N. Venturi,[158] A. Venturini,[24] V. Vercesi,[121a] M. Verducci,[132a,132b] W. Verkerke,[107] J. C. Vermeulen,[107] A. Vest,[45,nn] M. C. Vetterli,[142,e] O. Viazlo,[82] I. Vichou,[165] T. Vickey,[139] O. E. Vickey Boeriu,[139] G. H. A. Viehhauser,[120] S. Viel,[15] R. Vigne,[63] M. Villa,[21a,21b] M. Villaplana Perez,[92a,92b] E. Vilucchi,[48] M. G. Vincter,[30] V. B. Vinogradov,[66] C. Vittori,[21a,21b] I. Vivarelli,[149] S. Vlachos,[10] M. Vlasak,[128] M. Vogel,[174] P. Vokac,[128] G. Volpi,[124a,124b] M. Volpi,[89] H. von der Schmitt,[101] E. von Toerne,[22] V. Vorobel,[129] K. Vorobev,[98] M. Vos,[166] R. Voss,[31] J. H. Vossebeld,[75] N. Vranjes,[13] M. Vranjes Milosavljevic,[13] V. Vrba,[127] M. Vreeswijk,[107] R. Vuillermet,[31] I. Vukotic,[32] Z. Vykydal,[128] P. Wagner,[22] W. Wagner,[174] H. Wahlberg,[72] S. Wahrmund,[45] J. Wakabayashi,[103] J. Walder,[73] R. Walker,[100] W. Walkowiak,[141] V. Wallangen,[146a,146b] C. Wang,[151] C. Wang,[34d,86] F. Wang,[172] H. Wang,[15] H. Wang,[41] J. Wang,[43] J. Wang,[150] K. Wang,[88] R. Wang,[6] S. M. Wang,[151] T. Wang,[22] T. Wang,[36] X. Wang,[175] C. Wanotayaroj,[116] A. Warburton,[88] C. P. Ward,[29] D. R. Wardrope,[79] A. Washbrook,[47] P. M. Watkins,[18] A. T. Watson,[18] I. J. Watson,[150] M. F. Watson,[18] G. Watts,[138] S. Watts,[85] B. M. Waugh,[79] S. Webb,[84] M. S. Weber,[17] S. W. Weber,[173] J. S. Webster,[6] A. R. Weidberg,[120] B. Weinert,[62] J. Weingarten,[55] C. Weiser,[49] H. Weits,[107] P. S. Wells,[31] T. Wenaus,[26] T. Wengler,[31] S. Wenig,[31] N. Wermes,[22] M. Werner,[49] P. Werner,[31] M. Wessels,[59a] J. Wetter,[161] K. Whalen,[116] N. L. Whallon,[138] A. M. Wharton,[73] A. White,[8] M. J. White,[1] R. White,[33b] S. White,[124a,124b] D. Whiteson,[162] F. J. Wickens,[131] W. Wiedenmann,[172] M. Wielers,[131] P. Wienemann,[22] C. Wiglesworth,[37] L. A. M. Wiik-Fuchs,[22] A. Wildauer,[101] H. G. Wilkens,[31] H. H. Williams,[122] S. Williams,[107] C. Willis,[91] S. Willocq,[87] J. A. Wilson,[18] I. Wingerter-Seez,[5] F. Winklmeier,[116] O. J. Winston,[149] B. T. Winter,[22] M. Wittgen,[143] J. Wittkowski,[100] S. J. Wollstadt,[84] M. W. Wolter,[40] H. Wolters,[126a,126c] B. K. Wosiek,[40] J. Wotschack,[31] M. J. Woudstra,[85] K. W. Wozniak,[40] M. Wu,[56] M. Wu,[32] S. L. Wu,[172] X. Wu,[50] Y. Wu,[90] T. R. Wyatt,[85] B. M. Wynne,[47] S. Xella,[37] D. Xu,[34a] L. Xu,[26] B. Yabsley,[150] S. Yacoob,[145a] R. Yakabe,[68] D. Yamaguchi,[157] Y. Yamaguchi,[118] A. Yamamoto,[67] S. Yamamoto,[155] T. Yamanaka,[155] K. Yamauchi,[103] Y. Yamazaki,[68] Z. Yan,[23] H. Yang,[34e] H. Yang,[172] Y. Yang,[151] Z. Yang,[14] W-M. Yao,[15] Y. C. Yap,[81] Y. Yasu,[67] E. Yatsenko,[5] K. H. Yau Wong,[22] J. Ye,[41] S. Ye,[26] I. Yeletskikh,[66] A. L. Yen,[58] E. Yildirim,[43] K. Yorita,[170] R. Yoshida,[6] K. Yoshihara,[122] C. Young,[143] C. J. S. Young,[31] S. Youssef,[23] D. R. Yu,[15] J. Yu,[8] J. M. Yu,[90] J. Yu,[65] L. Yuan,[68] S. P. Y. Yuen,[22] I. Yusuff,[29,oo] B. Zabinski,[40] R. Zaidan,[34d] A. M. Zaitsev,[130,dd] N. Zakharchuk,[43] J. Zalieckas,[14] A. Zaman,[148] S. Zambito,[58] L. Zanello,[132a,132b] D. Zanzi,[89] C. Zeitnitz,[174] M. Zeman,[128] A. Zemla,[39a] J. C. Zeng,[165] Q. Zeng,[143] K. Zengel,[24] O. Zenin,[130] T. Ženiš,[144a] D. Zerwas,[117] D. Zhang,[90] F. Zhang,[172] G. Zhang,[34b,aa] H. Zhang,[34c] J. Zhang,[6] L. Zhang,[49] R. Zhang,[22] R. Zhang,[34b,pp] X. Zhang,[34d] Z. Zhang,[117] X. Zhao,[41] Y. Zhao,[34d,117] Z. Zhao,[34b] A. Zhemchugov,[66] J. Zhong,[120] B. Zhou,[90] C. Zhou,[46] L. Zhou,[36] L. Zhou,[41] M. Zhou,[148] N. Zhou,[34f] C. G. Zhu,[34d] H. Zhu,[34a] J. Zhu,[90] Y. Zhu,[34b] X. Zhuang,[34a] K. Zhukov,[96] A. Zibell,[173] D. Zieminska,[62] N. I. Zimine,[66] C. Zimmermann,[84] S. Zimmermann,[49] Z. Zinonos,[55] M. Zinser,[84] M. Ziolkowski,[141] L. Živković,[13] G. Zobernig,[172] A. Zoccoli,[21a,21b] M. zur Nedden,[16] G. Zurzolo,[104a,104b] and L. Zwalinski[31]

(ATLAS Collaboration)

[1]*Department of Physics, University of Adelaide, Adelaide, Australia*
[2]*Physics Department, SUNY Albany, Albany, New York, USA*
[3]*Department of Physics, University of Alberta, Edmonton AB, Canada*
[4a]*Department of Physics, Ankara University, Ankara, Turkey*
[4b]*Istanbul Aydin University, Istanbul, Turkey*
[4c]*Division of Physics, TOBB University of Economics and Technology, Ankara, Turkey*
[5]*LAPP, CNRS/IN2P3 and Université Savoie Mont Blanc, Annecy-le-Vieux, France*
[6]*High Energy Physics Division, Argonne National Laboratory, Argonne, Illinois, USA*
[7]*Department of Physics, University of Arizona, Tucson, Arizona, USA*
[8]*Department of Physics, The University of Texas at Arlington, Arlington, Texas, USA*

[9]*Physics Department, University of Athens, Athens, Greece*
[10]*Physics Department, National Technical University of Athens, Zografou, Greece*
[11]*Institute of Physics, Azerbaijan Academy of Sciences, Baku, Azerbaijan*
[12]*Institut de Física d'Altes Energies (IFAE), The Barcelona Institute of Science and Technology, Barcelona, Spain*
[13]*Institute of Physics, University of Belgrade, Belgrade, Serbia*
[14]*Department for Physics and Technology, University of Bergen, Bergen, Norway*
[15]*Physics Division, Lawrence Berkeley National Laboratory and University of California, Berkeley, California, USA*
[16]*Department of Physics, Humboldt University, Berlin, Germany*
[17]*Albert Einstein Center for Fundamental Physics and Laboratory for High Energy Physics, University of Bern, Bern, Switzerland*
[18]*School of Physics and Astronomy, University of Birmingham, Birmingham, United Kingdom*
[19a]*Department of Physics, Bogazici University, Istanbul, Turkey*
[19b]*Department of Physics Engineering, Gaziantep University, Gaziantep, Turkey*
[19c]*Faculty of Engineering and Natural Sciences, Istanbul Bilgi University, Istanbul, Turkey*
[19d]*Faculty of Engineering and Natural Sciences, Bahcesehir University, Istanbul, Turkey*
[20]*Centro de Investigaciones, Universidad Antonio Narino, Bogota, Colombia*
[21a]*INFN Sezione di Bologna, Bologna, Italy*
[21b]*Dipartimento di Fisica e Astronomia, Università di Bologna, Bologna, Italy*
[22]*Physikalisches Institut, University of Bonn, Bonn, Germany*
[23]*Department of Physics, Boston University, Boston, Massachusetts, USA*
[24]*Department of Physics, Brandeis University, Waltham, Massachusetts, USA*
[25a]*Universidade Federal do Rio De Janeiro COPPE/EE/IF, Rio de Janeiro, Brazil*
[25b]*Electrical Circuits Department, Federal University of Juiz de Fora (UFJF), Juiz de Fora, Brazil*
[25c]*Federal University of Sao Joao del Rei (UFSJ), Sao Joao del Rei, Brazil*
[25d]*Instituto de Fisica, Universidade de Sao Paulo, Sao Paulo, Brazil*
[26]*Physics Department, Brookhaven National Laboratory, Upton, New York, USA*
[27a]*Transilvania University of Brasov, Brasov, Romania*
[27b]*National Institute of Physics and Nuclear Engineering, Bucharest, Romania*
[27c]*National Institute for Research and Development of Isotopic and Molecular Technologies, Physics Department, Cluj Napoca, Romania*
[27d]*University Politehnica Bucharest, Bucharest, Romania*
[27e]*West University in Timisoara, Timisoara, Romania*
[28]*Departamento de Física, Universidad de Buenos Aires, Buenos Aires, Argentina*
[29]*Cavendish Laboratory, University of Cambridge, Cambridge, United Kingdom*
[30]*Department of Physics, Carleton University, Ottawa ON, Canada*
[31]*CERN, Geneva, Switzerland*
[32]*Enrico Fermi Institute, University of Chicago, Chicago, Illinois, USA*
[33a]*Departamento de Física, Pontificia Universidad Católica de Chile, Santiago, Chile*
[33b]*Departamento de Física, Universidad Técnica Federico Santa María, Valparaíso, Chile*
[34a]*Institute of High Energy Physics, Chinese Academy of Sciences, Beijing, China*
[34b]*Department of Modern Physics, University of Science and Technology of China, Anhui, China*
[34c]*Department of Physics, Nanjing University, Jiangsu, China*
[34d]*School of Physics, Shandong University, Shandong, China*
[34e]*Department of Physics and Astronomy, Shanghai Key Laboratory for Particle Physics and Cosmology, Shanghai Jiao Tong University, Shanghai; (also affiliated with PKU-CHEP), China*
[34f]*Physics Department, Tsinghua University, Beijing 100084, China*
[35]*Laboratoire de Physique Corpusculaire, Clermont Université and Université Blaise Pascal and CNRS/IN2P3, Clermont-Ferrand, France*
[36]*Nevis Laboratory, Columbia University, Irvington, New York, USA*
[37]*Niels Bohr Institute, University of Copenhagen, Kobenhavn, Denmark*
[38a]*INFN Gruppo Collegato di Cosenza, Laboratori Nazionali di Frascati, Italy*
[38b]*Dipartimento di Fisica, Università della Calabria, Rende, Italy*
[39a]*AGH University of Science and Technology, Faculty of Physics and Applied Computer Science, Krakow, Poland*
[39b]*Marian Smoluchowski Institute of Physics, Jagiellonian University, Krakow, Poland*
[40]*Institute of Nuclear Physics Polish Academy of Sciences, Krakow, Poland*
[41]*Physics Department, Southern Methodist University, Dallas, Texas, USA*
[42]*Physics Department, University of Texas at Dallas, Richardson, Texas, USA*

[43]*DESY, Hamburg and Zeuthen, Germany*
[44]*Institut für Experimentelle Physik IV, Technische Universität Dortmund, Dortmund, Germany*
[45]*Institut für Kern- und Teilchenphysik, Technische Universität Dresden, Dresden, Germany*
[46]*Department of Physics, Duke University, Durham, North Carolina, USA*
[47]*SUPA—School of Physics and Astronomy, University of Edinburgh, Edinburgh, United Kingdom*
[48]*INFN Laboratori Nazionali di Frascati, Frascati, Italy*
[49]*Fakultät für Mathematik und Physik, Albert-Ludwigs-Universität, Freiburg, Germany*
[50]*Section de Physique, Université de Genève, Geneva, Switzerland*
[51a]*INFN Sezione di Genova, Genova, Italy*
[51b]*Dipartimento di Fisica, Università di Genova, Genova, Italy*
[52a]*E. Andronikashvili Institute of Physics, Iv. Javakhishvili Tbilisi State University, Tbilisi, Georgia*
[52b]*High Energy Physics Institute, Tbilisi State University, Tbilisi, Georgia*
[53]*II Physikalisches Institut, Justus-Liebig-Universität Giessen, Giessen, Germany*
[54]*SUPA—School of Physics and Astronomy, University of Glasgow, Glasgow, United Kingdom*
[55]*II Physikalisches Institut, Georg-August-Universität, Göttingen, Germany*
[56]*Laboratoire de Physique Subatomique et de Cosmologie, Université Grenoble-Alpes, CNRS/IN2P3, Grenoble, France*
[57]*Department of Physics, Hampton University, Hampton, Virginia, USA*
[58]*Laboratory for Particle Physics and Cosmology, Harvard University, Cambridge, Massachusetts, USA*
[59a]*Kirchhoff-Institut für Physik, Ruprecht-Karls-Universität Heidelberg, Heidelberg, Germany*
[59b]*Physikalisches Institut, Ruprecht-Karls-Universität Heidelberg, Heidelberg, Germany*
[59c]*ZITI Institut für technische Informatik, Ruprecht-Karls-Universität Heidelberg, Mannheim, Germany*
[60]*Faculty of Applied Information Science, Hiroshima Institute of Technology, Hiroshima, Japan*
[61a]*Department of Physics, The Chinese University of Hong Kong, Shatin, N.T., Hong Kong, China*
[61b]*Department of Physics, The University of Hong Kong, Hong Kong, China*
[61c]*Department of Physics, The Hong Kong University of Science and Technology, Clear Water Bay, Kowloon, Hong Kong, China*
[62]*Department of Physics, Indiana University, Bloomington, Indiana, USA*
[63]*Institut für Astro- und Teilchenphysik, Leopold-Franzens-Universität, Innsbruck, Austria*
[64]*University of Iowa, Iowa City, Iowa, USA*
[65]*Department of Physics and Astronomy, Iowa State University, Ames, Iowa, USA*
[66]*Joint Institute for Nuclear Research, JINR Dubna, Russia*
[67]*KEK, High Energy Accelerator Research Organization, Tsukuba, Japan*
[68]*Graduate School of Science, Kobe University, Kobe, Japan*
[69]*Faculty of Science, Kyoto University, Kyoto, Japan*
[70]*Kyoto University of Education, Kyoto, Japan*
[71]*Department of Physics, Kyushu University, Fukuoka, Japan*
[72]*Instituto de Física La Plata, Universidad Nacional de La Plata and CONICET, La Plata, Argentina*
[73]*Physics Department, Lancaster University, Lancaster, United Kingdom*
[74a]*INFN Sezione di Lecce, Lecce, Italy*
[74b]*Dipartimento di Matematica e Fisica, Università del Salento, Lecce, Italy*
[75]*Oliver Lodge Laboratory, University of Liverpool, Liverpool, United Kingdom*
[76]*Department of Physics, Jožef Stefan Institute and University of Ljubljana, Ljubljana, Slovenia*
[77]*School of Physics and Astronomy, Queen Mary University of London, London, United Kingdom*
[78]*Department of Physics, Royal Holloway University of London, Surrey, United Kingdom*
[79]*Department of Physics and Astronomy, University College London, London, United Kingdom*
[80]*Louisiana Tech University, Ruston, Los Angeles, USA*
[81]*Laboratoire de Physique Nucléaire et de Hautes Energies, UPMC and Université Paris-Diderot and CNRS/IN2P3, Paris, France*
[82]*Fysiska institutionen, Lunds universitet, Lund, Sweden*
[83]*Departamento de Fisica Teorica C-15, Universidad Autonoma de Madrid, Madrid, Spain*
[84]*Institut für Physik, Universität Mainz, Mainz, Germany*
[85]*School of Physics and Astronomy, University of Manchester, Manchester, United Kingdom*
[86]*CPPM, Aix-Marseille Université and CNRS/IN2P3, Marseille, France*
[87]*Department of Physics, University of Massachusetts, Amherst, Massachusetts, USA*
[88]*Department of Physics, McGill University, Montreal QC, Canada*
[89]*School of Physics, University of Melbourne, Victoria, Australia*
[90]*Department of Physics, The University of Michigan, Ann Arbor, Michigan, USA*
[91]*Department of Physics and Astronomy, Michigan State University, East Lansing, Michigan, USA*
[92a]*INFN Sezione di Milano, Milano, Italy*

[92b]*Dipartimento di Fisica, Università di Milano, Milano, Italy*
[93]*B.I. Stepanov Institute of Physics, National Academy of Sciences of Belarus, Minsk, Republic of Belarus*
[94]*National Scientific and Educational Centre for Particle and High Energy Physics, Minsk, Republic of Belarus*
[95]*Group of Particle Physics, University of Montreal, Montreal QC, Canada*
[96]*P.N. Lebedev Physical Institute of the Russian Academy of Sciences, Moscow, Russia*
[97]*Institute for Theoretical and Experimental Physics (ITEP), Moscow, Russia*
[98]*National Research Nuclear University MEPhI, Moscow, Russia*
[99]*D.V. Skobeltsyn Institute of Nuclear Physics, M.V. Lomonosov Moscow State University, Moscow, Russia*
[100]*Fakultät für Physik, Ludwig-Maximilians-Universität München, München, Germany*
[101]*Max-Planck-Institut für Physik (Werner-Heisenberg-Institut), München, Germany*
[102]*Nagasaki Institute of Applied Science, Nagasaki, Japan*
[103]*Graduate School of Science and Kobayashi-Maskawa Institute, Nagoya University, Nagoya, Japan*
[104a]*INFN Sezione di Napoli, Napoli, Italy*
[104b]*Dipartimento di Fisica, Università di Napoli, Napoli, Italy*
[105]*Department of Physics and Astronomy, University of New Mexico, Albuquerque, New Mexico, USA*
[106]*Institute for Mathematics, Astrophysics and Particle Physics, Radboud University Nijmegen/Nikhef, Nijmegen, Netherlands*
[107]*Nikhef National Institute for Subatomic Physics and University of Amsterdam, Amsterdam, Netherlands*
[108]*Department of Physics, Northern Illinois University, DeKalb, Illinois, USA*
[109]*Budker Institute of Nuclear Physics, SB RAS, Novosibirsk, Russia*
[110]*Department of Physics, New York University, New York, New York, USA*
[111]*Ohio State University, Columbus, Ohio, USA*
[112]*Faculty of Science, Okayama University, Okayama, Japan*
[113]*Homer L. Dodge Department of Physics and Astronomy, University of Oklahoma, Norman, Oklahoma, USA*
[114]*Department of Physics, Oklahoma State University, Stillwater, Oklahoma, USA*
[115]*Palacký University, RCPTM, Olomouc, Czech Republic*
[116]*Center for High Energy Physics, University of Oregon, Eugene, Oregon, USA*
[117]*LAL, Univ. Paris-Sud, CNRS/IN2P3, Université Paris-Saclay, Orsay, France*
[118]*Graduate School of Science, Osaka University, Osaka, Japan*
[119]*Department of Physics, University of Oslo, Oslo, Norway*
[120]*Department of Physics, Oxford University, Oxford, United Kingdom*
[121a]*INFN Sezione di Pavia, Pavia, Italy*
[121b]*Dipartimento di Fisica, Università di Pavia, Pavia, Italy*
[122]*Department of Physics, University of Pennsylvania, Philadelphia, Pennsylvania, USA*
[123]*National Research Centre "Kurchatov Institute" B.P.Konstantinov Petersburg Nuclear Physics Institute, St. Petersburg, Russia*
[124a]*INFN Sezione di Pisa, Pisa, Italy*
[124b]*Dipartimento di Fisica E. Fermi, Università di Pisa, Pisa, Italy*
[125]*Department of Physics and Astronomy, University of Pittsburgh, Pittsburgh, Pennsylvania, USA*
[126a]*Laboratório de Instrumentação e Física Experimental de Partículas—LIP, Lisboa, Portugal*
[126b]*Faculdade de Ciências, Universidade de Lisboa, Lisboa, Portugal*
[126c]*Department of Physics, University of Coimbra, Coimbra, Portugal*
[126d]*Centro de Física Nuclear da Universidade de Lisboa, Lisboa, Portugal*
[126e]*Departamento de Fisica, Universidade do Minho, Braga, Portugal*
[126f]*Departamento de Fisica Teorica y del Cosmos and CAFPE, Universidad de Granada, Granada, Spain*
[126g]*Dep Fisica and CEFITEC of Faculdade de Ciencias e Tecnologia, Universidade Nova de Lisboa, Caparica, Portugal*
[127]*Institute of Physics, Academy of Sciences of the Czech Republic, Praha, Czech Republic*
[128]*Czech Technical University in Prague, Praha, Czech Republic*
[129]*Faculty of Mathematics and Physics, Charles University in Prague, Praha, Czech Republic*
[130]*State Research Center Institute for High Energy Physics (Protvino), NRC KI, Russia*
[131]*Particle Physics Department, Rutherford Appleton Laboratory, Didcot, United Kingdom*
[132a]*INFN Sezione di Roma, Roma, Italy*
[132b]*Dipartimento di Fisica, Sapienza Università di Roma, Roma, Italy*
[133a]*INFN Sezione di Roma Tor Vergata, Roma, Italy*
[133b]*Dipartimento di Fisica, Università di Roma Tor Vergata, Roma, Italy*
[134a]*INFN Sezione di Roma Tre, Roma, Italy*
[134b]*Dipartimento di Matematica e Fisica, Università Roma Tre, Roma, Italy*

[135a]*Faculté des Sciences Ain Chock, Réseau Universitaire de Physique des Hautes Energies—Université Hassan II, Casablanca, Morocco*
[135b]*Centre National de l'Energie des Sciences Techniques Nucleaires, Rabat, Morocco*
[135c]*Faculté des Sciences Semlalia, Université Cadi Ayyad, LPHEA-Marrakech, Morocco*
[135d]*Faculté des Sciences, Université Mohamed Premier and LPTPM, Oujda, Morocco*
[135e]*Faculté des sciences, Université Mohammed V, Rabat, Morocco*
[136]*DSM/IRFU (Institut de Recherches sur les Lois Fondamentales de l'Univers), CEA Saclay (Commissariat à l'Energie Atomique et aux Energies Alternatives), Gif-sur-Yvette, France*
[137]*Santa Cruz Institute for Particle Physics, University of California Santa Cruz, Santa Cruz, California, USA*
[138]*Department of Physics, University of Washington, Seattle, Washington, USA*
[139]*Department of Physics and Astronomy, University of Sheffield, Sheffield, United Kingdom*
[140]*Department of Physics, Shinshu University, Nagano, Japan*
[141]*Fachbereich Physik, Universität Siegen, Siegen, Germany*
[142]*Department of Physics, Simon Fraser University, Burnaby BC, Canada*
[143]*SLAC National Accelerator Laboratory, Stanford, California, USA*
[144a]*Faculty of Mathematics, Physics & Informatics, Comenius University, Bratislava, Slovak Republic*
[144b]*Department of Subnuclear Physics, Institute of Experimental Physics of the Slovak Academy of Sciences, Kosice, Slovak Republic*
[145a]*Department of Physics, University of Cape Town, Cape Town, South Africa*
[145b]*Department of Physics, University of Johannesburg, Johannesburg, South Africa*
[145c]*School of Physics, University of the Witwatersrand, Johannesburg, South Africa*
[146a]*Department of Physics, Stockholm University, Stockholm, Sweden*
[146b]*The Oskar Klein Centre, Stockholm, Sweden*
[147]*Physics Department, Royal Institute of Technology, Stockholm, Sweden*
[148]*Departments of Physics & Astronomy and Chemistry, Stony Brook University, Stony Brook, New York, USA*
[149]*Department of Physics and Astronomy, University of Sussex, Brighton, United Kingdom*
[150]*School of Physics, University of Sydney, Sydney, Australia*
[151]*Institute of Physics, Academia Sinica, Taipei, Taiwan*
[152]*Department of Physics, Technion: Israel Institute of Technology, Haifa, Israel*
[153]*Raymond and Beverly Sackler School of Physics and Astronomy, Tel Aviv University, Tel Aviv, Israel*
[154]*Department of Physics, Aristotle University of Thessaloniki, Thessaloniki, Greece*
[155]*International Center for Elementary Particle Physics and Department of Physics, The University of Tokyo, Tokyo, Japan*
[156]*Graduate School of Science and Technology, Tokyo Metropolitan University, Tokyo, Japan*
[157]*Department of Physics, Tokyo Institute of Technology, Tokyo, Japan*
[158]*Department of Physics, University of Toronto, Toronto ON, Canada*
[159a]*TRIUMF, Vancouver BC, Canada*
[159b]*Department of Physics and Astronomy, York University, Toronto ON, Canada*
[160]*Faculty of Pure and Applied Sciences, and Center for Integrated Research in Fundamental Science and Engineering, University of Tsukuba, Tsukuba, Japan*
[161]*Department of Physics and Astronomy, Tufts University, Medford, Massachusetts, USA*
[162]*Department of Physics and Astronomy, University of California Irvine, Irvine, California, USA*
[163a]*INFN Gruppo Collegato di Udine, Sezione di Trieste, Udine, Italy*
[163b]*ICTP, Trieste, Italy*
[163c]*Dipartimento di Chimica, Fisica e Ambiente, Università di Udine, Udine, Italy*
[164]*Department of Physics and Astronomy, University of Uppsala, Uppsala, Sweden*
[165]*Department of Physics, University of Illinois, Urbana, Illinois, USA*
[166]*Instituto de Física Corpuscular (IFIC) and Departamento de Física Atómica, Molecular y Nuclear and Departamento de Ingeniería Electrónica and Instituto de Microelectrónica de Barcelona (IMB-CNM), University of Valencia and CSIC, Valencia, Spain*
[167]*Department of Physics, University of British Columbia, Vancouver BC, Canada*
[168]*Department of Physics and Astronomy, University of Victoria, Victoria BC, Canada*
[169]*Department of Physics, University of Warwick, Coventry, United Kingdom*
[170]*Waseda University, Tokyo, Japan*
[171]*Department of Particle Physics, The Weizmann Institute of Science, Rehovot, Israel*
[172]*Department of Physics, University of Wisconsin, Madison, Wisconsin, USA*
[173]*Fakultät für Physik und Astronomie, Julius-Maximilians-Universität, Würzburg, Germany*

[174]*Fakultät für Mathematik und Naturwissenschaften, Fachgruppe Physik, Bergische Universität Wuppertal, Wuppertal, Germany*
[175]*Department of Physics, Yale University, New Haven, Connecticut, USA*
[176]*Yerevan Physics Institute, Yerevan, Armenia*
[177]*Centre de Calcul de l'Institut National de Physique Nucléaire et de Physique des Particules (IN2P3), Villeurbanne, France*

[a]Deceased.
[b]Also at Department of Physics, King's College London, London, United Kingdom.
[c]Also at Institute of Physics, Azerbaijan Academy of Sciences, Baku, Azerbaijan.
[d]Also at Novosibirsk State University, Novosibirsk, Russia.
[e]Also at TRIUMF, Vancouver BC, Canada.
[f]Also at Department of Physics & Astronomy, University of Louisville, Louisville, KY, USA.
[g]Also at Department of Physics, California State University, Fresno CA, USA.
[h]Also at Department of Physics, University of Fribourg, Fribourg, Switzerland.
[i]Also at Departament de Fisica de la Universitat Autonoma de Barcelona, Barcelona, Spain.
[j]Also at Departamento de Fisica e Astronomia, Faculdade de Ciencias, Universidade do Porto, Portugal.
[k]Also at Tomsk State University, Tomsk, Russia.
[l]Also at Universita di Napoli Parthenope, Napoli, Italy.
[m]Also at Institute of Particle Physics (IPP), Canada.
[n]Also at Department of Physics, St. Petersburg State Polytechnical University, St. Petersburg, Russia.
[o]Also at Department of Physics, The University of Michigan, Ann Arbor MI, USA.
[p]Also at Louisiana Tech University, Ruston LA, USA.
[q]Also at Institucio Catalana de Recerca i Estudis Avancats, ICREA, Barcelona, Spain.
[r]Also at Graduate School of Science, Osaka University, Osaka, Japan.
[s]Also at Department of Physics, National Tsing Hua University, Taiwan.
[t]Also at Department of Physics, The University of Texas at Austin, Austin TX, USA.
[u]Also at Institute of Theoretical Physics, Ilia State University, Tbilisi, Georgia.
[v]Also at CERN, Geneva, Switzerland.
[w]Also at Georgian Technical University (GTU),Tbilisi, Georgia.
[x]Also at Ochadai Academic Production, Ochanomizu University, Tokyo, Japan.
[y]Also at Manhattan College, New York NY, USA.
[z]Also at Hellenic Open University, Patras, Greece.
[aa]Also at Institute of Physics, Academia Sinica, Taipei, Taiwan.
[bb]Also at Academia Sinica Grid Computing, Institute of Physics, Academia Sinica, Taipei, Taiwan.
[cc]Also at School of Physics, Shandong University, Shandong, China.
[dd]Also at Moscow Institute of Physics and Technology State University, Dolgoprudny, Russia.
[ee]Also at Section de Physique, Université de Genève, Geneva, Switzerland.
[ff]Also at International School for Advanced Studies (SISSA), Trieste, Italy.
[gg]Also at Department of Physics and Astronomy, University of South Carolina, Columbia SC, USA.
[hh]Also at School of Physics and Engineering, Sun Yat-sen University, Guangzhou, China.
[ii]Also at Institute for Nuclear Research and Nuclear Energy (INRNE) of the Bulgarian Academy of Sciences, Sofia, Bulgaria.
[jj]Also at Faculty of Physics, M.V.Lomonosov Moscow State University, Moscow, Russia.
[kk]Also at National Research Nuclear University MEPhI, Moscow, Russia.
[ll]Also at Department of Physics, Stanford University, Stanford CA, USA.
[mm]Also at Institute for Particle and Nuclear Physics, Wigner Research Centre for Physics, Budapest, Hungary.
[nn]Also at Flensburg University of Applied Sciences, Flensburg, Germany.
[oo]Also at University of Malaya, Department of Physics, Kuala Lumpur, Malaysia.
[pp]Also at CPPM, Aix-Marseille Université and CNRS/IN2P3, Marseille, France.